The Dissertation Committee for Minhye Shin Certifies that this is the approved version of the following dissertation:

CHARACTERIZATION OF THE ROLE OF THE MITOCHONDRIAL ONE-CARBON METABOLISM DURING EMBRYONIC DEVELOPMENT

Committee:

Dean Appling, Supervisor

Richard Finnell

David Hoffman

Walter Fast

Steven Vokes

CHARACTERIZATION OF THE ROLE OF THE MITOCHONDRIAL ONE-CARBON METABOLISM DURING EMBRYONIC DEVELOPMENT

by

Minhye Shin, B.S.; M.S.

Dissertation

Presented to the Faculty of the Graduate School of

The University of Texas at Austin

in Partial Fulfillment

of the Requirements

for the Degree of

Doctor of Philosophy

The University of Texas at Austin

December 2016

Dedication

To my parents for all your love, guidance, and support that you have given me, and to my family, Hoon, Chloe, and Luke, for all your love, patience, and support

Acknowledgements

First and foremost, I would like to thank my advisor, Dr. Dean Appling for all his guidance, advice, warm consideration, and encouragement. I am very lucky person to have him as my Ph.D. advisor.

I would like to thank all the members of my dissertation committee: Dr. Richard Finnell, Dr. David Hoffman, Dr. Walter Fast, and Dr. Steven Vokes for their precious feedback and advice.

I would like to thank Dr. Gail Grabner for all her help and warm consideration. Without her help, it would not have been possible for me to finish my degree.

I would like to thank my lab members, Jessica Momb and Josh Bryant as my best mentor ever and my best senior ever, respectively. I appreciate all your encouragement and support.

I also would like to all my friends and colleagues at The University of Texas at Austin.

CHARACTERIZATION OF THE ROLE OF THE MITOCHONDRIAL ONE-CARBON METABOLISM DURING EMBRYONIC DEVELOPMENT

Minhye Shin, Ph.D.

The University of Texas at Austin, 2016

Supervisor: Dean Appling

Neural tube defects (NTDs) are one of serious structural birth defects resulting from failure of neural tube closure. Folic acid supplementation is the essential factor for prevention of NTDs. Folate-dependent one-carbon metabolism is a central metabolic pathway participating in a diverse range of metabolic reactions. Mitochondrial one-carbon metabolism is crucial for production of formate as a major 1C donor to the cytoplasm and regeneration of redox cofactors. Mitochondrial MTHFD family enzymes, MTHFD2, MTHFD2L, and MTHFD1L, are major contributors for formate production in mammalian mitochondria.

The MTHFD2 and MTHFD2L isozymes possess both CH_2-THF dehydrogenase and CH^+-THF cyclohydrolase activities, catalyzing the reaction of 10-CHO-THF production in mitochondria. The dehydrogenase activity of these bifunctional enzymes can use either NAD^+ or $NADP^+$ with dual redox cofactor specificity, but requires both phosphate and Mg^{2+} when using NAD^+. The $NADP^+$-dependent dehydrogenase activity is inhibited by inorganic phosphate. With polyglutamylated THF substrate, both of MTHFD2 and MTHFD2L show higher $NADP^+$-dependent activity than the monoglutamylated

substrate. Phylogenetic analysis indicates that MTHFD2L may be evolved from invertebrate MTHFD2 which is homologous to a primitive fungal MTHFD1.

MTHFD1L is expressed ubiquitously throughout the embryogenesis during neural tube closure, and significantly detected at the basal surface of the dorsal neuroepithelium. Lacking *Mthfd1l* causes retardation in growth and developmental progression. *Mthfd1l* knockout mouse embryos show defects in proliferation during late neural tube closure and head mesenchyme development during early neural tube closure. However, proliferation during early neural tube closure, apoptosis, and neural crest cell migration were not affected by the loss of *Mthfd1l*. Finally, we show that maternal formate supplementation significantly improves the dysregulated cellular processes in *Mthfd1l*$^{E/z}$ embryos. This study elucidates the specific metabolic mechanisms underlying folate-associated birth defects, including NTDs.

Table of Contents

List of Figures

List of Tables

Chapter 1. INTRODUCTION

1.1. NEURAL TUBE DEFECTS AND FOLATE SUPPLEMENTATION

1.1.1. Neural Tube Defects

Neural tube closure (NTC), also known as neurulation, is the embryonic process in vertebrates where the neural plate transforms into the neural tube which further differentiates into the central nervous system including the spinal cord and the brain. Neurulation is initiated at the hindbrain/cervical boundary at 3 weeks post-fertilization in humans (at embryonic day 8.5 in mouse), when the embryo has 6-7 pairs of somites (Copp, 2005). Initially, the central nervous system develops as a flat sheet, then rolls up and fuses to form the hollow neural tube (Figure 1.1) (Wallingford, Niswander, Shaw, & Finnell, 2013). The neural tube closure begins after neural induction of neuroepithelium to differentiate from the dorsal midline ectoderm (Yamaguchi & Miura, 2013). Subsequently, the neural plate bends at medial hinge point, is elevated to form the neural fold, bends at dorsolateral hinge point, and further apposes and fuses the edges forming the neural tube.

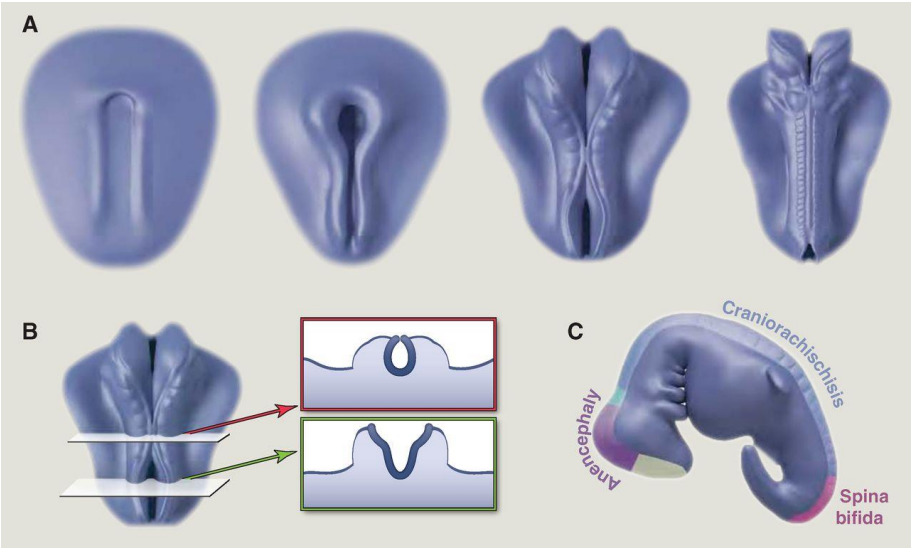

Figure 1.1 The progression of neural tube closure in a stylized vertebrate embryo. "A. The central nervous system is initially a flat sheet, then paired neural folds elevate along the rostrocaudal axis and move medially, eventually fusing to enclose the neural tube. B. Cross-sections illustrate closed (red) and open (green) regions of the neural tube. C. Region-specific neural tube defects." (Wallingford, Niswander, Shaw, & Finnell, 2013)

Neural tube defects (NTDs) are a category of serious structural birth defects, resulting from failure of the neural tube closure. NTDs occur in several forms: anencephaly (NTDs restricted to the cranial regions), spina bifida (NTDs restricted to the caudal regions), craniorachischisis (NTDs occurred over the entire body axis), and encephalocele (NTDs having protrusion of brain enclosed by a membrane) (Copp, Stanier, & Greene, 2013; Wallingford et al., 2013). It is estimated that NTDs occur approximately 6.0 per 10,000 births in the world, ranging from 0.3 to 199.4 per 10,000 births in specific geographical locations (Atta et al., 2016; Zaganjor et al., 2016). Relative frequency of each NTD type is 40% for anencephaly, 50% for spina bifida, 3% for craniorachischisis, and 7% for encephalocele (Copp et al., 2013). Babies with anencephaly are stillborn or die shortly after birth and 75 % of the babies only live up to 10 days (Jaquier, Klein, &

Boltshauser, 2006). Children with spina bifida have a much better chance for postnatal survival, although most of them may have lifelong physical and mental handicap with an economic burden (annual direct medical costs per patient with spina bifida are $65,177 (2003 USD) and total lifetime costs are $620,484 (2002 USD) (Yi, Lindemann, Colligs, & Snowball, 2011). Craniorachischisis, like anencephaly, is also lethal but relatively rare. Encephalocele is not lethal and can be treated with surgical treatment by removal of sac and closure (Copp et al., 2013).

1.1.2. Folate Supplementation

Folic acid is one of the B vitamins and occurs naturally in many foods especially dark green leafy vegetables and liver. It was first isolated from spinach leaves by Esmond Snell and his group in 1941 here at the University of Texas (Mitchell, Snell, & Williams, 1941). The importance of folic acid in neural tube development was first suggested in the 1965 (Hibbard & Smithells, 1965). Later, a randomized, double-blind trial led by the Medical Research Council showed 4 mg of folic acid supplementation is the essential factor for prevention of 72 % of NTDs (MRC Vitamin Study Research Group, 1991). Based on these findings, mandatory fortification of all enriched cereal grain products with folic acid was introduced in the United States in 1998. Fortification has contributed substantially to a reduction in the number of pregnancies affected by NTDs with upward of a 20 % decline of anencephaly and a 34 % decline in spina bifida (Eichholzer, Tönz, & Zimmermann, 2006; Wallingford et al., 2013). In addition to the prevention of NTDs, there is suggestive evidence of protection from congenital orofacial defects, cardiovascular defects, Down syndrome, limb defects, urinary tract anomalies and hydrocephalus with folic acid supplementation (Coppedè, 2009; De-Regil, Peña-Rosas, Fernández-Gaxiola, & Rayco-

Solon, 2015; Eskes, 2006; Goh, Bollano, Einarson, & Koren, 2006), although the effect of folic acid on other congenital birth defects beyond NTDs is still controversial.

Although maternal folic acid fortification has dramatically reduced the incidence of NTDs, there is a subset of NTDs (~30 % of NTDs prevalence before folic acid fortification) that still occurs, and causes/treatments of these folate-resistant NTDs are unknown. Also, a concern has been raised with respect to potential adverse effects of folic acid supplementation, such as accumulation of unmetabolized folic acid in cells, cognitive dysfunction, austism, and promotion of malignant tumors (Strickland, Krupenko, & Krupenko, 2013). Unfortunately, although there are a number of studies confirming the positive clinical and epidemiological aspects of folic acid supplementation, the fundamental question of how folic acid prevents NTDs and promotes closure of the neural tube remains largely a mystery.

1.2. FOLATE-DEPENDENT ONE-CARBON METABOLISM

1.2.1. Overview

In cells, folic acid is reduced to 7,8-dihydrofolate and then to 5,6,7,8-tetrahydrofolate (THF, the biologically active form of folic acid) by dihydrofolate reductase (DHFR) (Tibbetts & Appling, 2010). The folates enter the cell via folate transporters, which are the reduced folate carrier (RFC), folate receptors (Folr, also known as folate binding proteins, FolBP), and the proton-coupled folate transporter. The folates are further modified by polyglutamylation, catalyzed by folylpolyglutamate synthetase to aid in cytosolic and mitochondrial retention, and mediation of one-carbon metabolism (Fox & Stover, 2008).

Folate-dependent one-carbon metabolism is a central metabolic pathway in which activated one-carbon (1C) units are carried by THF at various oxidation states, participating in a diverse range of metabolic reactions. It is integral to many cellular processes including purine biosynthesis, amino acid metabolism, methyl group biogenesis, and redox cofactor regeneration. Uniquely, this metabolic pathway is highly compartmentalized in eukaryotes between cytoplasm, mitochondria, and nucleus (Tibbetts & Appling, 2010). These compartments, especially cytoplasmic and mitochondrial, are metabolically connected by transport of the 1C donors across the mitochondrial membranes, supporting a mostly unidirectional flow (in clockwise direction) of 1C units from serine to formate and onto methionine (Figure 1.2).

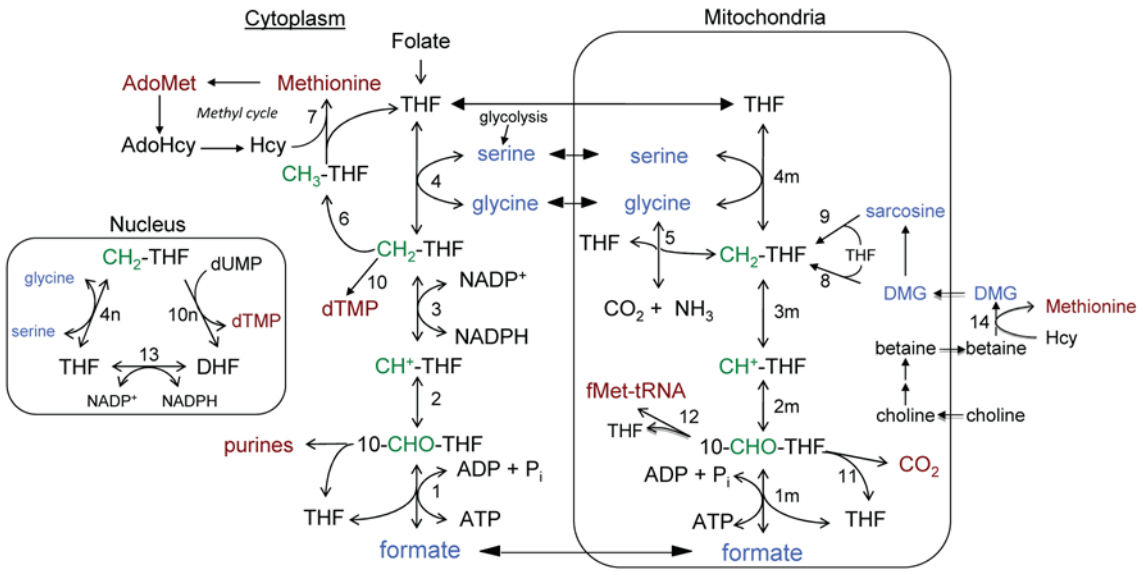

Figure 1.2 Mammalian one-carbon metabolism. Reactions 1, 2, and 3 are catalyzed by trifunctional C1-THF synthase in the cytoplasm (MTHFD1) with 10-formyl-THF synthetase, 5,10-methenyl-THF cyclohydrolase, and 5,10-methylene-THF dehydrogenase activities, respectively. In mitochondria, reaction 1m is catalyzed by MTHFD1L (monofunctional 10-formyl-THF synthetase), and reaction 2m and 3m are catalyzed by MTHFD2 or MTHFD2L (bifunctional 5,10-methylene-THF dehydrogenase/5,10-methenyl-THF cyclohydrolase) (Tibbetts & Appling, 2010).

1.2.2. Cytoplasmic One-Carbon Metabolism

Cytoplasmic 1C metabolism starts with transportation of formate produced from mitochondria (Figure 1.2). Formate is reattached to THF to produce 10-formyl-THF in a reaction catalyzed by the 10-formyl-THF synthetase activity of trifunctional C_1-THF synthase in the cytoplasm (MTHFD1, reaction 1). Synthesis of purines is critically dependent on the 1C pathway, requiring two moles of 10-formyl-THF per mole of purine ring (Tibbetts & Appling, 2010). 10-Formyl-THF can be further reduced to 5,10-methylene-THF via 5,10-methenyl-THF in reactions catalyzed by the 5,10-methenyl-THF cyclohydrolase and $NADP^+$-dependent 5,10-methylene-THF dehydrogenase activities, respectively, of MTHFD1 (reaction 2 and 3). It is noteworthy that 5,10-methylene-THF

also can be made from other 1C donors such as serine, glycine, dimethylglycine, or sarcosine. The level of 5,10-methylene-THF is highly regulated in cells by producing thymidylate, 5-methyl-THF, or serine catalyzed by TS (thymidylate synthase; reaction 10), MTHFR (5,10-methylene-THF reductase; reaction 6), or SHMT (serine hydroxymethyltransferase; reaction 4), respectively. 5,10-Methylene-THF is reduced to 5-methyl-THF by MTHFR, 5-methyl-THF is used to remethylate homocysteine to produce methionine and S-adenosylmethionine, the universal methyl donor for DNA and proteins. The 1C unit from methylene-THF may be used to produce serine from glycine, and this serine may be transported across the mitochondrial membrane, where it can be used to produce formate (Figure 1.2).

1.2.3. Mitochondrial One-Carbon Metabolism

Whereas the cytoplasmic one-carbon metabolism produces purines, thymidylate, universal methyl donors, NADPH, and serine, mitochondrial one-carbon metabolism is crucial for production of formate as a major 1C donor to the cytoplasm, formylation of initiator methionyl-tRNA, and regeneration of redox cofactors. The first step in the mitochondrial pathway begins with the donation of a 1C unit to THF from serine or glycine (Momb & Appling, 2014). Serine donates its third carbon to THF via the SHMT reaction, forming 5,10-methylene-THF and glycine (reaction 4m). Glycine can further donate its carbon to THF via the glycine cleavage system (reaction 5, GCS) composed of glycine decarboxylase, aminomethyltransferase, and GCS-H protein (Pai et al., 2015). In contrast to the single trifunctional enzyme in the cytoplasmic MTHFD1, three distinct isozymes, encoded by three distinct nuclear genes, are known to metabolize mitochondrial reaction of 5,10-methylene-THF in mammalian mitochondria (Shin, Bryant, Momb, & Appling,

2014). The 5,10-methylene-THF dehydrogenase and 5,10-methenyl-THF cyclohydrolase reactions are catalyzed by two homologous enzymes, MTHFD2 (bifunctional methylenetetrahydrofolate dehydrogenase 2) and MTHFD2L (bifunctional methylenetetrahydrofolate dehydrogenase 2-like), converting 5,10-methylene-THF to 10-formyl-THF (reaction 3m and 2m). The redox cofactors NADH and NADPH are also products of dehydrogenase activity of MTHFD2 and MTHFD2L. 10-Formyl-THF donates the 1C unit to formylate initiator methionyl-tRNA for mitochondrial proteins synthesis (reaction 12). The final step in the mammalian mitochondrial pathway, reaction 1m, is catalyzed by MTHFD1L (monofunctional 10-formyl-THF synthetase), producing mitochondrial formate. Metabolic tracer experiments in mouse embryonic fibroblasts demonstrated that more than 75 % of 1C units entering the cytoplasmic methyl cycle are mitochondrially derived as formate (Pike, Rajendra, Artzt, & Appling, 2010). MTHFD1L thus controls the flux of 1C units from mitochondria into cytoplasmic processes such as purine and thymidylate biosynthesis and the methyl cycle (Momb & Appling, 2014). MTHFD2, MTHFD2L, and MTHFD1L are the focus of this dissertation and further details about these enzymes will be described in sections 1.3 and 1.4.

1.2.4. Animal Models in One-Carbon Metabolism

Folate-mediated one-carbon metabolism is central to many cellular processes such as purine and thymidylate biosynthesis, mitochondrial protein biosynthesis, amino acid metabolism, and universal methyl donor production. To bring insight into the mechanisms by which folic acid acts during neural tube closure, knockout (KO) mouse models have been generated to aid in understanding how 1C metabolism influences embryonic development. Up to date, about 15 mouse models with mutations affecting 1C metabolism

exist (Karen E. Christensen, Patel, Kuzmanov, Mejia, & MacKenzie, 2005; Harris, 2009; Harris & Juriloff, 2010; Momb & Appling, 2014; Narisawa et al., 2012; Pai et al., 2015). Genes targeted in mice include *Folr1* (encoding folate receptor 1), *Folr2* (folate receptor 2), *Cbs* (cystathionine beta-synthase), *Mthfd1* (methylene-THF dehydrogenase 1), *Mthfd2* (methylene-THF dehydrogenase 2), *Mthfr* (methylene-THF reductase), *Shmt1* (serine hydroxymethyltransferase 1), *Mtr* (methionine synthase), *Mtrr* (methionine synthase reductase), *Rfc1* (reduced folate carrier 1), *Slc46a1* (proton-coupled folate transporter), *Mthfd1S* (cytoplasmic 10-formylTHF synthetase domain in MTHFD1), *Amt* (aminomethyltransferase in glycine cleavage system), *Gldc* (glycine decarboxylase in glycine cleavage system), and *Mthfd1l* (mitochondrial 10-formyl-THF synthetase). Surprisingly, many of the null mutants in the folate pathway show normal neural tube closure which is unexpected given the dramatic effect of folic acid supplementation on the prevention of NTDs in human populations. Folate-pathway KO mice that display NTDs include *Folr1* (5-30 % of null mutants partially rescued by maternal folate supplementation have exencephaly), *Amt, Gldc*, and *Mthfd1l*. Null mutants for *Mtr, Mtrr*, and *Rfc1* die before gestational day 9, and *Mthfd1S* null mutant embryos die shortly after 10.5 days gestation.

NTDs are observed in only five mutated genes (*Shmt1*, *Folr1, Amt, Gldc*, and *Mthfd1l*). *Shmt1* encodes a cytoplasmic serine hydroxymethyltransferase, and homozygous KO of the gene brings about a low frequence of NTDs when $Shmt^{-/-}$ dams fed a folate-deficient diet (Beaudin et al., 2011, 2012). *Folr1* encodes folate receptor 1, and homozygous KO of *Folr1* produces severe morphogenetic abnormalities and died in utero by embryonic day 10 (Piedrahita et al., 1999). Maternal supplementation with folinic acid (5-formyl-THF) reversed the embryonic lethality in nullizygous pups. Low maternal doses of folic acid produces *Folr1* null embryos with NTDs, while higher doses rescue embryos

to birth. While NTDs caused by the *Shmt1* and *Folr1* mutations are folate-sensitive depending on maternal folate level, NTDs from mutation of mitochondrial folate genes (*Amt, Gldc*, and *Mthfd1l*) are folate-resistant and not rescued by folate supplementation. *Amt* and *Gldc* encode an aminomethyltransferase and a glycine decarboxylase, respectively, which are subunits of the mitochondrially localized glycine cleavage system. Homozygous deletion of *Amt* is embryonic lethal and causes NTDs with 87 % penetrance (Narisawa et al., 2012), whereas hypomorphic *Gldc* mutation is not embryonic lethal and partially causes NTDs with 24 % penetrance (Pai et al., 2015). Interestingly, maternal formate supplementation rescues folate-resistant NTDs from the *Gldc* mutation. Details on *Mthfd2* and *Mthfd1l* KO mouse models will be explained in the following sections 1.3 and 1.4.

1.3. MITOCHONDRIAL 5,10-METHYLENE-THF DEHYDROGENASE/5,10-METHENYL-THF CYCLOHYDROLASE ENZYMES, MTHFD2 AND MTHFD2L

1.3.1. Enzymatic Properties

MTHFD2 and MTHFD2L are homologous enzymes, responsible for mitochondrial 5,10-methylene-THF oxidation to 10-formyl-THF. MTHFD2 was initially discovered in 1960 (Scrimgeour & Huennekens, 1960) and identified in 1985 as an NAD^+-dependent 5,10-methylene-THF dehydrogenase (Mejia & MacKenzie, 1985). Upon purification, this protein was found to be a bifunctional enzyme, also possessing 5,10-methenyl-THF cyclohydrolase activity (Mejia, Rios-Orlandi, & MacKenzie, 1986). The enzyme channels 5,10-methenyl-THF from the dehydrogenase to cyclohydrolase with 50-60 % efficiency (Pawelek & MacKenzie, 1998). The dehydrogenase activity of MTHFD2 is widely considered to be NAD^+-dependent, requiring Mg^{2+} and P_i. The MTHFD2 gene is expressed

throughout embryo development, but its expression declines dramatically as the embryo approaches birth (Erminia Di Pietro, Wang, & MacKenzie, 2004). The MTHFD2 transcript is absent from most adult tissues with exception of testis and spleen (Shin et al., 2014).

In 2011, my lab reported the discovery of a new mammalian mitochondrial methylene-THF dehydrogenase, termed MTHFD2L (Bolusani et al., 2011). Amino acid sequence of MTHFD2L is homologous to MTHFD2 (60-65 % sequence identity). In the study, crude rat MTHFD2L expressed in yeast exhibits $NADP^+$-dependent methylene-THF dehydrogenase activity (Bolusani et al., 2011). However, the enzyme was not purified in that study, and it could not be determined whether MTHFD2L was bifunctional because methenyl-THF cyclohydrolase assays are unreliable in crude extracts. The transcript for the MTHFD2L isozyme has low expression in early mouse embryos but begins to increase at embryonic day 10.5, remaining elevated through birth. *Mthfd2l* is also expressed in adult mitochondria, with the highest levels in brain and lung (Shin et al., 2014).

The existence of these two methylene-THF dehydrogenases (MTHFD2 and MTHFD2L) in mammalian mitochondria raises a question: Do the two enzymes differ in their catalytic activity or in their substrate or cofactor specificity? Chapter 2 will describe enzymatic characterization of MTHFD2 and MTHFD2L including their bifunctional dehydrogenase/cycohydrolase activities and redox cofactor specificities.

1.3.2. Human Studies

MTHFD2 is the most differentially expressed metabolic enzyme in cancer versus normal cells, including acute myeloid leukemia, breast cancer, lung cancer and liver cancer (Koufaris et al., 2016; Lehtinen et al., 2013; F. Liu et al., 2014; Moran et al., 2014; Nilsson

et al., 2014; Pikman et al., 2016). Nilsson et al. compared mRNA profiles of more than 1,000 metabolic enzymes in tumors spanning 19 cancer types, and discovered that the highest scoring pathway is mitochondrial 1C metabolism centered on MTHFD2. Especially, MTHFD2 gene expression was correlated with poor survival in breast cancer (Nilsson et al., 2014). Although the cellular functions of MTHFD2 in cancer cells have not been well-defined, it has been suggested that MTHFD2 may be associated with migration and epithelial-to-mesenchymal transition progression in cancer cells and connected with metastatic disease (Lehtinen et al., 2013; X. Liu et al., 2016).

Partly due to its more recent discovery, there are few human studies of MTHFD2L to date. MTHFD2L was highly associated with cardiovascular risk in Northern Finland Birth Cohort (Marttinen et al., 2014). Kennedy et al. reported that the MTHFD2L gene was highly associated with cytokine secretion stimulated by smallpox vaccine, suggesting a possibility of its involvement in immune responses in adults (Kennedy et al., 2012). Interestingly, activation of $CD4^+$ T cells (mature T-helper cells) derived from a mouse spleen induced 7-fold higher expression of MTHFD2L protein along with elevation of other enzymes in the mitochondrial 1C metabolism (Ron-Harel et al., 2016). This further supports the potential role of MTHFD2L in the adult immune response.

1.3.3. Animal Model

Homozygous deletion of *Mthfd2* in mice was first reported in 2002 (E. Di Pietro, Sirois, Tremblay, & MacKenzie, 2002). MTHFD2 homozygous null embryos die in utero by embryonic day (E) 15.5. These mutant embryos exhibit no obvious developmental defects, but are smaller and paler than wild-type littermates, a property attributed to defective hematopoiesis (Figure 1.3). Compared to other animal models in 1C metabolism

having NTDs such as *Folr1, Amt, Gldc*, and *Mthfd1l* KO mice, it was surprising that *Mthfd2* does not affect neural tube closure despite of its high expression in embryos. We now know that MTHFD2L is expressed in adults as well as embryos, supporting production of 10-formyl-THF and thus formate in mitochondria (Bolusani et al., 2011; Shin et al., 2014). The lack of developmental defects observed in *Mthfd2*-KO embryos may be due to compensation within the mitochondrial pathway from expression of MTHFD2L.

Figure 1.3 "Phenotypic comparison of E12.5 littermates from a mating between mice heterozygous for MTHFD2. A mutant embryo is shown on the right, and a wild-type embryo is shown on the left. The mutant embryo appears to be developmentally normal in comparison with its littermate except for its paleness and smaller size."(E. Di Pietro et al., 2002)

1.4. MITOCHONDRIAL 10-FORMYL-THF SYNTHETASE, MTHFD1L

1.4.1. Enzymatic Properties

MTHFD1L, mitochondrial 10-formyl-THF synthetase, is a mono-functional enzyme catalyzing the final step in the mammalian mitochondrial pathway to formate. A gene encoding MTHFD1L with high similarity to human cytoplasmic C_1-THF synthase, was first identified from human uterine RNA in 2003 (Prasannan, Pike, Peng, Shane, & Appling, 2003). This gene spans 236 kilobase pairs on chromosome 6 at 6q25.2 and

consists of 28 exons plus one alternative exon, encoding a protein of 978 amino acids. Enzymatic characterization of purified MTHFD1L revealed that the protein exists as a homodimer and possesses only 10-formyl-THF synthetase activity (Walkup & Appling, 2005).

Interestingly, despite possessing an N-terminal domain homologous to the 5,10-methylene-THF dehydrogenase/5,10-methenyl-THF cyclohydrolase domain of cytoplasmic C_1-THF synthase, these enzyme activities are not detected in MTHFD1L (Karen E. Christensen, Patel, et al., 2005; Walkup & Appling, 2005). Christensen et al. noted that several residues in the N-terminal domain involved in $NAD(P)^+$ cofactor binding or critical 5,10-methenyl-THF cyclohydrolase function are substituted, explaining the loss of dehydrogenase and cyclohydrolase activities in this domain (Christensen, Patel, et al., 2005).

The MTHFD1L gene is expressed in most human tissues, including adults and embryos. In adults, the gene is highly expressed in placenta, thymus, and brain, while expression is low in liver, skeletal muscle, and heart (Prasannan et al., 2003). The MTHFD1L transcript is also detected at all stages of mouse embryogenesis throughout the embryo, but with localized regions of higher expression such as the neural tube, the developing forebrain and midbrain, the craniofacial region, somites, and limb buds (Pike et al., 2010).

1.4.2. Human Studies

Three polymorphisms (rs3832406, rs6922269, and rs11754661) of MTHFD1L are known to be strongly associated with human diseases including NTDs, coronary heart diseases, and Alzheimer disease. A common deletion/insertion polymorphism,

rs3832406, is statistically associated with NTD risk in the Irish population (Parle-McDermott et al., 2009). This polymorphism possesses three alleles with varying numbers of ATT repeats (7 to 9) and influences splicing efficiency of the alternate MTHFD1L mRNA transcripts. Allele 1 with seven ATT repeats is the risk allele for NTDs and associated with the highest expression of the long transcript (thus potentially more functional mitochondrial 10-formyl-THF synthetase activity). However, it is unclear why increased expression of the full-length transcript increases NTD risk.

A polymorphism in MTHFD1L [rs6922269 (G>A) variant] has been implicated in risk for coronary heart disease (Angelakopoulou et al., 2012; Franceschini et al., 2011; Hubacek et al., 2015; Morgan et al., 2011; B. R. Palmer et al., 2014; Saade et al., 2011). This polymorphism was strongly associated with cardiovascular mortality in patients after acute coronary syndrome. Hyperhomocysteinemia is a risk factor for coronary heart diseases, and folate is well known to be the most important determinant to control plasma homocysteine level (Ward, 2001). It has been shown to significantly lower homocysteine concentration when administered at doses ranging from 0.2 to 10 mg daily. Based on the finding that mitochondrial formate provides at least 75 % of the 1C units entering the methyl cycle (conversion of homocysteine to methionine) (Pike et al., 2010), it is expected that MTHFD1L may be critical for homocysteine regulation and thus prevention of coronary heart disease.

Late-onset Alzheimer disease is a neurodegenerative disorder with memory and cognitive impairment, affecting more than 13 % of individuals aged 65 years and older (Naj et al., 2010). A common single nucleotide polymorphism rs11754661 in the MTHFD1L gene is significantly associated with late-onset Alzheimer disease (Ma et al., 2012; Naj et al., 2010; Ren et al., 2011). Naj et al. suggested a possible mechanism for the association of MTHFD1L in Alzheimer's disease (Naj et al., 2010): MTHFD1L catalyzes

an important step for homocysteine conversion to methionine. Dysfunction in MTHFD1L may cause hyperhomocysteinemia, a risk factor for the disease, and it may influence by causing vascular alterations and cholinergic deficit. Decreased expression of MTHFD1L in the hippocampus and increased homocysteic acid level in a mouse model of Alzheimer disease also support the hypothesis (Hasegawa, Mikoda, Kitazawa, & LaFerla, 2010; Martin et al., 2008).

1.4.3. Animal Models

A mouse model with homozygous deletion of *Mthfd1l* was firstly reported in 2013 (Momb et al., 2013). The *Mthfd1l* knockout mouse embryos show NTDs with 100 % penetrance, and the mutation causes embryonic lethality with death occurring around embryonic day 12.5 (Figure 1.4). The NTD phenotype of *Mhfd1l* null embryos is variable including craniorachischisis, exencephaly, and wavy neural tube. Deletion of *Mthfd1l* also triggers orofacial defects where the maxillary and mandibular processes are immature. The incidence of NTDs decreases with maternal supplementation with formate, and growth delay also is partially improved. However, folinic acid supplementation does not prevent the NTDs, suggesting that loss of MTHFD1L causes folate-resistant NTDs.

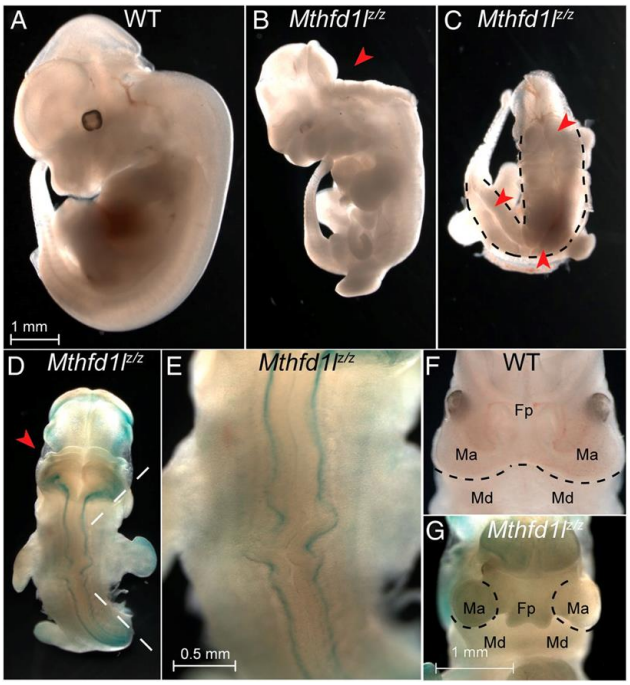

Figure 1.4 Neural tube defects and orofacial defects in *Mthfd1l*$^{z/z}$ embryos. "Compared with WT E12.5 embryos (A), E12.5 *Mthfd1l*$^{z/z}$ embryos (B-E) exhibit a spectrum of neural tube defects including exencephaly (B, red arrowhead). (C) Embryo with completely open neural folds (craniorachischisis) is indicated by the dashed lines. Note that the embryo curves to the left so the entire open neural tube is visible (red arrowheads). (D) Embryo with exencephaly (red arrowhead) and a wavy neural tube. (F) WT, 51-somite embryo showing normal facial development. (G) Same Mthfd1lz/z embryo (51 somites) imaged (D and E) displaying facial defects." (Momb et al., 2013)

Interestingly, Sudiwala et al. reported that MTHFD1L expression is significantly reduced in the curly tail mouse model known to develop folate-resistant NTDs (Sudiwala et al., 2016). Like the *Mthfd1l* knockout mouse model, maternal supplementation with formate prevents NTDs in the curly tail embryos and also increases litter size. How does formate prevent NTDs in the curly tail mouse? Although the reason for low expression of MTHFD1L in this mouse model is still unclear, the authors hypothesized that mitochondrial formate produced by MTHFD1L can provide 1C units for nucleotides

biosynthesis, resulting in stimulation of proliferation and normalization of growth imbalance in the mouse embryos.

Despite the clear association of MTHFD1L and folate-mediated 1C metabolism with NTDs, how folate and 1C metabolism contribute to normal NTC to prevent NTDs is not well known. The *Mthfd1l* KO mouse model is useful for elucidating roles of folate and 1C metabolism on NTC because: 1) MTHFD1L is a key enzyme in 1C metabolism for the provision of formate; 2) *Mthfd1l* KO mouse model develops fully penetrant NTDs which does not require feeding a folate-deficient diet to cause this phenotype; and 3) NTDs caused by *Mthfd1l* mutation are folate-resistant, and representative of folic acid-resistant NTDs.

1.5. OBJECTIVES

MTHFD2 and MTHFD2L are homologous enzymes, responsible for mitochondrial 5,10-methylene-THF oxidation to 10-formyl-THF. The experiments described in this dissertation were designed to determine if MTHFD2L possesses 5,10-methenyl-THF cyclohydrolase activity. This discovery would fill the remaining gap in the adult mammalian 1C metabolic pathway. I also examine the redox cofactor specificity of the dehydrogenase reaction of MTHFD2L, the differences in catalytic activity between MTHFD2 and MTHFD2L, and investigate potential reasons why mammals have these two isozymes in their mitochondrial pathway. Chapter 2 describes the enzymatic characterization of MTHFD2L including its bifunctional dehydrogenase/cycohydrolase activities and comparison of catalytic activities of the two isozymes, MTHFD2 and MTHFD2L, focusing on redox cofactor specificity.

MTHFD1L, mitochondrial 10-formyl-THF synthetase, is a mono-functional enzyme catalyzing the final step in the mammalian mitochondrial pathway to formate. The

Mthfd1l knockout mouse embryos show NTDs with 100 % penetrance. The incidence of NTDs decreases with maternal supplementation with formate, and growth delay also is partially improved. However, despite the clear association of MTHFD1L and folate-mediated 1C metabolism with NTDs, the mechanism by which folate and 1C metabolism contribute to normal NTC to prevent NTDs is not well understood. Chapter 3 identifies cellular processes regulated by MTHFD1L and mitochondrial 1C metabolism and demonstrates a role for formate supplementation during embryonic development.

Chapter 2. Mammalian Mitochondrial MTHFD2 and MTHFD2L Are Dual Redox Cofactor-specific Methylenetetrahydrofolate Dehydrogenase/Methenyltetrahydrofolate Cyclohydrolase Enzymes

2.1. INTRODUCTION

One-carbon (1C) metabolism is a universal folate-dependent metabolic pathway to generate one-carbon units for supporting de novo purine and thymidylate synthesis, interconversion of several amino acids, production of universal methyl donors, and regeneration of redox cofactors. Due to its essential roles in physiological processes, interest in recent years has been growing in the area of human health and diseases including fetal development, autoimmune disorders, cardiovascular disease, and cancer (Ducker & Rabinowitz, 2016; Momb et al., 2013; Pincus, Yazici, Sokka, Aletaha, & Smolen, 2003; Selhub, 2002)[1].

1C metabolism is highly compartmentalized in eukaryotes, and mitochondria play a critical role in cellular 1C metabolism by providing formate as a 1C unit for use in nucleic acid synthesis or homocysteine remethylation and regulating redox state (Momb & Appling, 2014). The 1C unit interconverting activities in mammalian mitochondria are catalyzed by three distinct MTHFD (methylenetetrahydrofolate dehydrogenase) enzymes; MTHFD1L, MTHFD2, and MTHFD2L (Figure 1.2) (Tibbetts & Appling, 2010). These enzymes are isozymes of the cytoplasmic MTHFD1 protein which is a trifunctional enzyme possessing 10-formyl-tetrahydrofolate (10-CHO-THF) synthetase, 5,10-methenyl-THF (CH^+-THF) cyclohydrolase, and 5,10-methylene-THF (CH_2-THF) dehydrogenase activities. MTHFD1L (mitochondrial 10-CHO-THF synthetase) catalyzes the final step in

[1] Portions of this work have been previously published (Shin, M, Bryant, JD, Momb, J, Appling DR (2014) J. Biol. Chem. 289 (22): 15507-15517). These sections will be indicated by quotation marks and additional indentation. For the paper, I designed and conducted research, analyzed data, and wrote the paper.

the mitochondrial pathway to produce formate, thus controlling the flux of 1C units from mitochondria into cytoplasmic processes.

The mitochondrial 5,10-methylene (CH_2)-THF dehydrogenase reaction is catalyzed by two homologous enzymes, MTHFD2 and MTHD2L. MTHFD2 was first discovered in 1960 (Scrimgeour & Huennekens, 1960) and identified in 1985 as an NAD^+-dependent 5,10-CH_2-THF dehydrogenase (Mejia & MacKenzie, 1985). This enzyme is known to be a bifunctional enzyme, also possessing 5,10-methyenyl (CH^+)-THF cyclohydrolase activity (Mejia et al., 1986). Interestingly, the *Mthfd2* gene is expressed only in transformed mammalian cells and in embryos, but not in adult mammalian tissues except for nondifferentiated adult tissues (Mejia & MacKenzie, 1985; Shin et al., 2014).

In 2011, a new mammalian mitochondrial 5,10-CH_2-THF dehydrogenase, termed MTHFD2L (MTHFD2-Like), was discovered in my lab (Bolusani et al., 2011). MTHFD2L is homologous to MTHFD2, sharing 60-65 % amino acid sequence identity among various mammals. However, it was not known if MTHFD2L is also bifunctional possessing 5,10-CH^+-THF cyclohydrolase activity. In addition, the redox cofactor specificity of the MTHFD2L enzyme had not been studied. The *Mthfd2l* gene is expressed in adult mitochondria (with high expression levels in brain and lung) and, also, at all stages of embryogenesis (Bolusani et al., 2011; Shin et al., 2014). The *Mthfd2l* expression was low at mouse embryonic day 8.5, but increased beginning at embryonic day 10.5, suggesting a switch between MTHFD2 and MTHFD2L expression at embryonic days 8.5 – 10.5 during mouse embryogenesis (Shin et al., 2014).

The tetrahydrofolates are composed of a fully reduced pterin ring, a p-aminobenzoyl group, and a polyglutamate peptide containing up to 9 glutamate residues linked by unusual γ-peptide linkages (Fox & Stover, 2008). Monoglutamylated THF is transported into mitochondria and converted to polyglutamylated THF to be retained in

mitochondria (Fox & Stover, 2008). Folylpolyglutamate specificity is one of the characteristic features of enzymes in the one-carbon metabolism (Schirch & Strong, 1989). In mammals, serum folates contain a single glutamate residue, whereas intracellular folates contain a polyglutamate residue (usually 5-8 glutamate residues) (Ross, Green, Baugh, MacKenzie, & Matthews, 1984). The polyglutamyl folates, which are physiologically active, affect transport properties of the folate derivatives, kinetic properties of enzymes in one-carbon metabolism, channeling efficiency between the enzymes, and regulation of metabolism (Schirch & Strong, 1989). Many enzymes in the 1C metabolism have a strong preference for polyglutamylated forms of THF, with increasing catalytic efficiency upon polyglutamylation. In the case of MTHFD2, it was reported by Mejia et al. (Mejia et al., 1986) that the enzyme showed greater specificity for the longer polyglutamylated derivatives than MTHFD1. However, specificity for the polyglutamyl folates of $NADP^+$-dependent activity of MTHFD2 as well as MTHFD2L is still unknown.

The existence of these two CH_2-THF dehydrogenases (MTHFD2 and MTHFD2L) in mammalian mitochondria raises several questions. Does MTHFD2L possess bifunctional activities of 5,10-CH_2-THF dehydrogenase and 5,10-CH^+-THF cyclohydrolase, like MTHFD2? What is its substrate or cofactor specificity? Do the two enzymes differ in their catalytic activity? And why do mammals have two isozymes in mitochondria? To answer these questions, I purified rat MTHFD2L and characterized enzymatic properties of MTHFD2L. Also, I compared enzymatic characteristics of MTHFD2 and MTHFD2L isozymes, focusing on their redox cofactor specificities using mono- and polyglutamylated CH_2-THF. Finally, I examined the evolutionary relationship between MTHFD2 and MTHFD2L.

Portions of this work have been previously published (Shin, M, Bryant, JD, Momb, J, Appling DR (2014) J. Biol. Chem. 289 (22): 15507-15517) (Shin et al., 2014). These sections will be indicated by quotation marks and additional indentation.

2.2. MATERIALS AND METHODS

2.2.1. Chemicals and Reagents

"All reagents were of the highest commercial grade available. NAD^+ and $NADP^+$ were purchased from US Biological (Swampscott, MA) and Sigma (St. Louis, MO), respectively. Tetrahydrofolate (THF) was prepared by the hydrogenation of folic acid (Sigma) using platinum oxide as a catalyst and purification of the THF product on a DEAE cellulose column (Sigma) (Blakley, 1957; Curthoys & Rabinowitz, 1971). CH_2-THF was prepared nonenzymatically from THF and formaldehyde (Fisher, Waltham, MA) (Appling & West, 1997). The yield of CH_2-THF was determined by solving the equilibria of THF, formaldehyde and β-mercaptoethanol (Kallen & Jencks, 1966). The preparation of CH^+-THF from 5-CHO-THF (MP Biomedicals, Solon, OH) was conducted as previously described (Walkup & Appling, 2005). Oligonucleotide primers were obtained from IDT (Coralville, IA). Tetrahydropteroylpentaglutamate ($H_4PteGlu_5$) was prepared by a modified $NaBH_4$ reduction from the corresponding pteroylpentaglutamate ($PteGlu_5$) (Schircks Laboratories, Jona, Switzerland), as previously described (Suliman, Sawyer, Appling, & Robertus, 2005). Further preparation of 5,10-CH_2-$H_4PteGlu_5$ was accomplished by incubating with formaldehyde as previously described (Appling & West, 1997)."

2.2.2. Cloning of Rat MTHFD2L

″RNA isolation and cDNA construction of rat MTHFD2L were conducted as previously described (Bolusani et al., 2011). Removal of the mitochondrial targeting sequence from the full-length rat MTHFD2L cDNA was accomplished by PCR-amplification using primers rMTHFD2LΔ1-40_forward (5'-GTCATCACCATCACCATCACGGATCCATGGCGACGCGGGCC-3' and rMTHFD2LΔ1-40_reverse (5'-ACCTTAGCGGCCGCAGATCTGGTACCCTAGTAGGTGATATTCT-3') (start codon in bold; underlined portions complementary to the rat MTHFD2L cDNA). The mitochondrial targeting sequence (amino acids 1-40) was predicted by MitoProt (Claros & Vincens, 1996). The resulting PCR-amplified fragment was cloned into the pET22b vector (Novagen, EMD Biosciences). The pET22b-rMTHFD2LΔ1-40 was further subcloned into a YEp24-based yeast expression vector containing the *Saccharomyces cerevisiae* MET6 promoter using sequence- and ligation-independent cloning (M. Z. Li & Elledge, 2007; Suliman et al., 2005). The YEp24 vector was modified to include a multiple cloning site and N-terminal His6 tag (Bolusani et al., 2011). This construct (YEp24-rMTHFD2LΔ1-40) should produce a protein of 307 residues (N-terminal Met + 2 Gly + 6 His + 298 MTHFD2L residues) with a calculated molecular mass of 33,180 kDa."

2.2.3. Expression and Purification of MTHFD2L

″The YEp24-rMTHFD2LΔ1-40 construct was transformed into yeast strain MWY4.4 (ser1 ura3-52 trp1 his4 leu2 ade3-65 Δmtd1) using a high efficiency lithium acetate yeast transformation procedure (Gietz & Woods, 2002; West,

Barlowe, & Appling, 1993). Transformed cells were grown in synthetic minimal medium (YMD) containing 0.7 % (w/v) yeast nitrogen base without amino acids (Difco Bacto) and 2 % (w/v) glucose, supplemented with L-serine (375 mg/L), L-tryptophan (20 mg/L), L-histidine (20 mg/L), L-leucine (30 mg/L), and adenine (20 mg/L). Cultures were grown at 30°C in a rotary shaker at 200 rpm and were harvested at 3-4 OD600 by centrifugation at 8,000 x g for 5 min at 4°C. The cell pellet was suspended in 2 ml of 25 mM Tris-Cl (pH 7.5) containing 1 % (w/v) sodium carbonate, 10 mM β-mercaptoethanol, and 1 mM phenylmethanesulfonylfluoride (PMSF) per gram wet weight. The suspended cells were disrupted with glass beads using a FastPrep FP120 cell disrupter (MP Biomedicals, Solon, OH), followed by incubation for 30 min at 4°C to facilitate dissociation of MTHFD2L from cellular membranes. Cell debris was removed by centrifuging at 30,000 x g for 30 min at 4°C. The extracted MTHFD2L protein was then dialyzed at 4°C overnight against 25 mM Tris-Cl, 10 mM β-mercaptoethanol, 1 mM PMSF, 20 % (v/v) glycerol and 500 mM KCl at pH 8.5. Concentrated cell lysate (~15 ml) was added to 9 ml of Ni^{2+}-charged His-Bind resin (Novagen, Darmstadt, Germany) in 15 ml of binding buffer (final concentration: 25 mM Tris-Cl, 10 mM β-mercaptoethanol, 1 mM PMSF, 20% (v/v) glycerol, 500 mM KCl, and 20 mM imidazole at pH 8.5). The slurry was mixed for 3 h at 4°C, and then packed into a column. The column was washed at room temperature with 40 column volumes of wash buffer containing 25 mM Tris-Cl, 10 mM β-mercaptoethanol, 1 mM PMSF, 500 mM KCl, 10% (v/v) isopropanol, and 60 mM imidazole (pH 8.5) at a flow rate of 2-3 ml/min. His-tagged MTHFD2L was eluted at 4°C at 0.5-1 ml/min with binding buffer containing 250 mM imidazole. Fractions containing active enzyme were determined by assaying for CH_2-THF dehydrogenase activity (see below) and protein concentration was determined using

Bio-Rad Protein Assay reagent (Bio-Rad, Hercules, CA). Purified MTHFD2L was stored at -20 °C in 25 mM Tris-Cl, 10 mM β-mercaptoethanol, 100 mM KCl, and 50% (v/v) glycerol at a final pH of 7.5. Purity of enzyme preparations was evaluated by SDS-PAGE. Enzyme stability was confirmed by assaying 5,10-CH_2-THF dehydrogenase activity in aliquots of stored enzyme over a 1-week period. Purified enzyme retained approximately 75% 5,10-CH_2-THF dehydrogenase activity after one-week of storage, and all kinetic analyses were performed within 1 week of enzyme purification."

2.2.4. 5,10-Methylene-THF Dehydrogenase and 5,10-Methenyl-THF Cyclohydrolase Assays

"A microplate assay was used for determination of kinetic parameters as previously described (Wagner, Breksa, Monzingo, Appling, & Robertus, 2005). 5,10-CH_2-THF dehydrogenase activity was determined by an endpoint assay (Walkup & Appling, 2005). Reaction buffer consisted of 50 mM HEPES (pH 8.0), 100 mM KCl, 5 mM $MgCl_2$, 0.4 mM CH_2-THF, 40 mM β-mercaptoethanol, and either NAD^+ (1 mM) or $NADP^+$ (6 mM). Potassium phosphate (25 mM) was also included for the NAD^+-dependent activity. To determine cofactor specificity of the MTHFD2L enzyme in conditions that more closely resemble physiological conditions, reaction buffer contained 50 mM HEPES (pH 8.0), 100 mM KCl, 0.5 mM $MgCl_2$, 10 mM potassium phosphate, 40 mM β-mercaptoethanol, and different cofactors including NAD^+ (0.2 mM) or $NADP^+$ (0.05 mM) and varying concentrations of CH_2-THF. Sixty µl of reaction cocktail without CH_2-THF and 20 µl of purified MTHFD2L were mixed and the enzyme reaction was initiated by addition of 20 µl of CH_2-THF, followed by incubation at 30°C for 5 min. The

reaction was quenched with 200 µl of 3% perchloric acid, and the plate was read at 350 nm on Infinite M200 (Tecan, Männedorf, Switzerland). Pathlength was corrected using near infra-red measurements (K. F. Palmer & Williams, 1974).

CH^+-THF cyclohydrolase activity was determined by a continuous assay (Barlowe & Appling, 1990) in microplate format. Enzyme reaction was incubated at 30°C with MTHFD2L containing 200 mM potassium maleate (pH 7.4), 20 mM β-mercaptoethanol, and varying concentrations of CH^+-THF. Activity was monitored by observing the decrease in absorbance of CH^+-THF at 355 nm.

For the determination of kinetic parameters, initial rate data was fitted to the Michaelis-Menten equation by non-linear regression using Prism (GraphPad, La Jolla, CA). Inhibition of $NADP^+$-dependent dehydrogenase activity by phosphate ion was examined by assays at four fixed phosphate ion concentrations at varying concentrations of $NADP^+$. Over the 5 minute period of measurement, 20% or less of the substrate was converted to product, ensuring that initial rates were observed. K_i was calculated from a global fit of the data to a competitive inhibition model using Prism."

2.2.5. Sequence Alignment

MTHFD2, MTHFD2L, MTHFD1 and MTHFD1L sequences for representative eukaryotic species were retrieved using HomoloGene (NCBI Resource Coordinators, 2015). HomoloGene is an automated system for constructing putative homology groups among the genes of 21 completely sequenced eukaryotic genomes including human, chimpanzee, mouse, rat, chicken, frog, zebrafish, insects, plants and fungi (Bettembourg, Diot, & Dameron, 2015; Z. Zhang, Hailat, Falk, & Chen, 2014). The amino acid sequences

were subjected to multiple sequence alignment using Clustal Omega (Sievers et al., 2011). The sequences of MTHFD1 and MTHFD1L were used for phylogenetic analyses.

2.2.6. Preparation of Human MTHFD2

Purified human MTHFD2 was a gift from Dr. Vipin Suri (Raze Therapeutics). Briefly, 6x histidine-tagged human MTHFD2 was expressed in *Escherichia coli* and purified using size exclusion chromatography. The resulting protein corresponded to a molecular weight of 36.7 kDa with the tag.

2.2.7. Phylogenetic Analysis

MTHFD2 and MTHFD2L sequences from different species were subjected to phylogenetic analysis using Phylogeny.fr (http://www.phylogeny.fr/). The portal enables alignment by MUSCLE, curation by Gblocks, phylogeny by PhyML, and tree rendering by TreeDyn to reconstruct a robust phylogenetic tree from a set of sequences (Dereeper et al., 2008). To identify origin of the enzymes during evolution, a phylogenetic tree was constructed for eukaryotic MTHFD2, MTHFD2L, MTHFD1 and MTHFD1L sequences. Genetic distance was evaluated by MEGA v7.0 (Kumar, Stecher, & Tamura, 2016).

2.3. RESULTS

2.3.1. Expression and Purification of Rat MTHFD2L

"Initial characterization of mammalian MTHFD2L relied on the recombinant full-length rat protein expressed in yeast crude extracts. Difficulties in purification, likely due to its tight association with membranes (Bolusani et al., 2011), prevented

from conducting a full enzymatic characterization of MTHFD2L in that study. In the present study, I overcame these problems using several strategies. To increase the yield of recombinant protein, I replaced the mitochondrial targeting sequence of the rat MTHFD2L with an N-terminal His tag for localization in the yeast cytosol (L. Zhang, Joshi, & Smith, 2003). Despite loss of its targeting sequence, the protein remained associated with cellular membranes, so I included sodium carbonate in the extraction buffer to release MTHFD2L from membranes (Prasannan et al., 2003). Finally, I washed the Ni^{2+}-column at room-temperature rather than 4°C to eliminate contamination from endogenous yeast proteins (Dihazi, Kessler, & Eschrich, 2001). This washing step allowed purification of MTHFD2L to greater than 95% homogeneity (Figure 2.1; cf. lanes 1 and 3). The mobility of the purified protein is consistent with the expected size of 33 KDa."

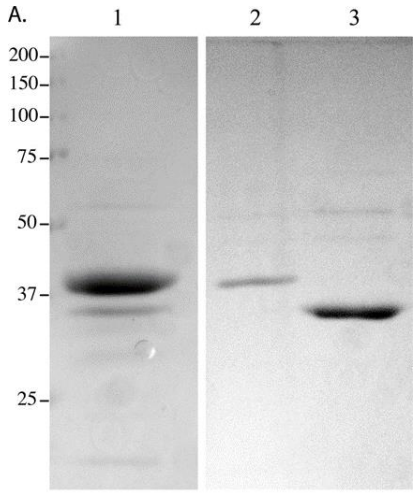

Figure 2.1 Purification of rat MTHFD2L. "6x His-tagged rat MTHFD2L was purified by immobilized nickel affinity chromatography as described under Materials and Methods. Lane 1 shows the imidazole elution after washing the column at 4 ºC. In a second experiment, the column was washed at room temperature instead of 4 ºC. Lane 2 shows the room temperature wash fractions. Lane 3 shows the imidazole elution after washing at room temperature." (Shin et al., 2014)

2.3.2. MTHFD2L Possesses 5,10-Methenyl-THF Cyclohydrolase Activity

"MTHFD2L exhibits robust CH^+-THF cyclohydrolase activity, confirming the bifunctional nature of this enzyme. The specific activity shown in Figure 2.2 is approximately 11-fold higher than the buffer-catalyzed rate. Cyclohydrolase activity could not be determined at saturating conditions due to the high absorbance of substrate, thus accurate values for k_{cat} and K_M could not be calculated."

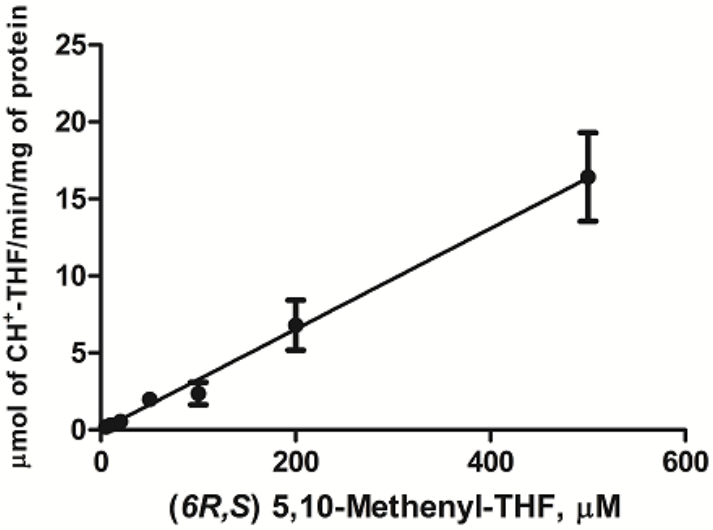

Figure 2.2 5,10-Methenyl-THF cyclohydrolase activity of MTHFD2L. "Results shown are the means ± S.E. of fie replicates (error bars are included for all data points but are obscured by the data symbol when the scatter is small)." (Shin et al., 2014)

2.3.3. Steady-state Kinetics and Cofactor Specificity of 5,10-Methylene-THF Dehydrogenase Activity of MTHFD2L

"It was previously reported that recombinant full-length rat MTHFD2L expressed in yeast exhibits $NADP^+$-dependent CH_2-THF dehydrogenase activity in

crude extracts (Bolusani et al., 2011). Purified MTHFD2L exhibited both NAD^+ and $NADP^+$-dependent CH_2-THF dehydrogenase activity using either mono- or penta-glutamylated CH_2-THF (CH_2-$H_4PteGlu_1$ and CH_2-$H_4PteGlu_5$, respectively). Kinetic parameters are given in Table 2.1. Values for k_{cat} and K_M differed between the polyglutamylation states of the CH_2-THF substrate, but were not sensitive to the redox cofactor in the dehydrogenase reaction (NAD^+ or $NADP^+$). The K_M values for CH_2-$H_4PteGlu_5$ were approximately 3.5 times higher than those of CH_2-$H_4PteGlu_1$ regardless of redox cofactor. However, this was accompanied by a similar increase in k_{cat}, resulting in similar k_{cat}/K_M values (Table 2.1). Using CH_2-$H_4PteGlu_1$, the K_M values for NAD^+ and $NADP^+$ were 147 ± 16 μM and 537 ± 54 μM, respectively (Table 2.1).

Table 2.1 Kinetic parameters for MTHFD2L 5,10-methylene-THF dehydrogenase activity. "Enzyme assays were performed as described under Materials and Methods. CH_2-THF kinetic parameters were determined using saturating concentrations of NAD^+ (1.0 mM) or $NADP^+$ (6.0 mM). When NAD^+ was used, potassium phosphate (25 mM) and $MgCl_2$ (5 mM) were also included. Redox cofactor kinetic parameters were determined using saturating concentrations of CH_2-$H_4PteGlu_{1/5}$ (400 μM)." (Shin et al., 2014)

Substrate	**K_M (μM)**		**k_{cat} (s^{-1})**	**k_{cat}/K_m ($s^{-1}\mu M^{-1}$)**
	$NAD^+/NADP^+$	**CH_2THF**		
NAD^+	147 ± 16	-	3.6 ± 0.1	0.025
CH_2-$H_4PteGlu_1$	-	40 ± 5	2.7 ± 0.07	0.067
CH_2-$H_4PteGlu_5$	-	130 ± 30	8.8 ± 0.4	0.068
$NADP^+$	537 ± 54	-	1.1 ± 0.04	0.002
CH_2-$H_4PteGlu_1$	-	42 ± 7	1.3 ± 0.05	0.030
CH_2-$H_4PteGlu_5$	-	153 ± 39	7.2 ± 0.5	0.047

Although the dehydrogenase activity of the bifunctional MTHFD2 (an isozyme of MTHFD2L) is classified as NAD^+-specific, it can also utilize $NADP^+$ at a reduced efficiency (Yang & MacKenzie, 1993). The NAD^+-dependent activity of MTHFD2 requires Mg^{2+} and inorganic phosphate (P_i). To explore redox cofactor specificity in MTHFD2L, I measured specific activity using saturating levels of NAD^+ or $NADP^+$ in the presence of Mg^{2+} and/or P_i (Figure 2.3). When NAD^+ was used, the dehydrogenase activity of MTHFD2L was strongly dependent on the presence of Mg^{2+} and P_i in combination. Using CH_2-H_4PteGlu$_1$ and NAD^+, the K_M values for Mg^{2+} and P_i were 233 ± 62 μM and 293 ± 59 μM, respectively. When $NADP^+$ was used, MTHFD2L activity was increased slightly with Mg^{2+}. Inorganic phosphate appeared to counteract the Mg^{2+} effect with $NADP^+$ (Figure 2.3).

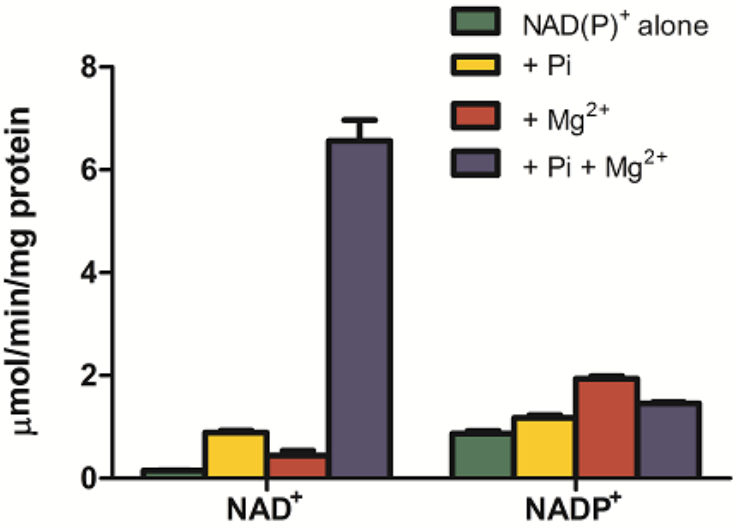

Figure 2.3 5,10-Methylene-THF dehydrogenase activity of MTHFD2L. "Purified MTHFD2L was assayed for NAD^+- and $NADP^+$-dependent 5,10-methylene-THF dehydrogenase activity in the presence or absence of P_i and Mg^{2+}. Enzyme activity is expressed as µmol product/min/mg of protein. Each column represents the mean ± S.E. of triplicate determinations. Reaction buffer contained 50 mM HEPES (pH 8.0), 100 mM KCl, 0.4 mM 5,10-CH_2-THF, and 40 mM β-mercaptoethanol. NAD^+ was used at 1.0 mM and $NADP^+$ at 6.0 mM. Mg^{2+} and P_i were tested by including 5.0 mM $MgCl_2$ and 25 mM potassium phosphate where indicated." (Shin et al., 2014)

Because MTHFD2 shows inhibition of $NADP^+$-dependent dehydrogenase activity by inorganic phosphate (Yang & MacKenzie, 1993), I sought to determine if MTHFD2L behaves in the same way. I observed that increasing concentrations of phosphate ion reduced the $NADP^+$-dependent dehydrogenase activity of MTHFD2L (Figure 2.4). The data fit best to a competitive inhibition model with a K_i of 1.9 ± 0.3 mM."

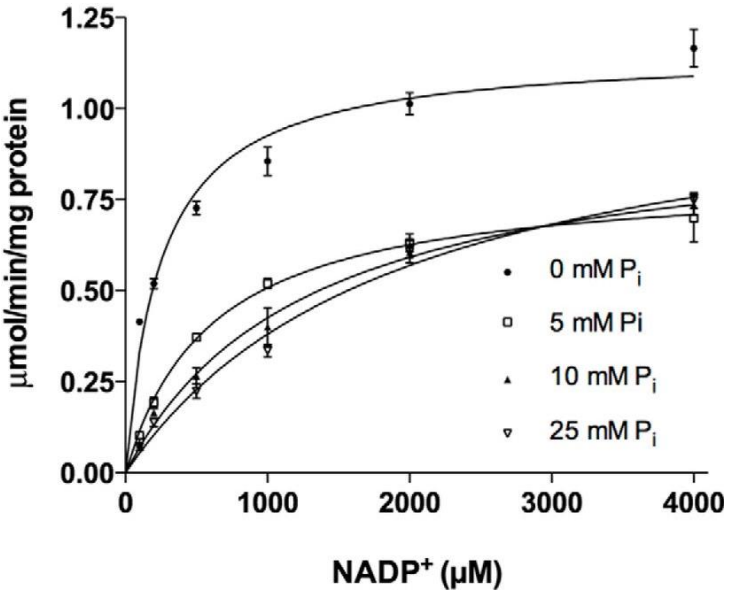

Figure 2.4 Competitive inhibition of $NADP^+$-dependent 5,10-methylene-THF dehydrogenase activity by inorganic phosphate. "Each point represents the mean ± S.E. of triplicate determinations (error bars are included for all data points but are obscured by the data symbol when the scatter is small). The curves represent nonlinear fits to the Michaelis-Menten model. The reaction buffer contained 5.0 mM $MgCl_2$ and varying concentrations of $NADP^+$. Potassium phosphate concentrations were 0 (●), 5 (□), 10 (▲), and 25 (▽) mM." (Shin et al., 2014)

2.3.4. Cofactor Specificity of MTHFD2L at Physiological Concentrations of Mg^{2+}, P_i and CH_2-THF

"To better understand the cofactor preference (NAD^+ vs. $NADP^+$) of the MTHFD2L dehydrogenase activity at physiologically relevant substrate conditions, I repeated the assay at a wide range of P_i, Mg^{2+}, and CH_2-THF concentrations. The range used includes concentrations estimated to exist in the matrix compartment of mammalian mitochondria: (CH_2-THF = 2.5 - 25 µM, Mg^{2+} = 0.5 mM, P_i = 10 mM; see legend to Figure 2.5 for references). For each component, the ratio of NAD^+-dependent to $NADP^+$-dependent dehydrogenase activities were plotted (Figure 2.5). The data indicate that there is an approximately 3.5-fold preference for NAD^+ at

physiological P_i concentrations (A in Figure 2.5) and a 5-6-fold preference for NAD^+ at physiological Mg^{2+} concentrations (B in Figure 2.5). At high concentrations of CH_2-THF, MTHFD2L clearly prefers NAD^+ (C in Figure 2.5). However, as the CH_2-THF concentration is lowered to more physiological levels, the ratio approaches 1, and at the lowest CH_2-THF concentrations, the enzyme is more active with $NADP^+$. This suggests that cofactor preference will be very sensitive to CH_2-THF concentration *in vivo*."

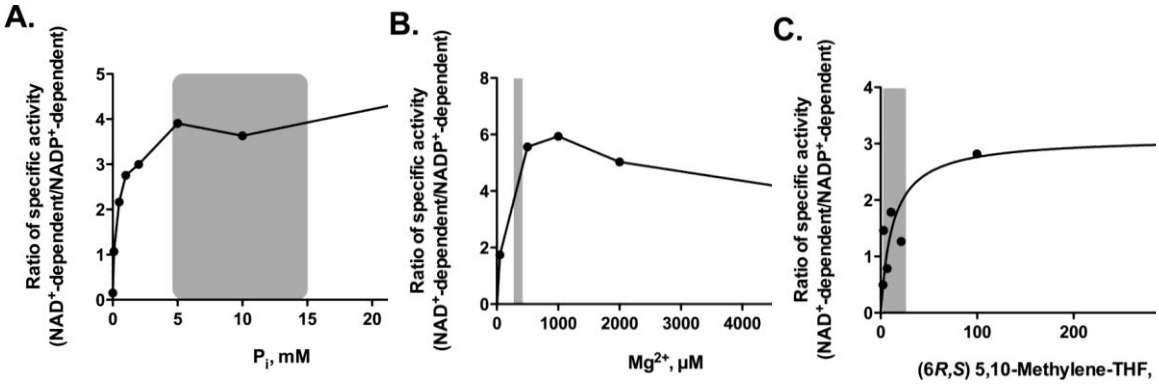

Figure 2.5 Redox cofactor specificity of MTHFD2L at physiological concentrations of P_i. "The ratio of NAD^+- to $NADP^+$-dependent 5,10-methylene-THF activity was plotted as a function of increasing concentrations of inorganic phosphate (A), Mg^{2+} (B), or 5,10-CH_2-THF (C). Reaction buffer contained either 1 mM NAD^+ or 6 mM $NADP^+$. 5,10-CH_2-THF was included at 0.4 mM (panels A and B), or varied (panel C). For dependence on P_i concentration (A), 5 mM $MgCl_2$ was included for both NAD^+- and $NADP^+$-dependent reactions. For dependence on Mg^{2+} concentration (B), 25 mM potassium phosphate was included in NAD^+-dependent, but not $NADP^+$-dependent reactions. For dependence on 5,10-CH_2-THF concentration, 5 mM $MgCl_2$ and 25 mM P_i were included in NAD^+-dependent reactions. For the $NADP^+$-dependent reactions, only 5 mM $MgCl_2$ was included. Reported mitochondrial matrix substrate concentration ranges (indicated by shaded boxes) are 5-15 mM for P_i (Albe, Butler, & Wright, 1990; Corkey, Duszynski, Rich, Matschinsky, & Williamson, 1986; Saleet Jafri & Kotulska, 2006), 0.3-0.4 mM for Mg^{2+} (Corkey et al., 1986; Saleet Jafri & Kotulska, 2006), and 2.5-25 µM for 5,10-CH_2THF (Eto & Krumdieck, 1982; Horne, Patterson, & Cook, 1989; Nijhout et al., 2006; Seither, Trent, Mikulecky, Rape, & Goldman, 1989), respectively. The best estimates found for in vivo mitochondrial $NADP^+$ and NAD^+ concentrations are $NADP^+$ = 80 µM and NAD^+ = 240 µM (Yang et al., 2007)." (Shin et al., 2014)

2.3.5. Cofactor Specificity of 5,10-Methylene-THF Dehydrogenase Activity of MTHFD2

Although the bifunctional MTHFD2 is well known as a NAD^+-dependent 5,10-CH_2-THF dehydrogenase, it also exhibits low 5,10-CH_2-THF dehydrogenase activity with $NADP^+$ (Yang & MacKenzie, 1993). It is not known whether the MTHFD2 isozyme might also exhibit dual redox cofactor specificity *in vivo*, as it was not characterized at physiologically relevant substrate concentrations. To understand redox cofactor specificity of MTHFD2 and MTHFD2L among different species, NAD(P) cofactor binding sequences in Rossman folds were compared by primary amino acid sequence alignment. Table 2.2 summarizes MTHFD2 and MTHFD2L genes from different species including human, chimpanzee, monkey, wolf, cow, mouse, rat, chicken, frog, zebrafish, fruit fly, and mosquito. Only MTHFD2 sequences, not MTHFD2L, are present in zebrafish, fruit fly, and mosquito. While most eukaryotes possess MTHFD1 (cytosolic trifunctional C_1-THF synthase) from human to fungi, either MTHFD2 or MTHFD2L sequence is not present in fungi, nematode, and plants.

Table 2.2 MTHFD (methylenetetrahydrofolate dehydrogenase) family enzymes, MTHFD1, MTHFD1L, MTHFD2, and MTHFD2L, in eukaryotes. The homologous sequences were derived from Homologene (http://www.ncbi.nlm.nih.gov/homologene).

<MTHFD1>

Common name	Species	Protein name	RefSeq ID_protein
Human	*Homo sapiens*	C-1-tetrahydrofolate synthase, cytoplasmic	NP_005947.3
Chimpanzee	*Pan troglodytes*	C-1-tetrahydrofolate synthase, cytoplasmic	XP_510001.3
Monkey	*Macaca mulatta*	C-1-tetrahydrofolate synthase, cytoplasmic	XP_001101708.2
Wolf	*Canis lupus*	C-1-tetrahydrofolate synthase, cytoplasmic	XP_537476.2
Cattle	*Bos taurus*	C-1-tetrahydrofolate synthase, cytoplasmic	NP_001076946.1
Mouse	*Mus musculus*	C-1-tetrahydrofolate synthase, cytoplasmic	NP_620084.2
Rat	*Rattus norvegicus*	C-1-tetrahydrofolate synthase, cytoplasmic	NP_071953.1
Chicken	*Gallus gallus*	C-1-tetrahydrofolate synthase, cytoplasmic	NP_001034392.1
Frog	*Xenopus tropicalis*	C-1-tetrahydrofolate synthase, cytoplasmic	NP_001008007.1
Zebrafish	*Danio rerio*	C-1-tetrahydrofolate synthase, cytoplasmic	NP_955823.1
Fruit fly	*Drosophila melanogaster*	pugilist, isoform B	NP_731489.2
Mosquito	*Anopheles gambiae*	AGAP002830-PA	XP_312083.5
Fungi	*Saccharomyces cerevisiae*	ADE3	NP_011720.3
Fungi	*Kluyveromyces lactis*	hypothetical protein	XP_454695.1
Fungi	*Eremothecium gossypii*	ACL121Cp	NP_983283.2
Fungi	*Schizosaccharomyces pombe*	C1-5,6,7,8-tetrahydrofolate (THF) synthase	NP_595256.1
Fungi	*Magnaporthe oryzae*	C-1-tetrahydrofolate synthase	XP_003717930.1
Fungi	*Neurospora crassa*	C-1-tetrahydrofolate synthase	XP_956550.1
Nematode	*Caenorhabditis elegans*	K07E3.4, isoform b	NP_509360.1
Plant	*Arabidopsis thaliana*	Formate--tetrahydrofolate ligase	NP_564571.1
Plant	*Oryza sativa*	Os09g0446800	NP_001063310.1

Table 2.2 Continued

<MTHFD1L>

Common name	Species	Protein name	RefSeq ID_protein
Human	*Homo sapiens*	monofunctional C1-tetrahydrofolate synthase, mitochondrial isoform 1 precursor	NP_001229696.1
Chimpanzee	*Pan troglodytes*	monofunctional C1-tetrahydrofolate synthase, mitochondrial isoform X2	XP_518807.3
Monkey	*Macaca mulatta*	monofunctional C1-tetrahydrofolate synthase, mitochondrial-like	XP_001098522.2
Wolf	*Canis lupus*	monofunctional C1-tetrahydrofolate synthase, mitochondrial	XP_533450.2
Cattle	*Bos taurus*	monofunctional C1-tetrahydrofolate synthase, mitochondrial precursor	NP_001069486.1
Mouse	*Mus musculus*	monofunctional C1-tetrahydrofolate synthase, mitochondrial precursor	NP_758512.3
Rat	*Rattus norvegicus*	monofunctional C1-tetrahydrofolate synthase, mitochondrial	NP_001101932.2
Chicken	*Gallus gallus*	monofunctional C1-tetrahydrofolate synthase, mitochondrial isoform X4	XP_004935675.1
Frog	*Xenopus tropicalis*	monofunctional C1-tetrahydrofolate synthase, mitochondrial	NP_001120171.1
Zebrafish	*Danio rerio*	monofunctional C1-tetrahydrofolate synthase, mitochondrial	NP_001229925.1

Table 2.2 Continued

<MTHFD2>

Common name	Species	Protein name	RefSeq ID_protein
Human	*Homo sapiens*	bifunctional methylenetetrahydrofolate dehydrogenase/cyclohydrolase, mitochondrial precursor	NP_006627.2
Chimpanzee	*Pan troglodytes*	bifunctional methylenetetrahydrofolate dehydrogenase/cyclohydrolase, mitochondrial	XP_001154612.1
Monkey	*Macaca mulatta*	-	-
Wolf	*Canis lupus*	bifunctional methylenetetrahydrofolate dehydrogenase/cyclohydrolase, mitochondrial	XP_005630608.1
Cattle	*Bos taurus*	bifunctional methylenetetrahydrofolate dehydrogenase/cyclohydrolase, mitochondrial	NP_001069223.1
Mouse	*Mus musculus*	bifunctional methylenetetrahydrofolate dehydrogenase/cyclohydrolase, mitochondrial precursor	NP_032664.1
Rat	*Rattus norvegicus*	bifunctional methylenetetrahydrofolate dehydrogenase/cyclohydrolase, mitochondrial	NP_001102868.1
Chicken	*Gallus gallus*	bifunctional methylenetetrahydrofolate dehydrogenase/cyclohydrolase, mitochondrial	NP_001026531.1
Frog	*Xenopus tropicalis*	bifunctional methylenetetrahydrofolate dehydrogenase/cyclohydrolase, mitochondrial precursor	NP_001123716.1
Zebrafish	*Danio rerio*	bifunctional methylenetetrahydrofolate dehydrogenase/cyclohydrolase, mitochondrial	NP_001002181.1
Fruit fly	*Drosophila melanogaster*	NAD-dependent methylenetetrahydrofolate dehydrogenase, isoform B	NP_476929.1
Mosquito	*Anopheles gambiae*	AGAP004677-PA	XP_001687783.1

Table 2.2 Continued

<MTHFD2L>

Common name	Species	Protein name	RefSeq ID_protein
Human	*Homo sapiens*	probable bifunctional methylenetetrahydrofolate dehydrogenase/cyclohydrolase 2	NP_001138450.1
Chimpanzee	*Pan troglodytes*	probable bifunctional methylenetetrahydrofolate dehydrogenase/cyclohydrolase 2	XP_517226.3
Monkey	*Macaca mulatta*	probable bifunctional methylenetetrahydrofolate dehydrogenase/cyclohydrolase 2-like	XP_001091218.2
Wolf	*Canis lupus*	probable bifunctional methylenetetrahydrofolate dehydrogenase/cyclohydrolase 2	XP_005628393.1
Cattle	*Bos taurus*	probable bifunctional methylenetetrahydrofolate dehydrogenase/cyclohydrolase 2	NP_001193024.1
Mouse	*Mus musculus*	probable bifunctional methylenetetrahydrofolate dehydrogenase/cyclohydrolase 2	NP_081064.1
Rat	*Rattus norvegicus*	probable bifunctional methylenetetrahydrofolate dehydrogenase/cyclohydrolase 2	NP_001100681.1
Chicken	*Gallus gallus*	probable bifunctional methylenetetrahydrofolate dehydrogenase/cyclohydrolase 2 isoform X1	XP_001233663.3
Frog	*Xenopus tropicalis*	probable bifunctional methylenetetrahydrofolate dehydrogenase/cyclohydrolase 2	XP_002941814.1

Sequence alignment results clearly showed highly conserved redox cofactor binding sequences (GRSKNVG) through evolution (Figure 2.6). For the cofactor binding, the classic Rossmann NAD binding site has the GXGXXG consensus sequence, while the sequence is not as strictly conserved in NADP-binding proteins. MTHFD2 and MTHFD2L share the consensus sequence of GRSXXXG, as does the cytoplasmic $NADP^+$-dependent trifunctional C_1-THF synthase (MTHFD1). MTHFD2 and MTHFD2L require phosphate and magnesium ions for proper binding of NAD^+, resembling the NADP binding site of MTHFD1. These ions compensate for the lack of a covalently bound phosphate group on

the cofactor $NADP^+$ (Karen E. Christensen, Mirza, Berghuis, & MacKenzie, 2005; Shin et al., 2014). As suggested by Christensen et al. (Karen E. Christensen, Mirza, et al., 2005), the mitochondrial enzymes (MTHFD2 and MTHFD2L) may have evolved from an $NADP^+$-dependent cytosolic enzyme, adapting an NADP binding site and changing the cofactor specificity to the mitochondrial environment.

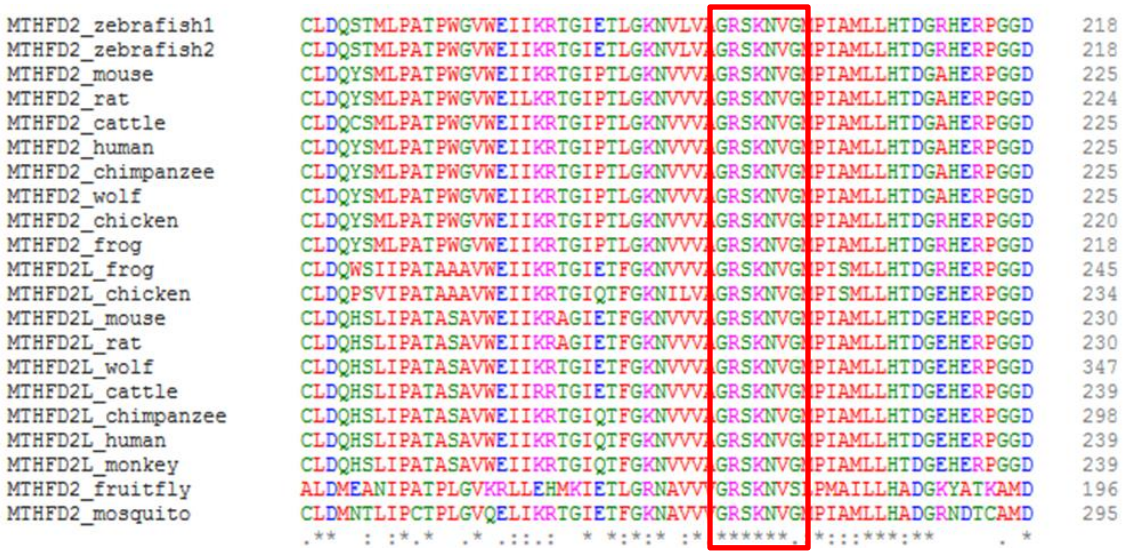

Figure 2.6 Sequence alignment of MTHFD2 and MTHFD2L proteins. Full-length MTHFD2 and MTHFD2L from various species are aligned showing Rossmann fold cofactor binding sequences indicated by a box (GRSKNVG sequences). "*" indicates identical residues; ":" similar alternate residues; and "." less similar alternate resides.

To experimentally verify redox cofactor specificity of MTHFD2 and MTHFD2L, I compared 5,10-CH_2-THF dehydrogenase activities of the enzymes with both cofactors under standard saturating substrate conditions (Figure 2.7). In order to allow direct comparisons between MTHFD2 and MTHFD2L, MTHFD2L activity assay were repeated alongside the new experiments with MTHFD2. With 5,10-CH_2-$H_4PteGlu_1$ substrate, NAD^+-dependent dehydrogenase activity of MTHFD2 was 8.5-fold higher than its

$NADP^+$-dependent activity, while NAD^+-dependent dehydrogenase activity of MTHFD2L was 3.7-fold higher than its $NADP^+$-dependent activity. Accordingly, MTHFD2 showed higher NAD^+ preference on its dehydrogenase activity than MTHFD2L with the monoglutamylated substrate.

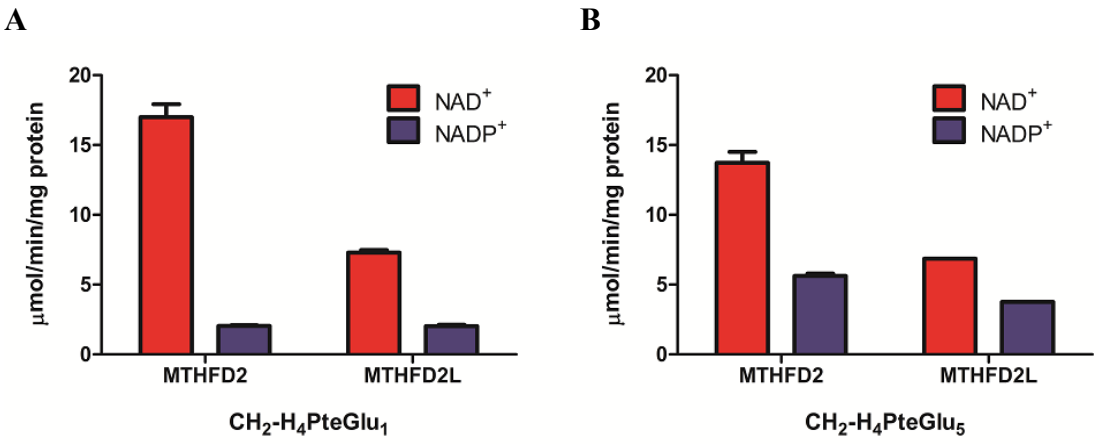

Figure 2.7 5,10-CH_2-THF dehydrogenase activity of MTHFD2 and MTHFD2L. Purified MTHFD2 and MTHFD2L were assayed for NAD^+- and NADP+-dependent 5,10-CH_2-THF dehydrogenase activity with saturating concentration of CH_2-H_4PteGlu$_1$ or CH_2-H_4PteGlu$_5$. Enzyme activity is expressed as μmol product/min/mg of protein. CH_2-H_4PteGlu$_1$ and CH_2-H_4PteGlu$_5$ concentrations were 354 μM and 429 μM, respectively. As a cofactor, NAD^+ was used at 1.0 mM and $NADP^+$ at 6.0 mM.

To further explore redox cofactor specificity in MTHFD2 under physiologically relevant substrate conditions, I repeated the assay with CH_2-H_4PteGlu$_5$. While NAD^+-dependent activities of the isozymes slightly decreased, their maximal $NADP^+$-dependent activities considerably increased with CH_2-H_4PteGlu$_5$ compared to CH_2-H_4PteGlu$_1$ (2.4-fold and 1.8-fold higher dehydrogenase activities of MTHFD2 and MTHFD2L,

respectively, with NAD^+ compared to $NADP^+$ (Figure 2.7). This result suggests that MTHFD2 and MTHFD2L may be dual redox cofactor-specific CH_2-THF dehydrogenases/CH^+-THF cyclohydrolases in mammalian mitochondria.

2.3.6. Steady-state Kinetics of 5,10-Methylene-THF Dehydrogenase Activity of MTHFD2

To further investigate redox cofactor specificity of MTHFD2 and MTHFD2L, steady-state kinetic parameters for CH_2-THF dehydrogenase activity were determined using CH_2-$H_4PteGlu_1$ (Figure 2.8). In order to allow direct comparisons between MTHFD2 and MTHFD2L, MTHFD2L kinetics were repeated alongside the new experiments with MTHFD2.MTHFD2 showed higher NAD^+-dependent activity than MTHFD2L at all concentrations of CH_2-THF substrate, while $NADP^+$-dependent activity was very similar in the two enzymes. The ratio of catalytic efficiency (k_{cat}/K_M) of NAD^+- versus $NADP^+$-dependent activities were 7.8 and 1.5 for MTHFD2 and MTHFD2L, respectively, indicating the higher preference for NAD^+ for MTHFD2 than for MTHFD2L (Table 2.3). For kinetic constants, it is noted that K_M values for MTHFD2 was higher than a published report in other research group (Pawelek & MacKenzie, 1998; Yang & MacKenzie, 1993). The same purified MTHFD2 enzyme showed similar K_M value within two folds when tested by a different group, demonstrating the numbers for kinetic constants are quite dependent on the buffer conditions so it's possible that some of those differences underlie different results from literature studies (personal communication with Dr. Vipin Suri, September 30, 2014).

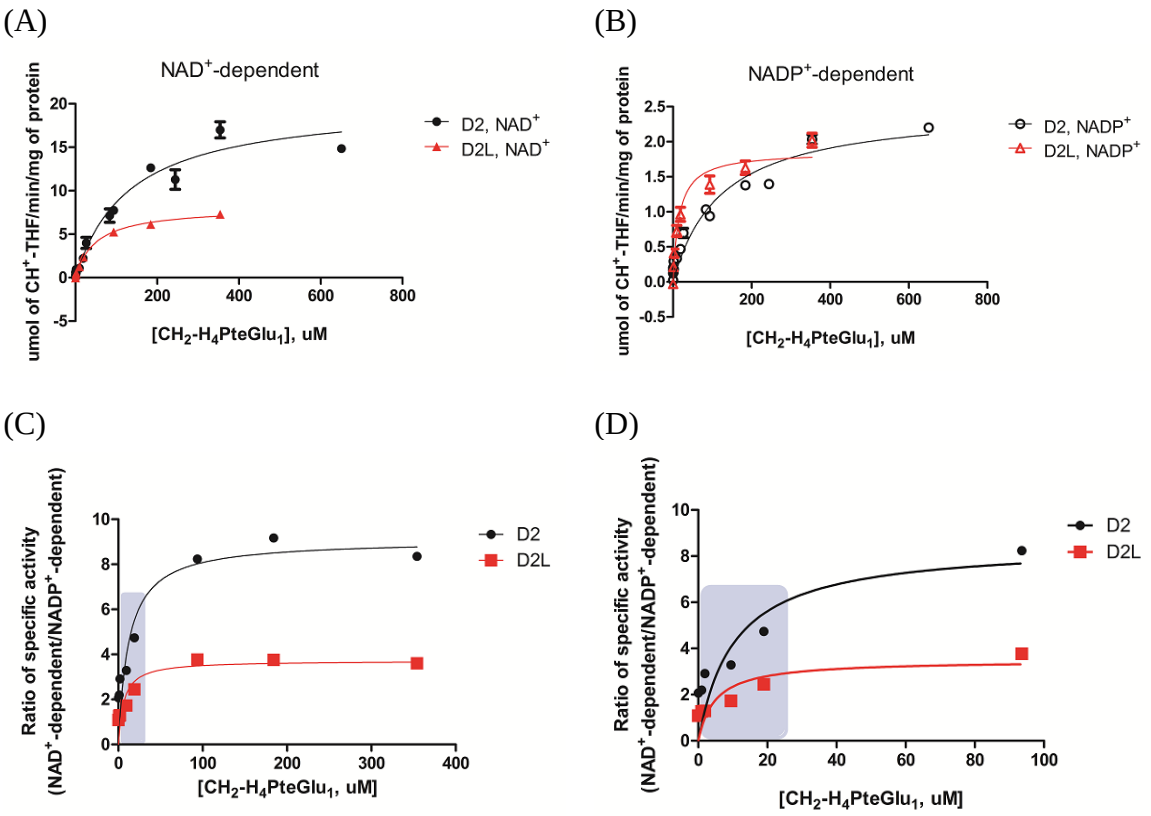

Figure 2.8 Redox cofactor specificity of MTHFD2 and MTHFD2L with CH_2-H_4PteGlu$_1$. Purified MTHFD2 and MTHFD2L were assayed for NAD^+- (A) and $NADP^+$- (B) dependent 5,10-CH_2-THF dehydrogenase activity with respect to CH_2-H_4PteGlu$_1$ concentration. The data were fit to the Michaelis-Menten equation. Enzyme activity is expressed as µmol product/min/mg of protein. Reaction buffer contained 50 mM HEPES (pH 8.0), 100 mM KCl, 0.4 mM 5,10-CH_2-THF, 40 mM β-mercaptoethanol, 5 mM $MgCl_2$, and 25 mM potassium phosphate. As a cofactor, NAD^+ was used at 1.0 mM and $NADP^+$ at 6.0 mM. (C) The ratio of NAD^+- to $NADP^+$-dependent activity was plotted as a function of increasing concentrations of CH_2-H_4PteGlu$_1$. Reported mitochondrial matrix concentration ranges 2.5 µM-25 µM for 5,10-CH_2-H_4PteGlu$_1$ indicated by shaded boxes, and plots in (D) were magnified the physiological range of 5,10-CH_2-H_4PteGlu$_1$.

Table 2.3 Kinetic parameters for MTHFD2 and MTHFD2L 5,10-CH_2-THF dehydrogenase activity. 5,10-CH_2-THF kinetic parameters were determined using saturating concentrations of NAD^+ (1.0 mM) or $NADP^+$ (6.0 mM). When NAD^+ was used, potassium phosphate (25 mM) and $MgCl_2$ (5 mM) were also included.

	CH_2-H_4PteGlu$_1$			**CH_2-H_4PteGlu$_5$**		
	K_M (μM)	k_{cat} (s^{-1})	k_{cat}/K_M ($s^{-1}\mu M^{-1}$)	K_M (μM)	k_{cat} (s^{-1})	k_{cat}/K_M ($s^{-1}\mu M^{-1}$)
NAD^+-dependent						
MTHFD2	133±20	12.4±0.71	0.093	359±32	15.4±0.55	0.043
MTHFD2L	49±4	4.5±0.09	0.092	156±25	5.7±0.29	0.037
$NADP^+$-dependent						
MTHFD2	123±24	1.5±0.11	0.012	302±35	6.4±0.29	0.021
MTHFD2L	16±3	1.0±0.05	0.063	216±81	3.8±0.49	0.018

To better understand the cofactor preference of the MTHFD2 dehydrogenase activity, the ratio of NAD^+-dependent activity versus $NADP^+$-dependent activity was calculated at each CH_2-H_4PteGlu$_1$ concentration. At high CH_2-H_4PteGlu$_1$ concentrations, both MTHFD2 and MTHFD2L clearly preferred NAD^+. However, as the folate substrate concentration was lowered into the physiological range (2.5-25 μM, reported mitochondrial matrix substrate concentration range), the ratio of $NAD^+/NADP^+$-dependent dehydrogenase activity for both enzymes decreased. MTHFD2L approached a ratio of 1, whereas the ratio for MTHFD2 dropped from 8 to 2-4 in the physiological folate range (Figure 2.8).

With the physiologically relevant substrate, CH_2-H_4PteGlu$_5$, the ratio of catalytic efficiency (k_{cat}/K_M) of NAD^+- versus $NADP^+$-dependent activities were 2.0 and 2.1 for MTHFD2 and MTHFD2L, respectively, further supporting that both enzymes increased

their activity with $NADP^+$ when polyglutamylated CH_2-THF is used as substrate (Figure 2.9 and Table 2.3).

The ratio of NAD^+-dependent versus $NADP^+$-dependent activity was similar between the two enzymes, ranging 0.5 to 2, and it was lower in MTHFD2 with polyglutamylated THF than monoglutamylated THF. Even at physiological CH_2-THF concentrations, the two enzymes were similarly active with NAD^+ or $NADP^+$, suggesting that MTHFD2 has a dual redox cofactor-specific dehydrogenase activity in physiological conditions, like MTHFD2L.

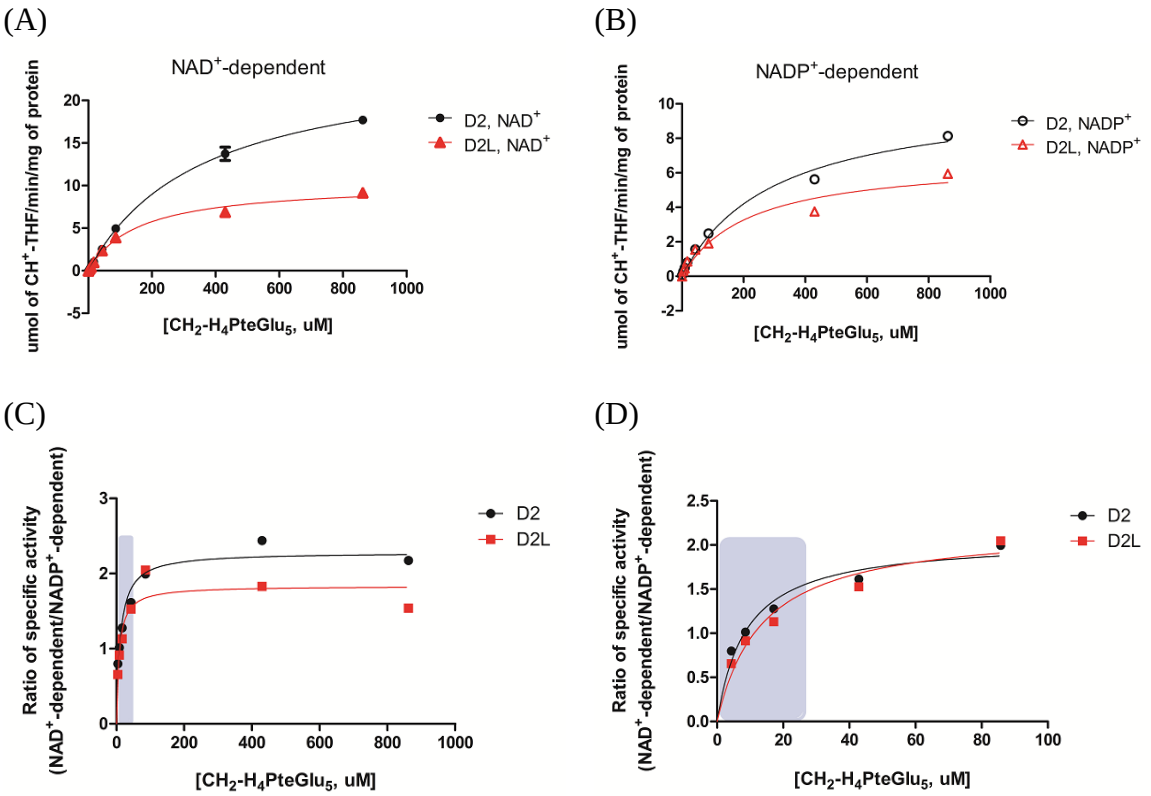

Figure 2.9 Redox cofactor specificity of MTHFD2 and MTHFD2L with CH_2-H_4PteGlu$_5$. Purified MTHFD2 and MTHFD2L were assayed for NAD^+- (A) and $NADP^+$- (B) dependent 5,10-CH_2-THF dehydrogenase activity with respect to CH_2-H_4PteGlu$_5$ concentration. The data were fit to the Michaelis-Menten equation. Enzyme activity is expressed as µmol product/min/mg of protein. Reaction buffer contained 50 mM HEPES (pH 8.0), 100 mM KCl, 0.4 mM 5,10-CH_2-THF, 40 mM β-mercaptoethanol, 5 mM $MgCl_2$, and 25 mM potassium phosphate. As a cofactor, NAD^+ was used at 1.0 mM and $NADP^+$ at 6.0 mM. (C) The ratio of NAD^+- to $NADP^+$-dependent activity was plotted as a function of increasing concentrations of CH_2-H_4PteGlu$_5$. Reported mitochondrial matrix concentration ranges 2.5 µM-25 µM for 5,10-CH_2-H_4PteGlu$_5$ indicated by shaded boxes, and plots in (D) were magnified the physiological range of 5,10-CH_2-H_4PteGlu$_5$.

2.3.7. Phylogeny and Evolution of MTHFD2 and MTHFD2L Sequences

In order to evaluate an evolutionary relationship between MTHFD2 and MTHFD2L, a phylogenetic tree was calculated by the alignment of twenty homologous MTHFD2 and MTHFD2L amino acid sequences. The unrooted phylogram demonstrates clustering of the sequences into three distinct groups during evolution, namely invertebrate MTHFD2, vertebrate MTHFD2L, and vertebrate MTHFD2 (Figure 2.10). The MTHFD2 and MTHFD2L groups were significantly different from each other showing relatively high bootstrap values of all of the nodes (>0.7/1). This supports that these two isozymes are distinct but related family groups. Invertebrate MTHFD2 sequences were distinctively separated from vertebrate MTHFD2 and MTHFD2L sequences, suggesting these vertebrate enzymes may be derived from an ancestral invertebrate MTHFD2 enzyme.

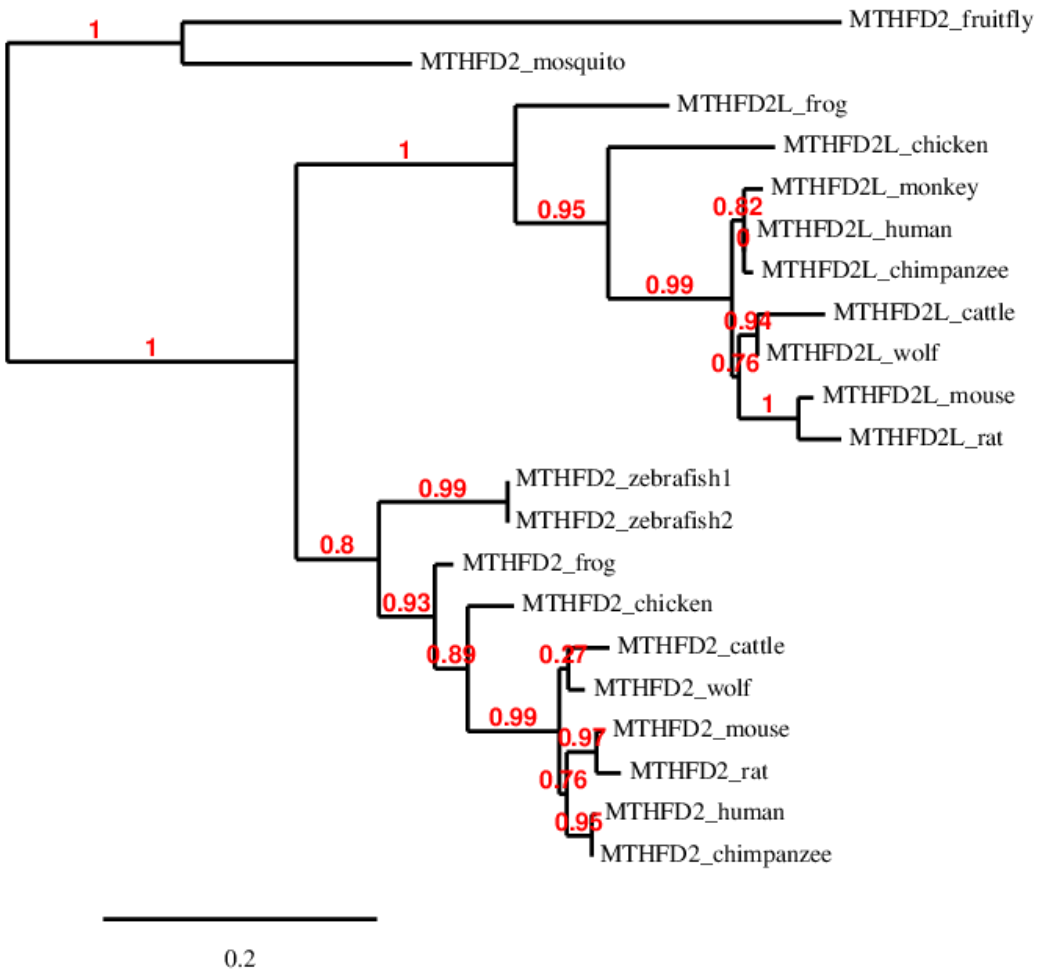

Figure 2.10 Phylogenetic analysis of MTHFD2 and MTHFD2L sequences. The tree is labeled with the enzyme name and the name of the species. The tree has three major clusters: invertebrate (insect) MTHFD2, vertebrate MTHFD2, and vertebrate MTHFD2L. A genetic distance scale is shown below the phylogenetic tree. The number of times a clade occurred in the bootstrap replicates is represented as a fraction out of 100.

Genetic distance values of MTHD2 sequences in fruit fly (*Drosophila melanogaster*) and mosquito (*Anopheles gambiae*) from the respective vertebrate sequences were significantly lower for the vertebrate MTHFD2 sequences, as compared with the respective MTHFD2L sequences ($p<0.0001$ by paired t-test), reflecting a possible derivation of vertebrate MTHFD2L genes from invertebrate MTHFD2 genes (Table 2.4).

Table 2.4 Pairwise genetic distances of MTHFD2 and MTHFD2L in various species from MTHFD2 for fruit fly and mosquito.

From	MTHFD2, fruit fly		MTHFD2, mosquito	
To	MTHFD2	MHTFD2L	MTHFD2	MTHFD2L
Human	0.581	0.642	0.497	0.535
Chimpanzee	0.581	0.636	0.497	0.530
Wolf	0.587	0.648	0.491	0.530
Cow	0.587	0.654	0.481	0.541
Mouse	0.605	0.642	0.497	0.524
Rat	0.599	0.642	0.513	0.541
Chicken	0.581	0.648	0.470	0.535
Frog	0.564	0.617	0.454	0.508

To further understand the evolutionary relationship of MTHFD2 and MTHFD2L in one-carbon metabolism, a phylogenetic tree was calculated by alignment of MTHFD2 and MTHFD2L amino acid sequences with MTHFD1 and MTHFD1L sequences from different species (Figure 2.11). It was notable that the MTHFD1 sequences for nematode and plants were absent because of poor sequence homology, and yeast MIS1 sequence (mitochondrial $NADP^+$-dependent trifunctional C_1-THF synthase) was added because of high sequence identity with MTHFD2 sequences. The phylogram showed that MTHFD2 and MTHFD2L are homologous from an ancestral fungal MTHFD1 gene. My results suggest that MTHFD2L may be evolved from invertebrate MTHFD2, originated from a primitive fungal gene.

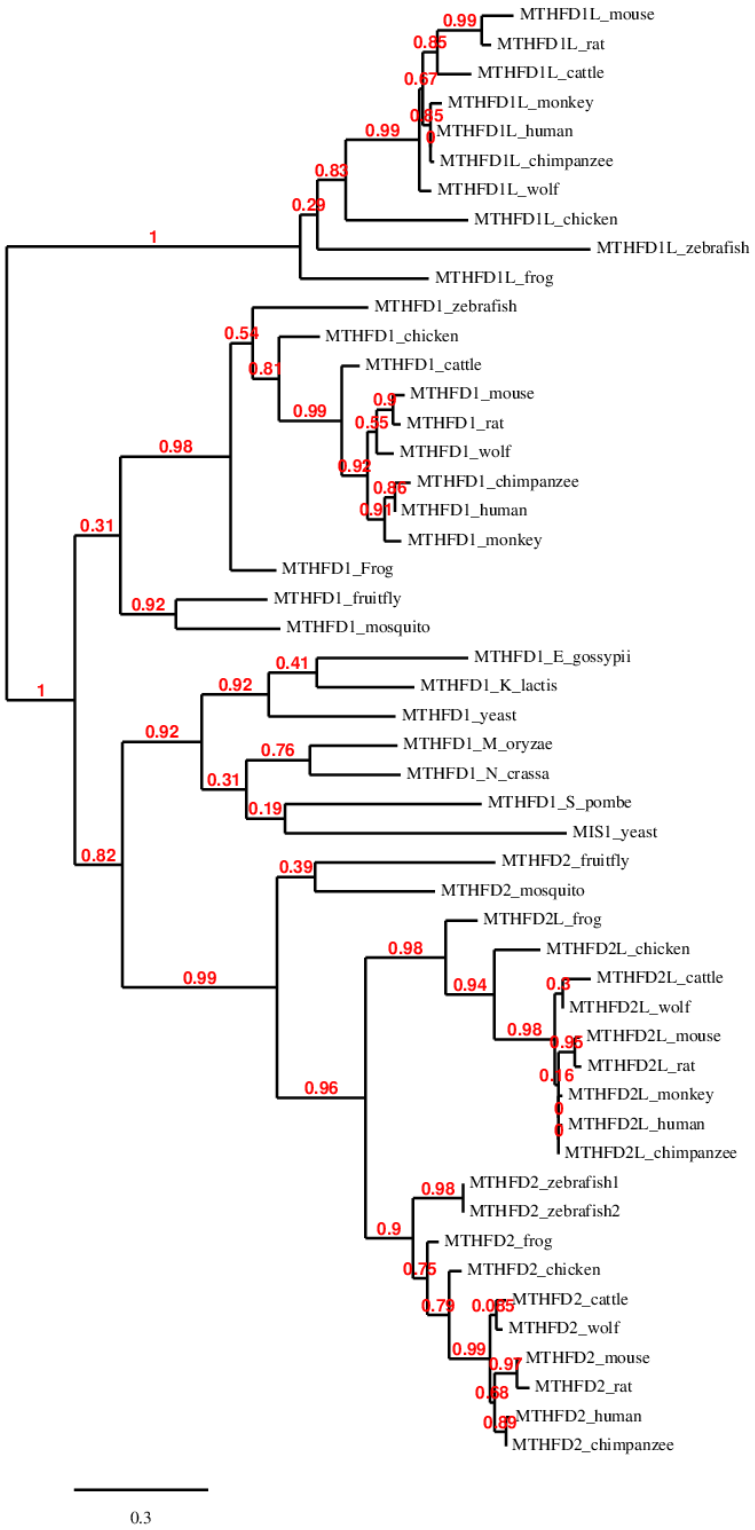

Figure 2.11: Caption on next page

Figure 2.11 Phylogenetic analysis of MTHFD family enzymes, MTHFD1, MTHFD1L, MTHFD2, and MTHFD2L. The tree is labeled with the protein name and the name of the species. The tree has five major clusters: MTHFD1L, animal MTHFD1, fungal MTHFD1, MTHFD2 and MTHFD2L. Fungal MTHFD1, MTHFD2, and MTHFD2L were clustered together. Note the absence of MTHFD1 for nematode and plants because of poor sequence similarity and the presence of yeast MIS1 sequence (yeast mitochondrial trifunctional C_1-THF synthase). A genetic distance scale is shown below the phylogenetic tree. The number of times a clade occurred in the bootstrap replicates is represented as a fraction out of 100.

2.4. DISCUSSION

The experiments described here demonstrate that the mammalian MTHFD2L isozyme, like MTHFD1 and MTHFD2, possesses both CH_2-THF dehydrogenase and CH^+-THF cyclohydrolase activities (Figure 2.2 and Figure 2.3). The dehydrogenase activity of this bifunctional enzyme can use either NAD^+ or $NADP^+$, but requires both phosphate and Mg^{2+} when using NAD^+ (Figure 2.3). The $NADP^+$-dependent dehydrogenase activity of MTHFD2L is inhibited by inorganic phosphate (Figure 2.4). MTHFD2L can use the mono- and polyglutamylated forms of CH2-THF with similar catalytic efficiencies (k_{cat}/K_M; Table 2.1). The mammalian MTHFD2 isozyme, like MTHFD2L, also possesses dual redox cofactor specificity. The dehydrogenase activity of MTHFD2 exhibits a higher preference for NAD^+ with monoglutamylated THF substrate than $NADP^+$ (Figure 2.7 and Figure 2.8). However, with polyglutamylated THF substrate, which is more similar to the physiologically relevant substrate present in mitochondria, MTHFD2 shows higher $NADP^+$-dependent activity than the monoglutamylated substrate, resulting in dual cofactor specificity of NAD^+ and $NADP^+$ (Figure 2.9). Phylogenetic analysis indicates that MTHFD2L may be evolved from invertebrate MTHFD2 which is homologous to a primitive fungal MTHFD1.

"How do these cofactor requirements compare to those of the other CH_2-THF dehydrogenase/CH^+-THF cyclohydrolase found in mammalian mitochondria? The MTFHD2 isozyme has been named NAD^+-dependent methylenetetrahydrofolate dehydrogenase-methenyltetrahydrofolate cyclohydrolase (Christensen, Mirza, et al., 2005; Yang & MacKenzie, 1993), but in fact exhibits dehydrogenase activity with $NADP^+$, albeit with a much higher K_M and lower V_{max} (Yang & MacKenzie, 1993). In fact, the redox cofactor requirements of the two isozymes are quite similar: both exhibit lower Km values for NAD^+ than for $NADP^+$; their NAD^+-dependent activities require phosphate and Mg^{2+}; and their $NADP^+$-dependent activities are inhibited by phosphate. The absolute requirement of the NAD^+-dependent activity of MTHFD2 for Mg^{2+} and P_i has been characterized in great detail by Mackenzie and coworkers (Karen E. Christensen, Mirza, et al., 2005). MTHFD2 uses Mg^{2+} and P_i to convert an NADP binding site into an NAD binding site. P_i binds in close proximity to the 2'-hydroxyl of NAD and competes with NADP binding. Mg^{2+} plays a role in positioning P_i and NAD. Mackenzie and coworkers identified several amino acid residues in MTHFD2 that are involved in the P_i and Mg^{2+} binding these residues are highly conserved in MTHFD2L in mammals. It is thus likely that Mg^{2+} and P_i play a mechanistically similar role in the NAD^+-dependent dehydrogenase activity of MTHFD2L as well.

The apparent preference of MTHFD2 and MTHFD2L for NAD^+ (Figure 2.3 and Figure 2.7) is most dramatic at non-physiological levels of phosphate, Mg^{2+}, and folate cofactor. When these experiments were repeated at more physiologically relevant substrate concentrations, MTHFD2 and MTHFD2L showed much less preference for NAD^+ (Figure 2.5 and Figure 2.7). Given that estimates for mitochondrial matrix levels of CH_2-THF range from 2.5-25 μM (Eto & Krumdieck,

1982; Horne et al., 1989; Nijhout et al., 2006; Seither et al., 1989), it is likely that MTHFD2 and MTHFD2L exhibits dual redox cofactor specificity *in vivo*."

Folylpolyglutamate specificity is one of the characteristic features of enzymes in the one-carbon metabolism (Schirch & Strong, 1989). In this study, I showed that MTHFD2L can use the mono- and polyglutamylated forms of CH_2-THF with similar catalytic efficiencies (k_{cat}/K_M), resulting from higher k_{cat} as well as higher K_M with polyglutamylated CH_2-THF. In the case of MTHFD2, it has higher dehydrogenase activity for the polyglutamylated substrate than the monoglutamylated form with $NADP^+$ as a cofactor, but not with NAD^+. Why does MTHFD2 show higher $NADP^+$-dependent activity with polyglutamylated CH_2-THF? There are two possible explanations: First, the polyglutamate "tails" on folate derivatives may facilitate dehydrogenase activity by increasing the affinity of the enzyme for its folate substrate or by enforcing a conformational change in the enzyme-folate complex. Second, polyglutamylation may enhance binding synergism between the folate and other substrates (Schirch & Strong, 1989)(Schirch and Strong, 1989). For example, 10-formyltetrahydrofolate synthetase uses formate as a substrate, and polyglutamate THF substrates decrease the K_M for formate 500-fold as the result of a conformational change induced by the binding of the third glutamyl residue of $H_4PteGlu_n$ (Strong, Joshi, Lura, Muthukumaraswamy, & Schirch, 1987). It may be possible for MTHFD2 to enhance its $NADP^+$ binding with polyglutamylated substrates, but this hypothesis needs to be further verified experimentally.

"The use of NAD^+ vs. $NADP^+$ in this step can have a dramatic effect on the rate and direction of flux of one-carbon units through this pathway in mitochondria. The oxidation state of mitochondrial pools of NAD^+ and $NADP^+$ is dictated by mitochondrial respiration, which is in turn linked to nutrition, differentiation and proliferation (Yang et al., 2007). Measurements in liver suggest that the redox

potential of the NAD^+/NADH matrix pool is typically 75-100 mV more positive than that of the $NADP^+$/NADPH matrix pool (Tibbetts & Appling, 2010). Thus, the ratio of CH_2-THF to 10-CHO-THF in the matrix will be shifted much further towards 10-CHO-THF with a CH_2-THF dehydrogenase linked to the NAD^+/NADH pool vs. the $NADP^+$/NADPH pool (Pelletier & MacKenzie, 1995; Yang & MacKenzie, 1993). A cyclohydrolase/dehydrogenase with dual-cofactor specificity such as MTHFD2 and MTHFD2L would be able to adapt immediately to changing metabolic conditions, shifting the equilibrium between CH_2-THF and 10-CHO-THF (and formate) depending on the relative levels of oxidized cofactor (NAD^+ or $NADP^+$) in the mitochondrial matrix."

So, now we return to the central question: why are there two of the mitochondrial CH_2-THF dehydrogenases in vertebrates? From kinetic characteristics and substrate specificity, it seems the enzymes are quite similar, except for higher NAD^+-dependent dehydrogenase activity of MTHFD2. In the previous study from my lab, both *Mthfd2* and *Mthfd2l* were expressed during embryogenesis, whereas *Mthfd2l* expression is low in early stages but begins to increase at embryonic day 10.5 and remains elevated through birth (Shin et al., 2014). I propose here that, from a developmental perspective, MTHFD2 may be expressed to boost flux through the mitochondrial pathway when MTHFD2L alone is not sufficient, to support high cell proliferation during the earlier stages of embryogenesis. As the embryo approaches birth, MTHFD2 turns off and stays off in most adult tissues where cell proliferation is not as rapid. MTHFD2L may be enough to handle the lower flux by itself.

Recently, a number of studies have shown that *Mthfd2* is the most overexpressed gene in proliferating cancers (Jain et al., 2012; F. Liu et al., 2014; Moran et al., 2014; Nilsson et al., 2014; Pikman et al., 2016). Its expression is associated with rapidly

proliferating cells such as acute myeloid leukemia, breast cancer, hepatocellular carcinoma, and lung cancer. Fan et al. (Fan et al., 2014) used quantitative flux analysis to show that a major contribution of NADPH in proliferating cells is via one-carbon metabolism. Surprisingly, knockdown of *Mthfd2* resulted in decrease of NADPH production. However, it was not clear if MTHFD2 produces NADPH in vivo because it was known as primarily NAD^+-dependent enzyme. Our results clearly support mitochondrial NADPH production from MTHFD2. Mitochondrial NADPH is used for a number of cellular processes including biosynthesis of fatty acids, maintenance of antioxidant species and apoptosis (Rydström, 2006). Further *in vivo* experiments such as overexpression/knockout of the genes in mammalian system will be required to compare mitochondrial redox cofactors production by MTHFD2 and MTFHD2L.

The results presented here are the first detailed description of phylogenetic analysis of MTHFD proteins from various organisms. My analysis indicates that MTHFD2L may be evolved from invertebrate MTHFD2 which is homologous to a primitive fungal MTHFD1. Robert Mackenzie's group, who have extensively researched MTHFD2, reported NAD^+-dependent 5,10-CH_2-THF dehydrogenase activity in insects including spruce budworm (*Choristoneura fumiferana*) and fruit fly (*Drosophila melanogaster*). Interestingly, all insect adult tissues had detectable levels of NAD^+-dependent CH_2-THF dehydrogenase activity (approximately 10-fold lower than $NADP^+$-dependent activity) (Tremblay, Sohi, Retnakaran, & MacKenzie, 1995), whereas normal mouse tissues had either very low or undetected levels of NAD^+-dependent activity (Mejia & MacKenzie, 1985). The requirement for higher levels of NAD^+-dependent CH_2-THF dehydrogenase in insect adult tissues is still unknown. Based on my phylogenetic findings, I speculate that evolutionary higher organisms may achieve fine-tuning on their proliferation through developmental stages using two different isozymes, MTHFD2 and MTHFD2L, in 1C

metabolism. Functional analysis and enzymatic characterization of insect MTHFD2 with developmental progression will be necessary to further investigate the reason for a system of two dehydrogenase/cyclohydrolase enzymes in mammalian mitochondrial 1C metabolism.

Chapter 3. Deletion of *Mthfd1l* Causes Defect in Head Mesenchyme Development in Mice

3.1. INTRODUCTION

Neural tube defects (NTDs) are serious structural birth defects of the central nervous system including brain and spinal cord, caused by failure of neural tube closure. It is well known that many NTDs can be prevented primarily by folic acid supplementation. However, compared with a number of studies on the clinical and epidemiological aspects of folic acid supplementation, the fundamental question of how folic acid prevents NTDs and promotes closure of the neural tube has received little attention (Copp et al., 2013).

Folic acid-mediated one-carbon (1C) metabolism is central to many cellular processes such as purine and thymidylate biosynthesis, mitochondrial protein biosynthesis, amino acid metabolism, and universal methyl donor production. To bring insight into the mechanisms by which folic acid acts during neural tube closure, 1C pathway knockout mouse models have been generated to be representative of human NTDs. Up to date, about 15 mouse models having mutations on 1C metabolism exist (K. E. Christensen et al., 2013; Harris, 2009; Momb & Appling, 2014; Narisawa et al., 2012; Pai et al., 2015). However, NTDs are observed in only five of these knock-out mouse models (*Shmt1*, *Folr1, Amt, Gldc,* and *Mthfd1l*).

The *Mthfd1l* gene encodes the monofunctional 10-formyl-tetrahydrofolate (THF) synthetase in the mitochondrial 1C pathway, producing formate for export to the cytoplasm. Homozygous deletion of *Mthfd1l* causes NTDs with 100 % penetrance and is embryonic lethal with death occurring around embryonic day 12.5 (Momb et al., 2013). Maternal supplementation with formate decreases the incidence of NTDs and partially improves growth delay. Supplementation with folinic acid (5-formyl-THF) is not protective in this mouse model. The *Mthfd1l* KO mouse model can be useful for elucidating

roles of folate and 1C metabolism on neural tube closure because: 1) MTHFD1L is a mitochondrial enzyme. The mitochondrial 1C pathway is crucial for flux of formate from the mitochondria into the cytoplasm, accounting for approximately 75 % of 1C units entering folate metabolism (Pike et al., 2010); 2) the *Mthfd1l* KO mouse model develops fully penetrant NTDs and does not require feeding a folate-deficient diet to cause these phenotypes; and 3) NTDs caused by *Mthfd1l* mutation are folate-resistant. Although maternal folic acid fortification has dramatically reduced the incidence of NTDs, there is a subset of NTDs (~30 % of NTD prevalence before folic acid fortification) that still occur, and causes/treatments of these folate-resistant NTDs are unknown.

Mouse neural tube first fuses at the hindbrain/cervical boundary (closure 1) at embryonic day 8.5 (6-7 somite stage) and neural tube fusion proceeds both rostrally and caudally (Golden & Chernoff, 1993). Around 10-13 somite stage, closure 2 is initiated at the forebrain/midbrain boundary in the cranial region, fuses bi-directionally, and further meets the rostrally directed closure 1 and the caudally directed closure 3, sealing the anterior neuropore at approximately 20 somite stage. Caudal neural tube from closure 1 continues fusion along the growing spinal region and finally finishes closure of the posterior neuropore during embryonic day 10 (35-39 somite stage) (Golden & Chernoff, 1993).

For successful closure of the neural tube, especially for the cranial neural tube, specific and precise cellular mechanisms are required. Several cellular mechanisms are essential for proper elevation and apposition of the cranial neural folds, including neuroepithelial cell proliferation, apoptosis, neural crest cell formation, and head mesenchymal expansion (Copp, 2005; Copp, Greene, & Murdoch, 2003). The neuroepithelium is completely proliferative during neural tube closure (Tuckett & Morriss-Kay, 1985). Cell proliferation has an important role in neural tube closure, encouraging a

hypothesis that increased cell proliferation could be a key effect of folic acid. Apoptotic cell death occurs in the neural folds during embryonic development and appears to be important for proper neural tube closure (Geelen & Langman, 1977). Cranial neural crest (NC) cells are generated at the dorsal edge of the neural folds. In mammals, the cranial NC cells begin detaching from the edge of the neural folds in the midbrain and hindbrain, and emigrate before neural tube closure is complete (Wagner et al., 2005). Since some mouse models lacking genes expressed in the NC cells often have exencephaly, NC cell formation is considered one of important cellular processes in regulating mammalian cranial neurulation (Soo et al., 2002). The cranial neural plate is surrounded mainly by the head mesenchyme, affecting neural fold elevation and dorsolateral hinge point formation during cranial neural tube closure (Copp et al., 2003; Zohn, Anderson, & Niswander, 2007; Zohn & Sarkar, 2012).

To investigate the role of 1C metabolism during cranial neural tube closure, I analyzed several cellular processes, including cell proliferation, apoptosis, neural crest cell formation, and head mesenchyme formation, in *Mthfd1l* knockout mice during neural tube closure at 7-13 somite stage (embryonic day 8.75 in wild-type embryo) and 18-24 somite stage (embryonic day 9.5 in wild-type embryo). I also examined the effects of maternal supplementation with calcium formate on the dysregulated cellular processes.

3.2. MATERIALS AND METHODS

3.2.1. Mouse Strains and Genotyping

All protocols used in this study were approved by the Institutional Animal Care and Use Committee of The University of Texas at Austin and performed within the guidelines of the National Institutes of Health for the Care and Use of Laboratory Animals. As

reported by a previous study (Momb et al., 2013), all mice were maintained on a C57BL/6 genetic background. Mice harboring a floxed conditional knockout cassette between exons 4 and 6 of *Mthfd1l* were mated to mice expressing Cre recombinase under control of the E2a promoter (E2a-Cre) to generate heterozygous *Mthfd1l*$^{+/+}$ embryos. All mice were fed standard commercially available laboratory chow (LabDiet 5K67), and exposed to a 12 h light-dark cycle.

Genotyping was carried out using a forward primer (5'-GAGTATGTGATTGCTTGGACCCCCAGGTTCC-3'), a reverse primer for wild type (5'-TGGCTCCCGAGGTTGTCTTCTGGCTATGAT-3'), and a reverse primer for the mutant allele (5'-CGGCGCCAGCCGCTTTTTTGTACAAACTTG-3').

3.2.2. Embryo Preparation

Embryos of three different genotypes were generated by matings between *Mthfd1l* heterozygous males and females. Appearance of a vaginal plug was designated as embryonic day (E) 0.5, and embryos were dissected within specific somite number ranges (7-13 somites at E8.5-E8.75 for wild types and E9.5 for nullizygotes; and 18-24 somites at E9.5 for wild types and E10.5 for nullizygotes) in order to represent the characteristic morphology of the neural tube closure.

For immunohistochemistry, embryos were fixed for 30 min (E8.5), 1.5 hr (E9.5), or 3 h (E10.5) at 4 °C in 4 % (w/v) paraformaldehyde in PBS, pH 7.2, followed by washing twice in PBS. Embryos were further infused in 30 % (w/v) sucrose in PBS overnight and frozen. For whole mount in situ hybridization and TUNEL assay, embryos were fixed overnight at 4 °C in 4 % (w/v) paraformaldehyde in PBS, pH 7.2, followed by washing

twice in PBS. Embryos were further dehydrated and stored in 100 % methanol at -20 °C before processed.

3.2.3. Immunohistochemistry

Cryosections (7 μm) were blocked in 0.5 % (v/v) Triton in PBS (PBST) containing 5 % normal goat serum for 30 min at room temperature. For cleaved caspase-3, 2 % (w/v) BSA was added to the blocking solution and the sections were blocked for 1.5 hr. Primary antibodies were applied overnight at 4 °C: anti-beta-galactosidase (MP Biomedicals; 1:50 dilution), anti-phosphohistone H3 (Millipore; 1:300 dilution), anti-cleaved caspase 3 (Cell Signaling; 1:200), and anti-Sox9 (Millipore; 1: 250). Secondary antibodies were goat anti-rabbit IgG Alexa Fluor 555 (Cell Signaling; 1:200 dilution) and goat anti-mouse IgG Alexa Fluor 488 (Life Technologies; 1:200 dilution). At least three embryos were assessed with each antibody. For nuclear staining, cells were incubated with anti-fade mounting medium with DAPI (Vectashield). Fluorescent images were collected on an Axiovert 200M fluorescent microscope (Zeiss). Images were analysed using ImageJ software (U.S. National Institutes of Health).

3.2.4. Whole Mount In Situ Hybridization

Mouse embryos ranging from E8.5 to E10.5 were hybridized using digoxigenin-labeled RNA probes (Yu et al., 2012). Plasmids harboring *Sox9* and *FoxD3* were a gift from Dr. Steve Vokes and purchased from Addgene (Cambridge, MA; plasmid #37098), respectively. Antisense probe for *Mthfd1l* was constructed as described previously (Pike et al., 2010) by *in vitro* transcription using T7 RNA polymerase to transcribe from a vector linearized with Sfi1.

3.2.5. Whole Mount TUNEL Assay

Whole-mount TUNEL assay was performed following the manufacturer's instructions with some modifications (Millipore; catalog # S7100). Dissected embryos were fixed in 4 % (w/v) paraformaldehyde in PBS (pH 7.2), dehydrated, and stored at -20 ° C until use. For TUNEL assay, embryos were rehydrated and fixed in ethanol/acetic solution (2:1) for 20 min at -20 °C, quenched in 3 % (v/v) hydrogen peroxide in PBS for 20 min at room temperature. Embryos were equilibrated, incubated with TdT enzyme (Terminal deoxynucleotidyl Transferase) overnight at 37 °C, and subsequently incubated with anti-digoxigenin-peroxidase conjugate antibody overnight at 4 °C. On the following day, embryos were stained with 0.05 % (w/v) DAB (3,3'-diaminobenzidine) solution for 1 min at room temperature.

3.2.6. Quantitative Analysis of Head Mesenchyme Cell Density

Quantitative analysis of head mesenchyme cell density was carried out based on Dunlevy et al (Dunlevy, Burren, Mills, et al., 2006). Areas for cell counting were defined by boxes of defined dimensions located in central site (8.5 % x 33.5 % of each section width) or in lateral site (8.5 % x 16.7 % of each section width). Image processing was conducted using ImageJ.

3.2.7. Ethynyl-deoxyuridine (EdU) Incorporation in Mouse Embryonic Fibroblasts (MEFs)

Mouse embryonic fibroblasts (MEFs), derived from pools of *Mthfd1l*$^{+/+}$ and *Mthfd1l*$^{z/z}$ embryos respectively, were plated (5,000 cells per well) and cultured for 24 hours prior to addition of 10 μM EdU (Invitrogen). EdU solution in PBS was added incubating 2 hours, then cells were fixed and processed for detection of EdU (Click-It EdU

Imaging Kit). Cells were washed in PBST buffer containing 0.5 % Triton-X100 and blocked for 30 min in PBST containing 5 % normal goat serum, 0.15 % (w/v) glycine, and 2 mg/ml BSA prior to immunohistochemistry for phosphohistone H3.

3.2.8. Maternal Supplementation with Calcium Formate

Formate supplementation was performed by the addition of calcium formate to the drinking water of females when *Mthfd1l*$^{tz/+}$ matings were set up. Concentration of the calcium formate was 0.1 M to deliver 2,500 mg formate·kg^{-1}·d^{-1}, based on an average water intake of 5 mL per day for a 25 g C57BL/6 mouse (Momb et al., 2013). The effect of formate supplementation was analyzed for somite numbers/crown-rump length, proliferation, and head mesenchyme density.

3.2.9. Statistical Analysis

All quantitative data were compared using Student's t-test and two-way ANOVA (analysis of variance). All statistical tests were performed using Prism version 5 (GraphPad, La Jolla, CA).

3.3. RESULTS

3.3.1. MTHFD1L is Widely Expressed in Early Development

The *Mthfd1l* gene is expressed at all stages of mammalian embryogenesis and ubiquitously throughout the embryo. Also, it has localized regions of higher expression along the neural tube, the brain, craniofacial structures, limb buds, and the tail bud (Momb et al., 2013; Pike et al., 2010; Shin et al., 2014). However, there is a lack of information on

the spatiotemporal expression of *Mthfd1l* throughout mouse neural tube closure from embryonic day (E) 8.75 to E10.5. Whole-mount *in-situ* hybridization verified ubiquitous expression in embryonic tissues but especially high expression of *Mthfd1l* in the forebrain, first branchial arch, and limb buds at E9.5 and E10.5 (Figure 3.1), as reported (Momb et al., 2013; Pike et al., 2010). At E8.75, during neural tube closure, the highest expression was detected in the folding neural plates.

In the *Mthfd1l* knock-out mice, the *Mthfd1l* locus is modified by the insertion of a cassette, containing a splice acceptor, internal ribosome entry site, the β-galactosidase gene (*LacZ*) followed by a polyadenylation signal, and the gene for neomycin phosphotransferase (*Neo*) between exons 4 and 6 of *Mthfd1l* (Momb et al., 2013). Transcription of the disrupted allele produces a transcript containing exons 1-4 sliced to *LacZ*. To verify expression of MTHFD1L protein in sections, immunofluorescence against β-galactosidase on *Mthfdth1l*$^{tz/tz}$ embryos was conducted. It is notable that β-galactosidase expression was significantly restricted and reduced in *Mthfd1l*$^{tz/+}$ embryos, while it was robustly detected in *Mthfd1l*$^{tz/tz}$ embryos. In sectioned *Mthfd1l*$^{tz/tz}$ embryos, β-galactosidase was significantly detected at the basal surface of the dorsal neuroepithelium, lateral region of head mesenchyme (Figure 3.1; E and F) and the first branchial arch (Figure 3.1; H and I).

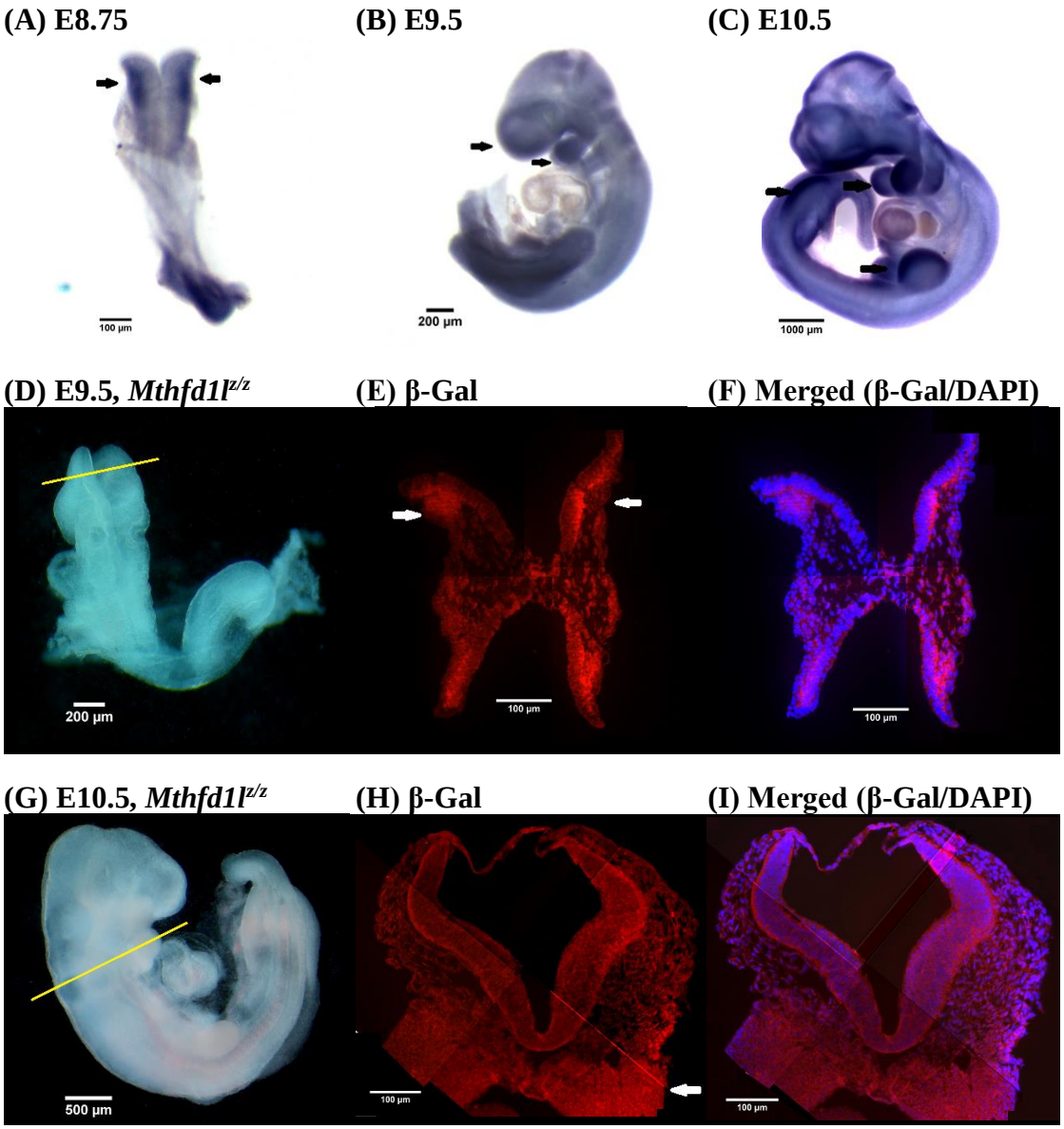

Figure 3.1 MTHFD1L is expressed ubiquitously but most highly in the basal neuroepithelium. Whole-mount *in-situ* hybridization at E8.75 (A), E9.5 (B), and E10.5 (C) show abundant expression of MTHFD1L in the developing forebrain, the limb buds, and the branchial arches (arrows). Expression is observed in the folding neural plates at E8.75 (arrows in A). Sections through *Mthfd1l*$^{z/z}$ embryos express β-galactosidase (immunostained) in the basal area of the dorsal neuroepithelium (E) and the first branchial arch (H). β-Galactosidase staining is red and DAPI-stained nuclei are blue, shown in F and I. Straight line in the embryos (D and G) indicates the level of sections (E/F and H/I, respectively).

3.3.2. Deletion of *Mthfd1l* Causes Retardation in Growth and Development

To analyze effects of the *Mthfd1l* mutation on the embryonic development and progression through the different stages of neural tube closure, litters were collected at a series of developmental stages from E8.5 to E10.5 (Table 3.1). The numbers of embryos of differing genotypes were not distributed as expected for Mendelian inheritance of the nonfunctional $Mthfd1l^{z}$ allele. The ratio of $Mthfd1l^{+/+}$ to $Mthfd1l^{z/+}$ to $Mthfd1l^{z/z}$ was 130:211:66, indicating that the $Mthfd1l^{z/z}$ genotype causes embryonic lethality before E8.5 ($P = 3.2 \times 10^{-5}$).

Previous report showed that all embryos lacking *Mthfd1l* exhibit aberrant neural tube closure including craniorachischisis and exencephaly and/or a wavy neural tube between E11.5 and E12.5 in previous study (Momb et al., 2013). In the current study, I found that 96% (24 of 25) at E9.5 and 68% (15 of 22) nullizygous embryos at E10.5 still had an open cranial neural tube (Table 3.1). The 7 $Mthfd1l^{z/z}$ embryos whose neural tubes had closed were small and pale. All $Mthfd1l^{z/z}$ embryos at E10.5 displayed a small, aberrantly formed head (Figure 3.2). While all $Mthfd1l^{z/z}$ embryos at E10.5 had distinguishable mutant phenotypes including open neural folds and aberrant head formation compared to wild types, $Mthfd1l^{z/z}$ embryos at E9.5 did not show any noticeable difference to wild types (E8.75), except for retarded growth.

Table 3.1 Mthfd1l nullizygous mice have delayed embryonic growth and open neural tube in the cranial region. Numbers of somites in *Mthfd1l*$^{z/z}$ were statistically lower compared to *Mthfd1l*$^{+/+}$ ($p < 0.0001$ for all ages; asterisk indicates significant difference at the 99.99 % level to *Mthfd1l*$^{+/+}$ by t-test). Number of embryos showing partially or completely open neural tube in the head were counted.

Age	Genotype	Dams	Embryos	Somites (mean±std)	Neural tube open (Embryos)
E8.5 /E8.75	*Mthfd1l*$^{+/+}$	16	34	6.3±2.8	100 % (34)
	Mthfd1l$^{z/+}$	20	59	5.7±3.2	100 % (59)
	Mthfd1l$^{z/z}$	12	19	1.4±2.1*	100 % (19)
E9.5	*Mthfd1l*$^{+/+}$	19	51	20.5±5.5	12 % (6)
	Mthfd1l$^{z/+}$	20	73	21.3±4.1	12 % (9)
	Mthfd1l$^{z/z}$	14	25	10.2±3.7*	96 % (24)
E10.5	*Mthfd1l*$^{+/+}$	17	45	33.5±5.7	2 % (1)
	Mthfd1l$^{z/+}$	20	79	32.6±5.3	9 % (7)
	Mthfd1l$^{z/z}$	12	22	22.9±6.0*	68 % (15)

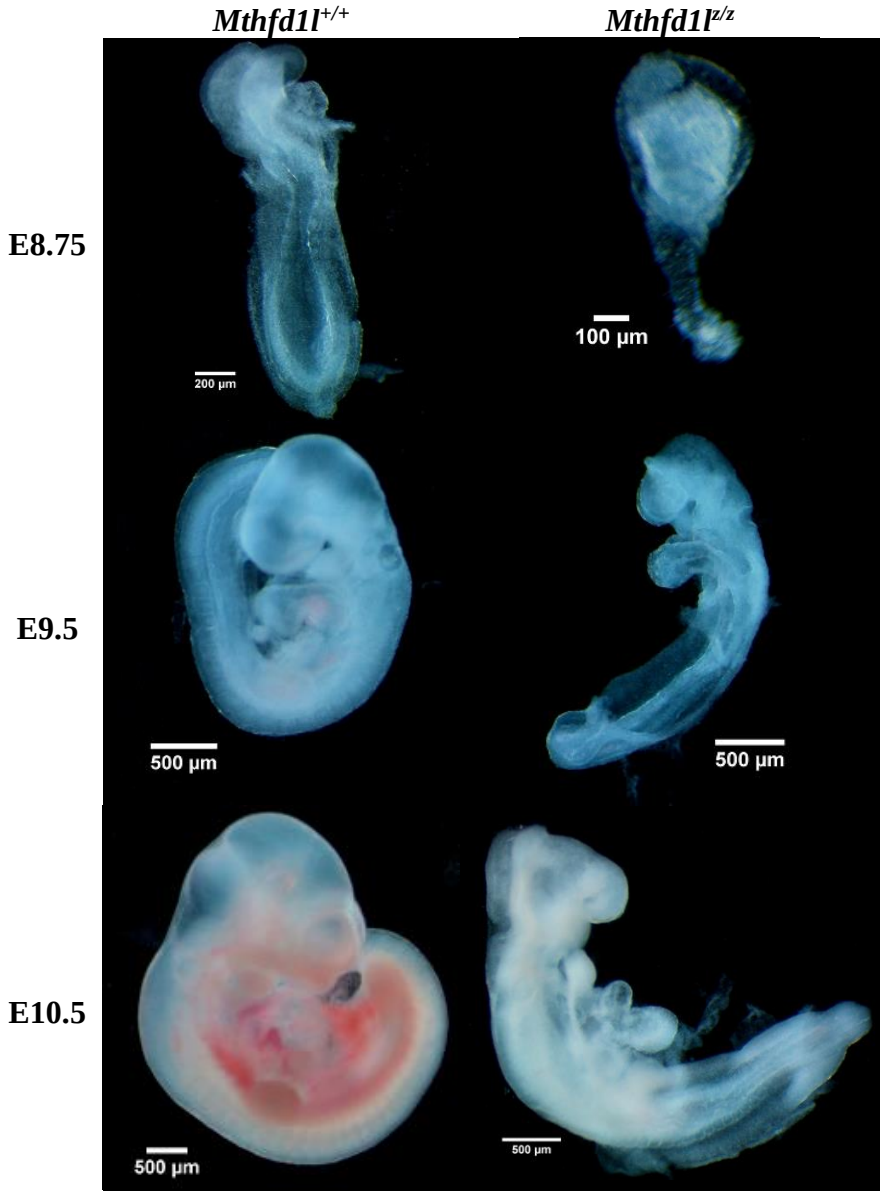

Figure 3.2 *Mthfd1l* nullizygous mice are smaller than wild-type littermates and have open neural tube. Compared with wild-type embryos, *Mthfd1l*$^{z/z}$ embryos show delayed growth and developmental progression at all embryonic stages (E8.75 to E10.5). *Mthfd1l*$^{z/z}$ embryos at E9.5 have similar morphology with *Mthfd1l*$^{+/+}$ embryos at E8.75. *Mthfd1l*$^{z/z}$ embryos at E10.5 are similar in size with *Mthfd1l*$^{+/+}$ embryos at E9.5, but have defects in neural tube closure and orofacial development.

The growth and development of *Mthfd1l*$^{z/z}$ embryos was also severely retarded. In comparison with wild type and heterozygous littermates, homozygous mutants had significantly fewer somites at all gestational time points (E8.5 to E10.5, $p<0.01$), equivalent to a developmental delay of around 0.75 day (Figure 3.3). The mean crown-rump length of *Mthfd1l*-deficient embryos was smaller at each stage. Plots of crown to rump length against somite number for individual embryos do not show a difference between genotypes, however, suggesting the relationship between growth and developmental progression is not disrupted in the nulls (Figure 3.4).

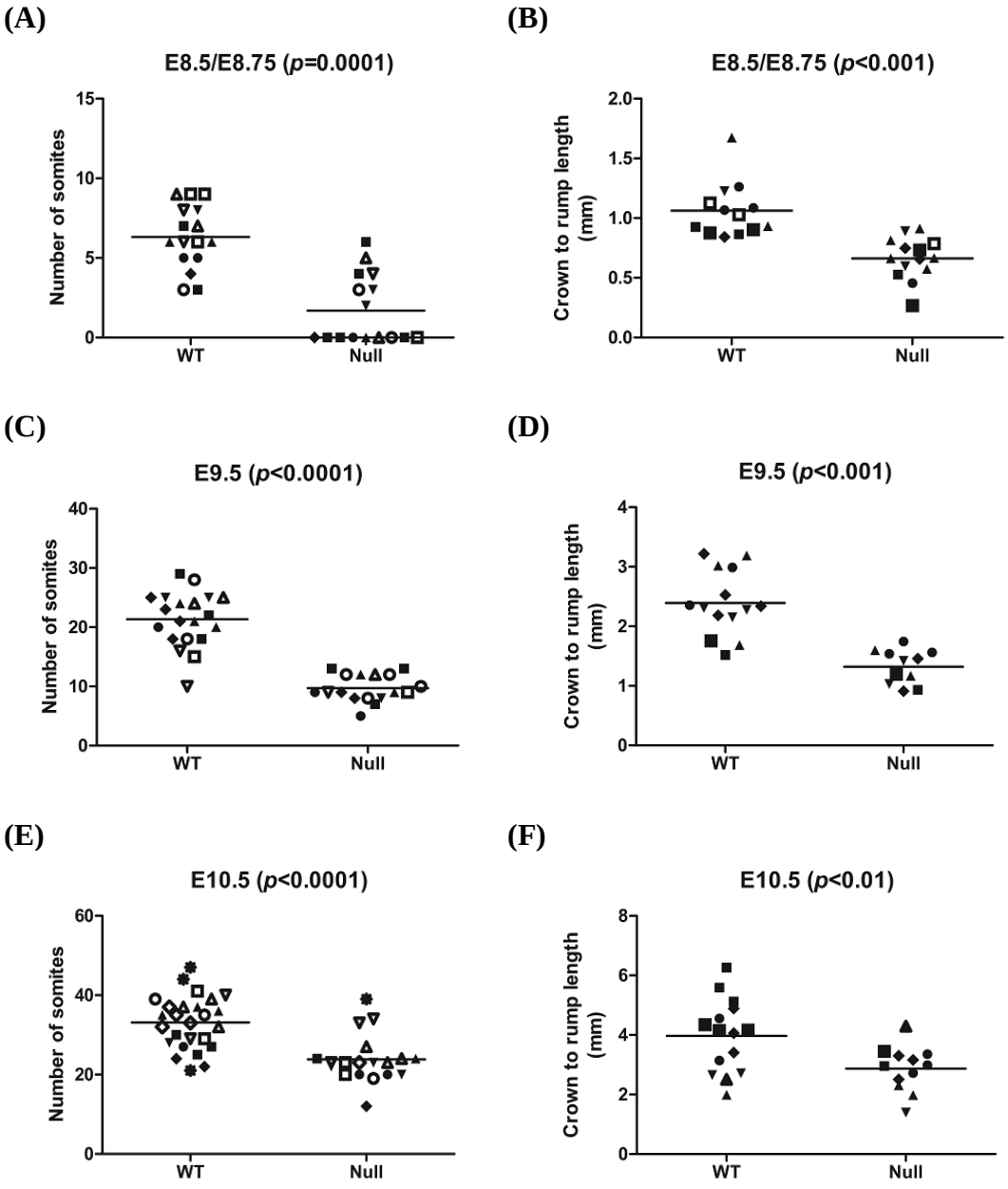

Figure 3.3 *Mthfd1l* nullizygous mice have delayed developmental progression and embryonic growth at all embryonic stages (E8.5 to E10.5). Reduced number of somites in *Mthfd1l*$^{z/z}$ show delayed developmental progression (A, C, and E), and shorter crown to rump length show growth retardation (B, D, and F). Each type of symbol represents littermates. P value was calculated by Student's t-test.

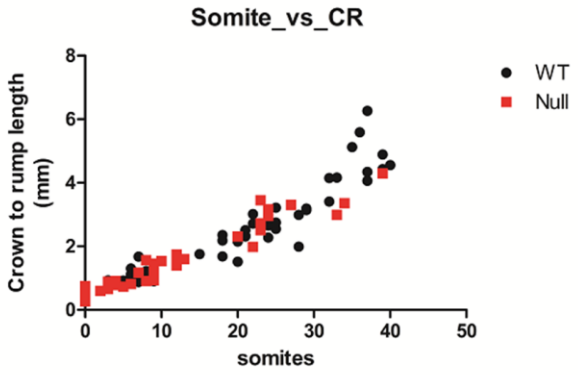

Figure 3.4 Relationship between growth and developmental progression is not disrupted in Mthfd1l nullizygous embryos. Plots of crown to rump length against somite number for individual embryos do not show difference between genotypes (●, wild-type; and ■, nullizygous embryos).

3.3.3. Deletion of *Mthfd1l* Causes Decrease in Proliferation during Late Neural Tube Closure

To assess effects of *Mthfd1l* mutation on proliferation, I compared mitotic index [phospho-histone H3 $(PHH3)^{+}$/total cells] in wild types and homozygous mutants. Cellular processes were investigated at two different somite stages: 7-13 somite stage after initiation of neural tube closure (E8.5-E8.75 for wild types and E9.5 for nullizygotes); and 18-24 somite stage after completion of neural tube closure (E9.5 for wild types and E10.5 for nullizygotes). Representative sections of PHH3 immunofluorescence staining show typical apical location of mitotic nuclei (Figure 3.5 and Figure 3.6). As shown in Figure 3.6, there was a decrease in the mitotic index of $Mthfd1l^{z/z}$ embryos at 18~24 somite stages at the time of completion of neural tube closure. The mutants showed lower proliferation at the hindbrain (two folds decrease) as well as in whole cranial regions. However, in earlier

developmental stages (7~13 somites) prior to the time of cranial neural closure, there was no significant difference in the mitotic index at the hindbrain regions between wild type and homozygous mutant embryos ($p=0.69$). The whole cranial regions also showed no difference in proliferation.

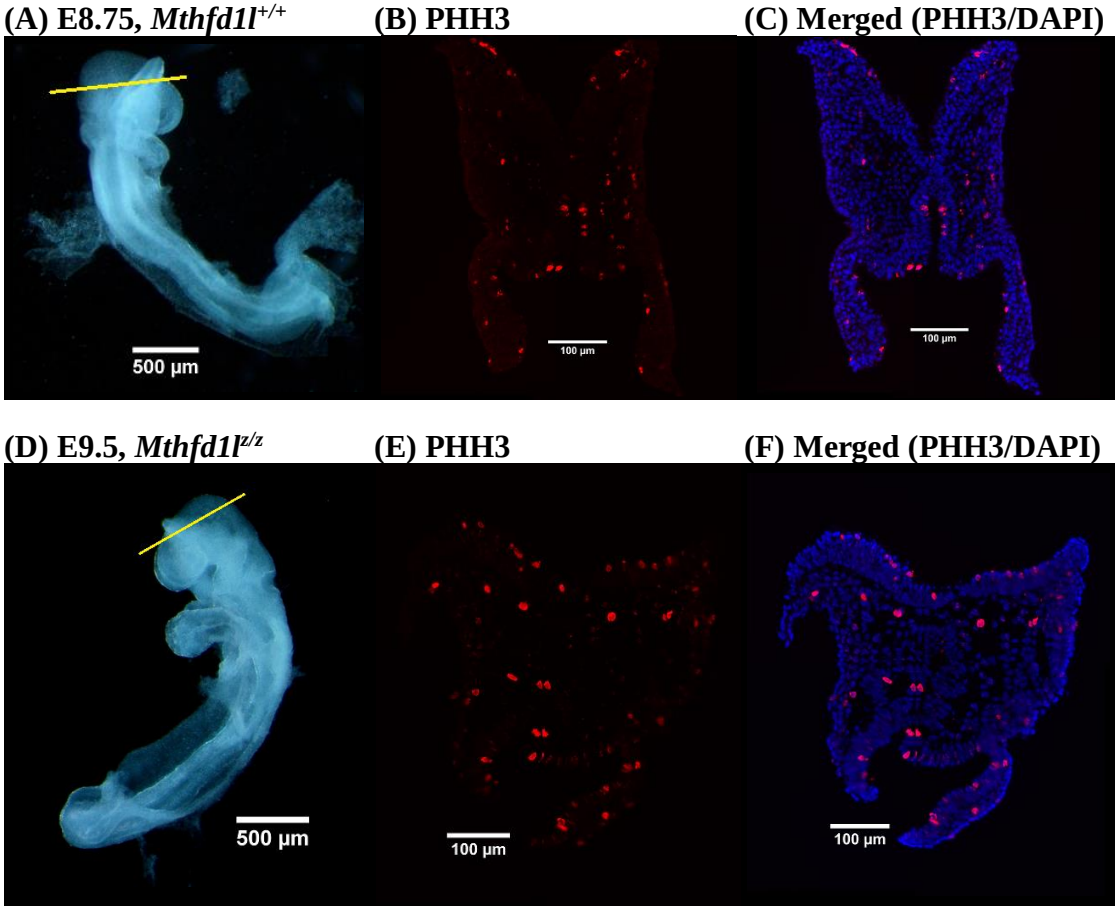

(G) Mitotic index

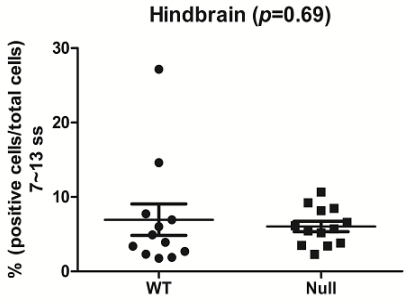

Figure 3.5 Deletion of *Mthfd1l* does not affect proliferation at 7-13 somite stages. At E8.75 (for *Mthfd1l*$^{+/+}$; A-C) and E9.5 (for *Mthfd1l*$^{z/z}$; D-F), during early cranial neural tube closure, the mitotic index (% phosphohistone H3-positive cells per total cells; G) was determined in the neuroepithelium at the developing hindbrain. Dashed line in the embryos (A and D) indicates the level of sections. Phosphohistone H3 (PHH3) staining is red and DAPI-stained nuclei are blue, shown in C and F. Mitotic index is not significantly different in the *Mthfd1l*$^{z/z}$ embryos compared with *Mthfd1l*$^{+/+}$ embryos. n = four embryos in each genotype with three to four sections analyzed per embryo. P value was calculated by Student's t-test.

(A) E9.5, *Mthfd1l*$^{+/+}$ **(B) PHH3** **(C) Merged (PHH3/DAPI)**

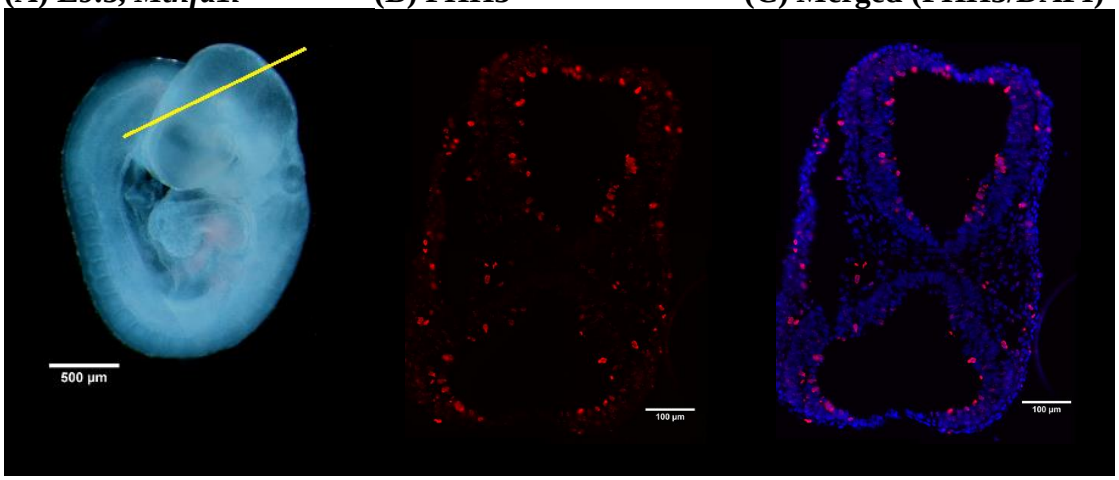

(D) E10.5, *Mthfd1l*$^{z/z}$ **(E) PHH3** **(F) Merged (PHH3/DAPI)**

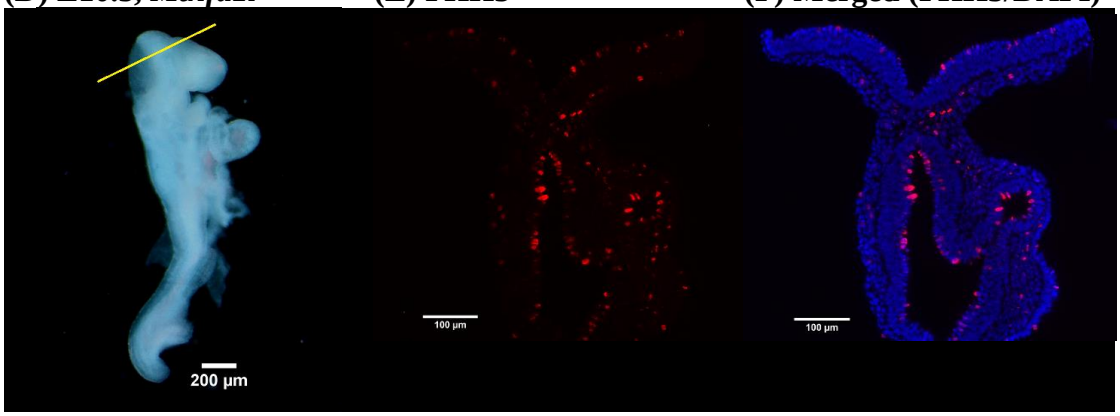

(G) Mitotic index

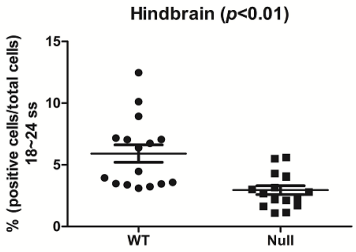

Figure 3.6 Deletion of *Mthfd1l* causes reduced proliferation at 18-24 somite stages. At E9.5 (for *Mthfd1l*$^{+/+}$; A-C) and E10.5 (for *Mthfd1l*$^{z/z}$; D-F), at the time of completion of neural tube closure, the mitotic index (% phosphohistone H3-positive cells per total cells; G) was determined in the neuroepithelium at the developing hindbrain. Dashed line in the embryos (A and D) indicates the level of sections. Phosphohistone H3 (PHH3) staining is red and DAPI-stained nuclei are blue, shown in C and F. Mitotic index is significantly different in the *Mthfd1l*$^{z/z}$ embryos compared with *Mthfd1l*$^{+/+}$ embryos. n = five wild-type and four nullizygous embryos with three to four sections analyzed per embryo. P value was calculated by Student's t-test.

To investigate whether the lower proliferation in *Mthfd1l*$^{z/z}$ embryos after the neural tube close is cell autonomous or a secondary defect, ethynyl-deoxyuridine (EdU) incorporation and PHH3 expression were measured on primary mouse embryonic fibroblast (MEF) cultures. The MEFs were grown in different growth conditions including basal medium (DMEM), minimal medium (MEM), and minimal medium with formate supplementation (MEM+F). Although *Mthfd1l*$^{z/z}$ MEFs grew slowly in the minimal medium, the EdU incorporation and the mitotic index were not different significantly between *Mthfd1l*$^{+/+}$ and *Mthfd1l*$^{z/z}$ MEFs (Table 3.2).

Table 3.2 Deletion of *Mthfd1l* does not affect proliferation in MEFs. In cultured embryonic fibroblasts, cell cycle analysis was performed using EdU incorporation for labelling cells in S-phase and phosphohistone H3 (PHH3) staining for labelling cells in mitosis. The experiment was conducted in different culture media condition: DMEM, nutrient-rich medium; MEM, nutrient-limited medium; and, MEM+F, nutrient-limited medium with formate supplementation. P value was calculated by Student's t-test.

	% EdU			% PHH3		
Media/Genotype	WT	Null	*p*	WT	Null	*p*
DMEM	19.2±2.7	25.4±3.5	0.18	16.3±6.9	19.3±5.1	0.73
MEM	27.8±2.0	32.1±4.8	0.42	17.4±6.6	16.7±5.6	0.94
MEM+F	24.5±1.9	26.6±2.0	0.46	15.1±5.7	15.8±4.4	0.92

3.3.4. Deletion of *Mthfd1l* Does Not Affect Apoptosis

To investigate the effect of loss of *Mthfd1l* on mouse neural tube closure, we examined distribution of apoptotic cells by analysis of activated caspase-3 and whole-mount TUNEL staining in the cranial region. Activated caspase-3 staining of embryos revealed the presence of apoptotic cells at the sites of dorsolateral bending of the neural plate, and at the tips of the fusing neural folds (Figure 3.7 and Figure 3.8). At 7~13 somite stages before neural tube closure, $Mthfd1l^{gt/gt}$ embryos showed slightly higher apoptotic index but it was not statistically significant (p=0.64, Figure 3.7). The number of apoptotic cells increased at the stage after neural tube closure (18~24 somite stages) by 6.1- and 3.6-fold in $Mthfd1l^{+/+}$ and $Mthfd1l^{gt/gt}$ embryos, respectively, compared to the stage before neural tube closure. However, there was no significant difference on the apoptotic index between wild types and nullizygous embryos at this stage (p=0.16, Figure 3.8). Whole-mount TUNEL staining further supported that there was no noticeable difference in apoptosis between the genotypes (Figure 3.9).

(A) E8.75, *Mthfd1l*$^{+/+}$ **(B) Caspase 3** **(C) Merged (Cas3/DAPI)**

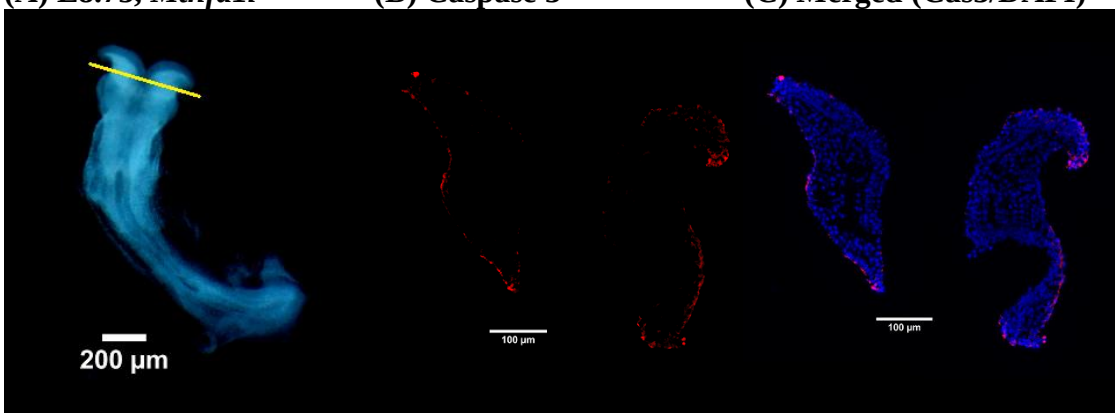

(D) E9.5, *Mthfd1l*$^{z/z}$ **(E) Caspase 3** **(F) Merged (Cas3/DAPI)**

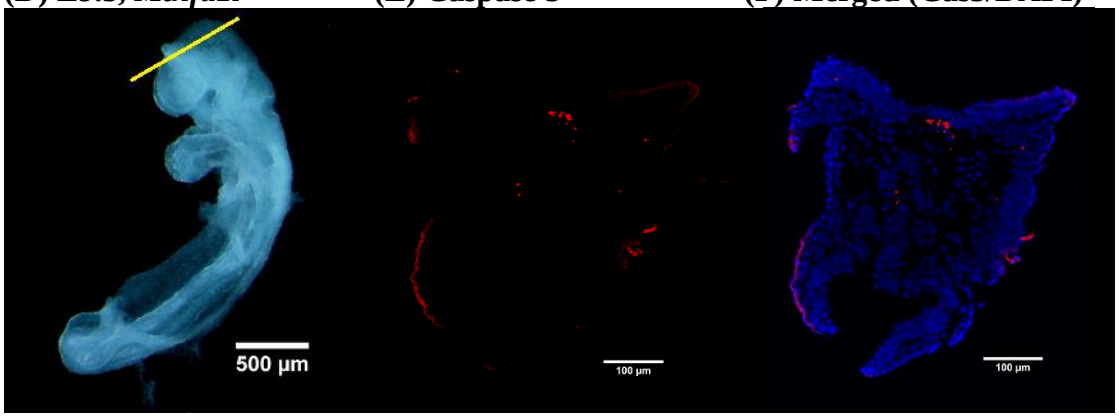

(G) Apoptotic index

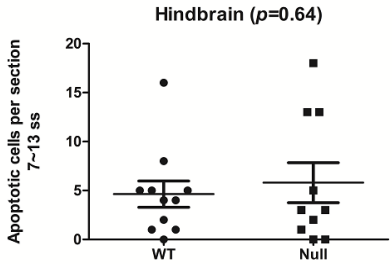

Figure 3.7 Deletion of *Mthfd1l* does not affect apoptosis at 7-13 somite stages. At E8.75 (for *Mthfd1l*$^{+/+}$; A-C) and E9.5 (for *Mthfd1l*$^{z/z}$; D-F), during early cranial neural tube closure, the apoptotic index (% cleaved caspase 3-positive cells per section; G) was determined in the whole section at the cranial region (top to the level of first branchial arch). Dashed line in the embryos (A and D) indicates the level of sections. Cleaved caspase 3 (Cas3) staining is red and DAPI-stained nuclei are blue, shown in C and F. Apoptotic index is not significantly different in the *Mthfd1l*$^{z/z}$ embryos compared with *Mthfd1l*$^{+/+}$ embryos. n = three wild-type and four nullizygous embryos with three to four sections analyzed per embryo. P value was calculated by Student's t-test.

(A) E9.5, *Mthfd1l*$^{+/+}$ **(B) Caspase 3** **(C) Merged (Cas3/DAPI)**

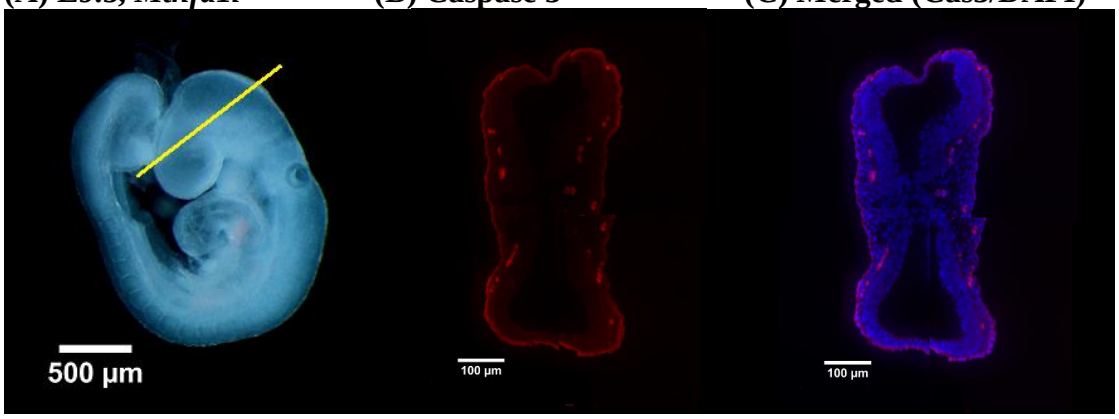

(D) E10.5, *Mthfd1l*$^{z/z}$ **(E) Caspase 3** **(F) Merged (Cas3/DAPI)**

(G) Apoptotic index

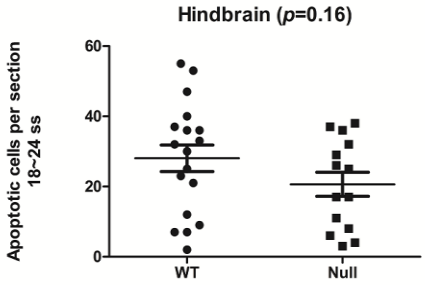

Figure 3.8 Deletion of *Mthfd1l* does not affect apoptosis at 18-24 somite stages. At E9.5 (for *Mthfd1l*$^{+/+}$; A-C) and E10.5 (for *Mthfd1l*$^{z/z}$; D-F), at the time of completion of neural tube closure, the apoptotic index (% cleaved caspase 3-positive cells per section; G) was determined in the whole section at the level of developing hindbrain (to the level of first branchial arch). Dashed line in the embryos (A and D) indicates the level of sections. Cleaved caspase 3 (Cas3) staining is red and DAPI-stained nuclei are blue, shown in C and F. Apoptotic index is not significantly different in the *Mthfd1l*$^{z/z}$ embryos compared with *Mthfd1l*$^{+/+}$ embryos. n = five wild-type and four nullizygous embryos with three to four sections analyzed per embryo. P value was calculated by Student's t-test.

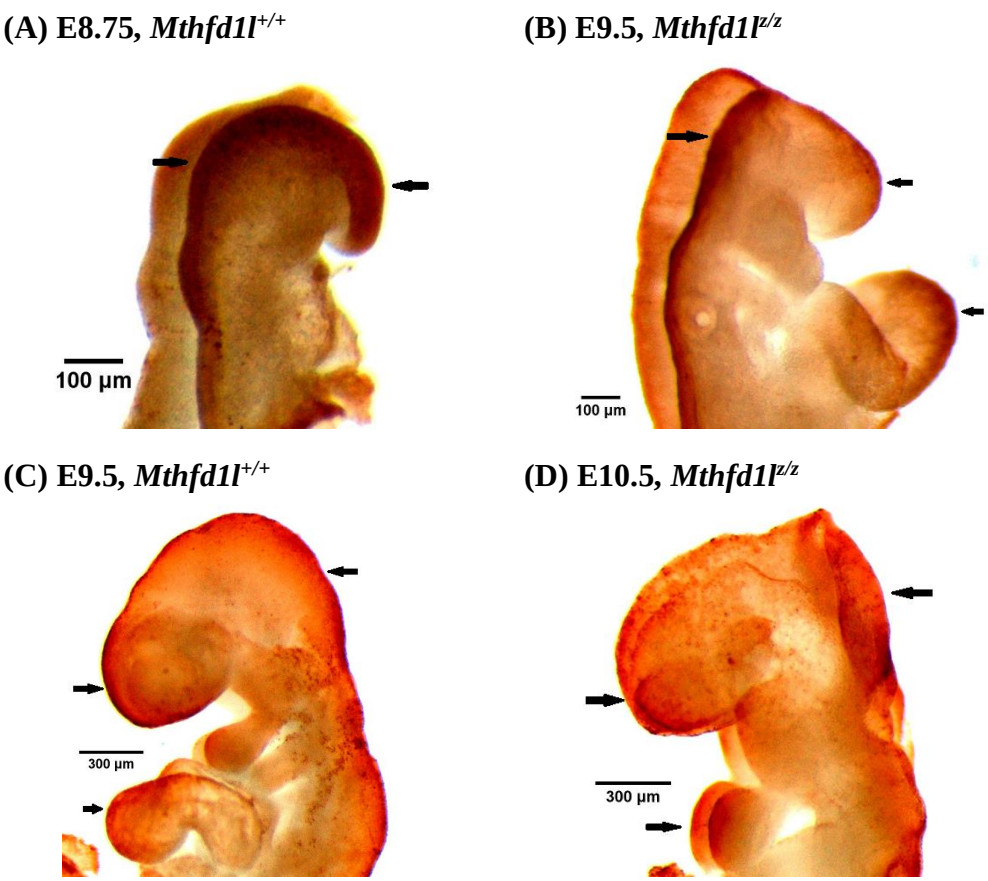

Figure 3.9 Deletion of *Mthfd1l* does not affect apoptosis during neural tube closure. Whole mount TUNEL analysis shows abundant expression of apoptotic cells in the developing forebrain, midbrain, hindbrain, the heart, and the branchial arches (arrows).

3.3.5. Deletion of *Mthfd1l* Does Not Affect Neural Crest Cell Formation

To investigate the effect of lacking MTHFD1L on mouse neural tube closure, I examined expression of markers for neural crest cells, *Sox9* and *FoxD3*, by whole-mount *in-situ* hybridization during the process of neural tube closure. *Sox9*, a number of the family of Sox (Sry-type high-mobiity-group box) genes containing transcription factors, regulates neural crest development (Wright et al., 1995). It is expressed in the prospective neural crest and its expression precedes expression of premigratory neural crest markers (Cheung & Briscoe, 2003). Whole-mount *in-situ* hybridization shows expression of *Sox9* in the developing hindbrain, otocyst, and within the cephalic mesenchyme tissue at 7-13 somite stages (Figure 3.10). It was also expressed in some surface ectodermal cells overlying the spinal cord. Compared to wild type embryos, the nullizygous embryos showed no significant difference in the expression of this gene. Further immunofluorescence examination using anti-Sox9 antibody confirmed that both genotypes expressed Sox9 in similar way (Figure 3.11). At 18-24 somite stages, *Sox9* was expressed in the first branchial arch, otocyst, somites, and within the forebrain. The expression pattern of *Sox9* in *Mthfd1l*$^{z/z}$ embryos was similar to the wild type embryos. Although *Sox9* was expressed clearly in each somite of the wild type, its expression was not distinctively separated in somites of the nullizygotes. It may result from abnormal somite formation in the nullizygous embryos by loss of MTHFD1L or somite degeneration by embryonic death at this stage. But, currently the reason in unknown.

(A) E8.75, *Mthfd1l*$^{+/+}$ **(B) E9.5, *Mthfd1l*$^{z/z}$**

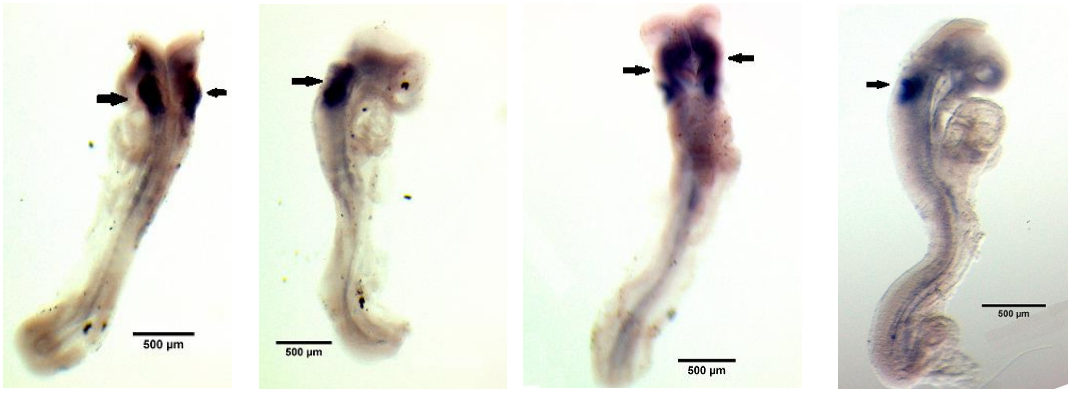

(C) E9.5, *Mthfd1l*$^{+/+}$ **(D) E10.5, *Mthfd1l*$^{z/z}$**

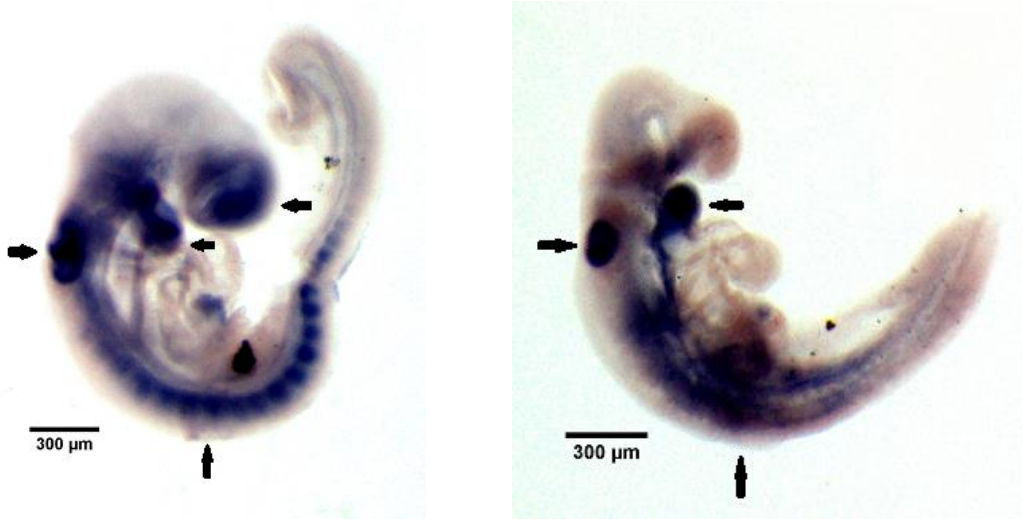

Figure 3.10 Deletion of *Mthfd1l* does not affect neural crest cell formation during neural tube closure. Whole mount *in-situ* hybridization for *Sox9* shows expression of premigratory and migrating neural crest cells in the developing forebrain, head mesenchyme, somites, and the branchial arches (arrows).

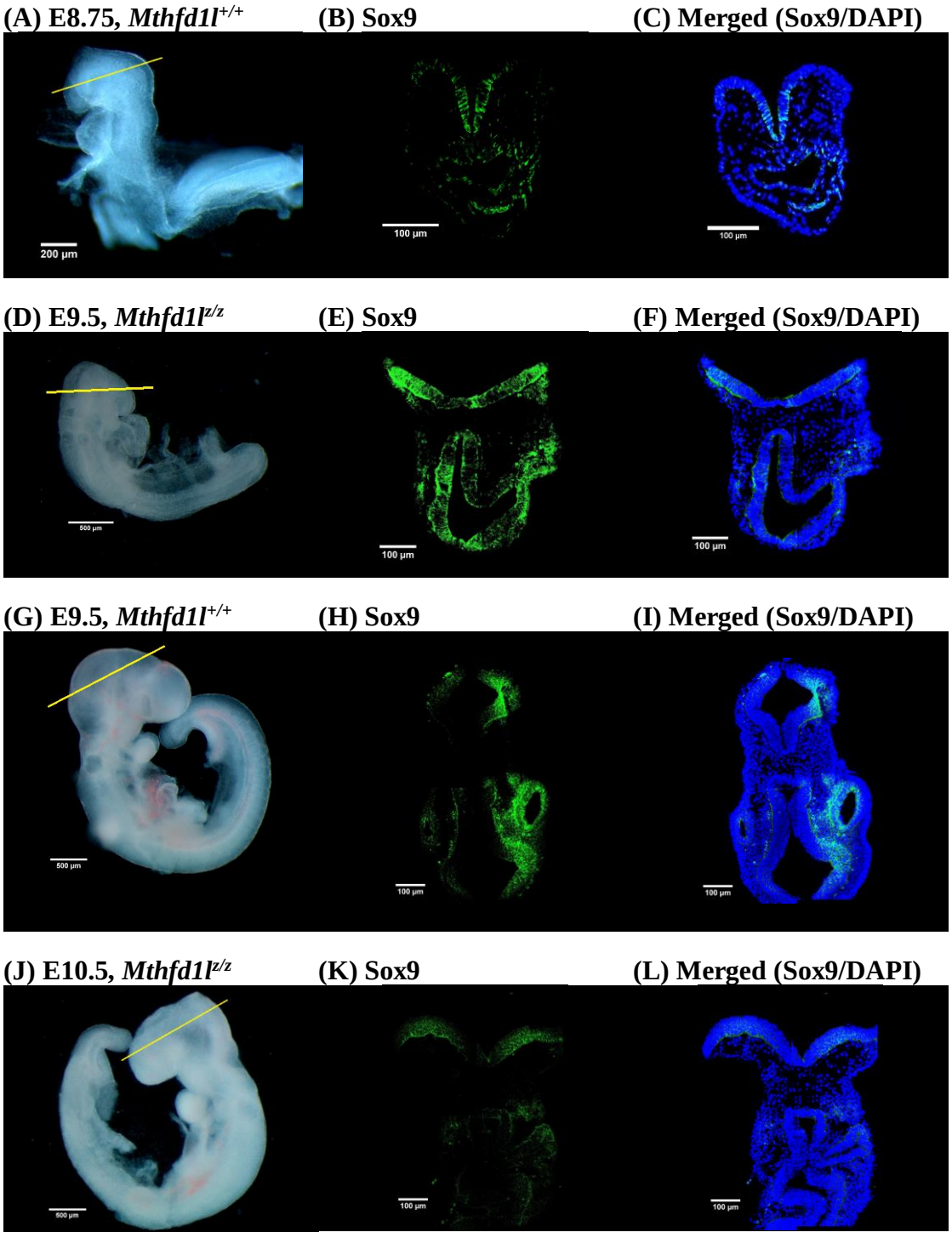

Figure 3.11 Deletion of *Mthfd1l* does not affect neural crest cell formation during neural tube closure. Immunofluorescence staining against Sox9 shows expression of neural crest cells in the developing forebrain and at the edge of neural plate in the hindbrain.

FoxD3, a member of the winged-helix class of transcription factors, is involved in the segregation of the neural crest lineage from the neuroepithelium (Kos, Reedy, Johnson, & Erickson, 2001). *FoxD3* is expressed transiently in neural crest cells prior to delamination (Cheung & Briscoe, 2003). Whole-mount *in-situ* hybridization show expression of *FoxD3* in the dorsal neural tube, otocyst, and some surface ectodermal cells overlying the spinal cord, similarly to the expression of *Sox9* at 7-13 somite stages (Figure 3.12). There was no significant difference in the expression of *FoxD3* in both genotypes. At 18-24 somite stages, *FoxD3* was extensively expressed in trigeminal ganglion and vestibular-acoustic ganglion, and posterior dorsal neural tube. The expression of *FoxD3* was similar between the two genotypes, confirming that neural crest cell formation is not affected by loss of MTHFD1L.

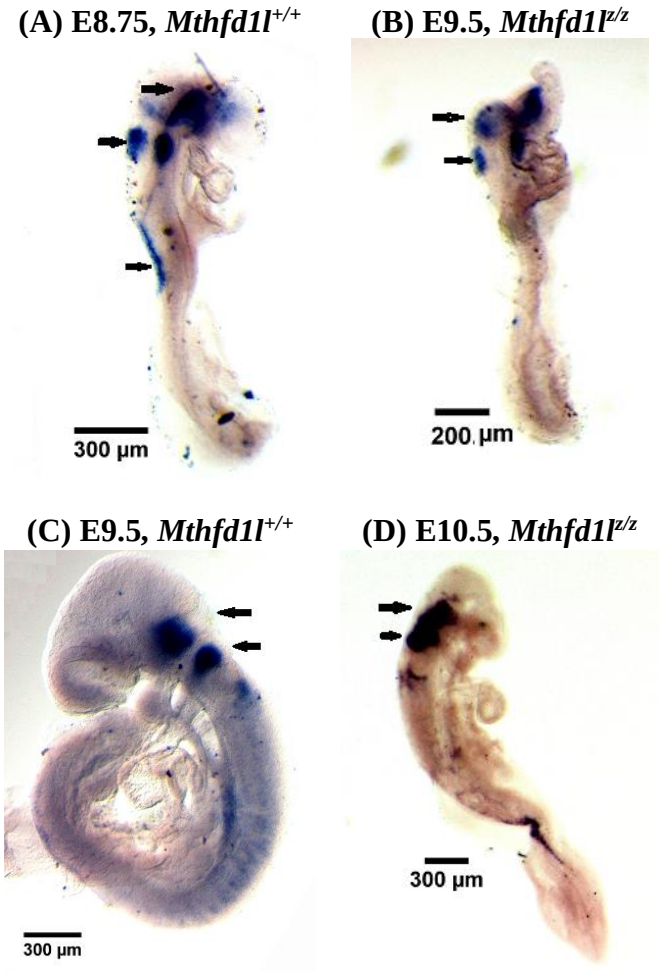

Figure 3.12 Deletion of *Mthfd1l* does not affect neural crest cell formation during neural tube closure. Whole mount *in-situ* hybridization for *FoxD3* shows expression of premigratory neural crest cells in the dorsal neural tube, otocyst, surface ectodermal cells overlying the spinal cord, trigeminal ganglion and vestibular-acoustic ganglion (arrows).

3.3.6. Deletion of *Mthfd1l* Causes Defect in Head Mesenchyme Development during early NTC

From the experiments investigating cellular processes (section 3.3.3-3.3.5), interestingly, I observed a failure of neural fold elevation and abnormal head mesenchyme formation in *Mthfd1l* mutant embryos at 7-13 somite stages. Although my analysis on cellular processes in *Mthfd1l* mutant embryos suggest a decrease in proliferation at the time of completion of neural tube closure, it is still unclear if there is a cellular process affected by mutation of *Mthfd1l* that precedes the event of neural tube closure.

In order to determine if the abnormal organization of head mesenchyme in *Mthfd1l* mutant embryos occurs before cranial neural tube closure, the head mesenchyme was examined at 7-13 somite stages (at E8.75 for $Mthfd1l^{+/+}$ and E9.5 for $Mthfd1l^{z/z}$ embryos). Transverse sections of embryos were stained for nuclei with DAPI and cell density in the head mesenchyme was quantified. As shown in Figure 3.13, the head mesenchyme in the nullizygous embryos is abnormal and appears to be sparser around the neural plate, especially underneath the neural plate. Quantification of the cell density in the head mesenchyme supported the abnormal head mesenchyme formation, showing decreased cell density underlying the neural plate (center area) as well as around the lateral edges of neural plate (lateral area) in the mutant embryos. Also, the center area seemed more affected by the mutation compared with the lateral area. As a result, total mesenchyme density was lower in the mutant embryos.

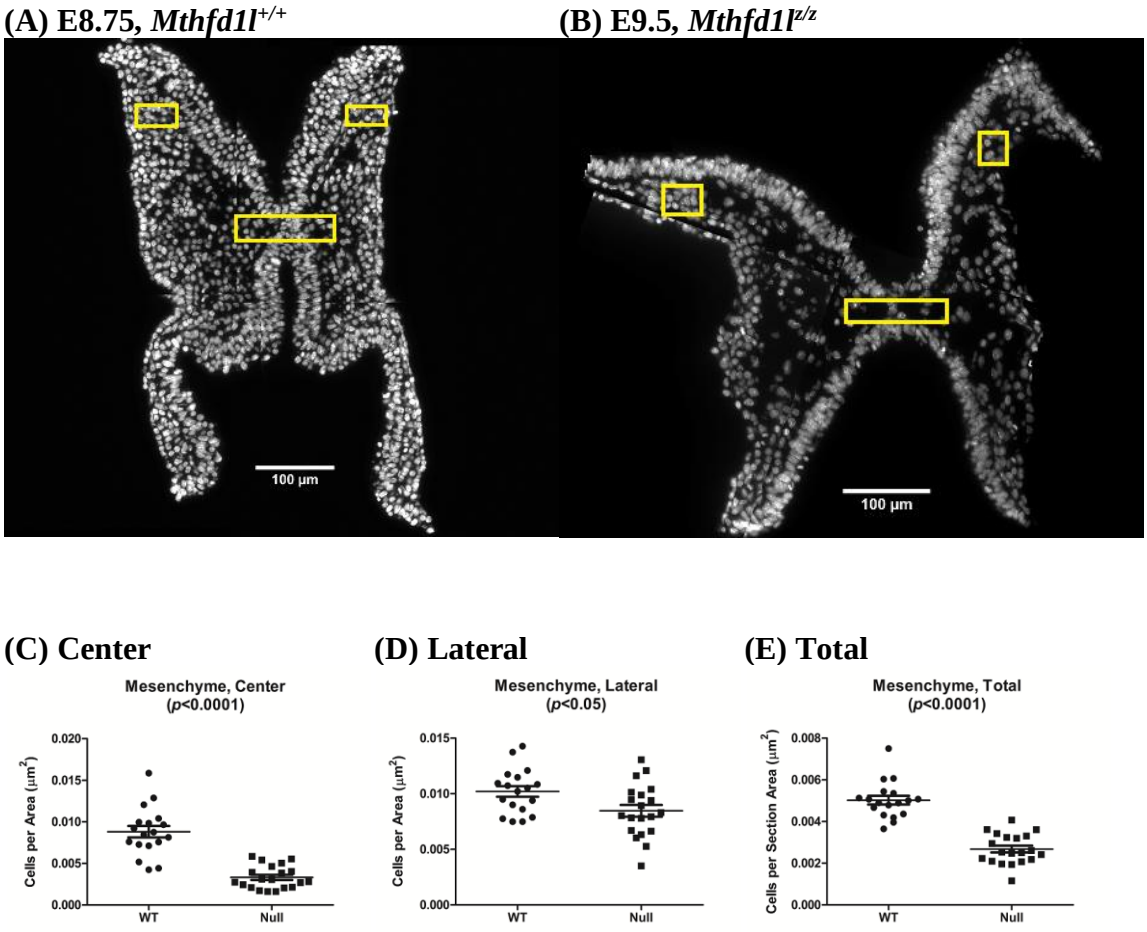

Figure 3.13 Deletion of *Mthfd1l* causes reduced head mesenchyme density at 7-13 somite stages. Representative transverse sections of wild type and nullizygous embryos at E8.75 (A) and E9.5 (B), respectively, show reduction in number of mesenchymal cells in the cranial region, especially underneath the neural plate. Head mesenchyme density is significantly different in the center area, later area (boxed region), as well as the total mesenchyme. n = eight embryos in wild type and nine embryos in nullizygotes with two to three sections analyzed per embryo. P value was calculated by Student's t-test.

To determine if the sparse head mesenchyme results from a change in proliferation, expression of phosphohistone H3 (PHH3) was examined in the mesenchyme at 7-13 somite stages (Figure 3.14). The mitotic index in the head mesenchyme of *Mthfd1l*$^{z/z}$ embryos were not significantly different compared with *Mthfd1l*$^{+/+}$ embryos, indicating there is no difference in proliferation of the abnormal head mesenchyme surrounding the neural tube.

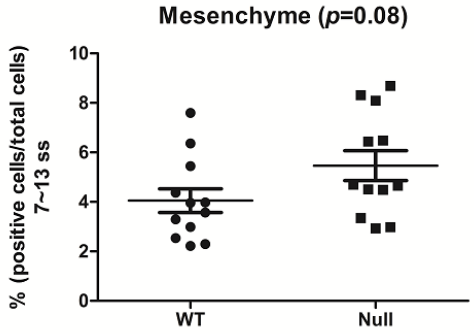

Figure 3.14 Deletion of *Mthfd1l* does not affect proliferation of mesenchymal cells at 7-13 somite stages. At E8.75 (for *Mthfd1l*$^{+/+}$) and E9.5 (for *Mthfd1l*$^{z/z}$), during early cranial neural tube closure, the mitotic index (% phosphohistone H3-positive cells per total cells) was determined in the mesenchyme. Mitotic index is not significantly different in the *Mthfd1l*$^{z/z}$ embryos compared with *Mthfd1l*$^{+/+}$ embryos. n = four embryos in each genotype with three to four sections analyzed per embryo. P value was calculated by Student's t-test.

3.3.7. Formate Supplementation Improves Disrupted Cellular Processes

Because disruption of *Mthfd1l* is expected to result in loss of mitochondrial formate production, maternal supplementation with sodium formate decreases the incidence of NTDs and partially improves the growth delay in embryos lacking *Mthfd1l* (Momb et al., 2013). However, still there is no information on the effects of formate supplementation on *Mthfd1l* mutant mouse embryos during neural tube closure (E8.5 to E9.5). In this study, to investigate the effects of formate supplementation on specific cellular processes in *Mthfd1l* mutant embryos, pregnant dams were given water containing calcium formate at a dose of 2,500 $mg \cdot kg^{-1} \cdot d^{-1}$ and cellular processes of embryos were analyzed during neural tube closure. It is noteworthy that calcium formate, not sodium formate, was given to the dams because calcium formate showed better outcomes for prevention of NTDs than sodium formate (data not shown; Jessica Momb).

As reported previously (Momb et al., 2013), maternal formate supplementation partially rescued growth defects (Table 3.3). The genotype distribution does not differ significantly from the expected Mendelian ratio (P = 0.70). Compared with nulls from unsupplemented dams having 96 % of open neural tube at E9.5, formate supplementation partially improved both neural tube closure (21 % of nulls exhibited a closed neural tube) and the growth defect (Table 3.3). Although the nullizygous embryos still had high a percentage of open neural tube, gross morphologic comparison of embryos from formate supplemented dams showed no significant difference between *Mthfd1l*$^{+/+}$ and *Mthfd1l*$^{z/z}$ embryos, except for smaller size of the nulls (Figure 3.15). This suggests that the high percentage of open neural tube possibly resulted from slightly slower growth of the mutant embryos compared to wild type embryos (mean of somite numbers: 22 versus 18 in wild type and nulls, respectively; Figure 3.16).

Table 3.3 Maternal formate supplementation improves delayed embryonic growth and partially prevents defective neural tube closure in *Mthfd1l* nullizygous embryos. Numbers of somites in *Mthfd1l*$^{z/z}$ were statistically lower compared to *Mthfd1l*$^{+/+}$ only at E9.5 ($p<0.001$; asterisk indicates significant difference to *Mthfd1l*$^{+/+}$ by t-test). Number of embryos showing partially or completely open neural tube in the head were counted.

Age	Genotype	Dams	Embryos	Somites (mean±std)	Neural tube open (Embryos)
E8.75	*Mthfd1l*$^{+/+}$	3	4	8.5±2.6	100 % (4)
	Mthfd1l$^{z/+}$	3	16	7.4±3.4	100 % (16)
	Mthfd1l$^{z/z}$	3	8	4.6±3.8	100 % (8)
E9.5	*Mthfd1l*$^{+/+}$	8	17	21.9±3.1	12 % (2)
	Mthfd1l$^{z/+}$	9	35	19.8±4.8	31 % (11)
	Mthfd1l$^{z/z}$	7	14	17.6±3.2*	79 % (11)

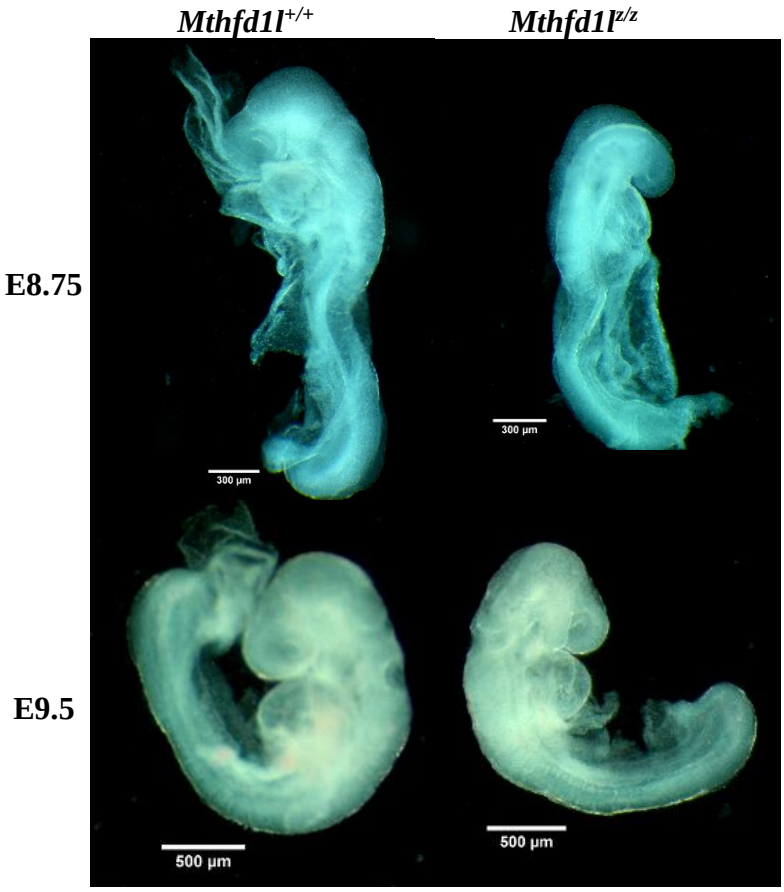

Figure 3.15 Maternal formate supplementation improves abnormal morphology of *Mthfd1l* nullizygous embryos. Supplemented *Mthfd1l*$^{z/z}$ embryos have similar morphology with *Mthfd1l*$^{+/+}$ embryos.

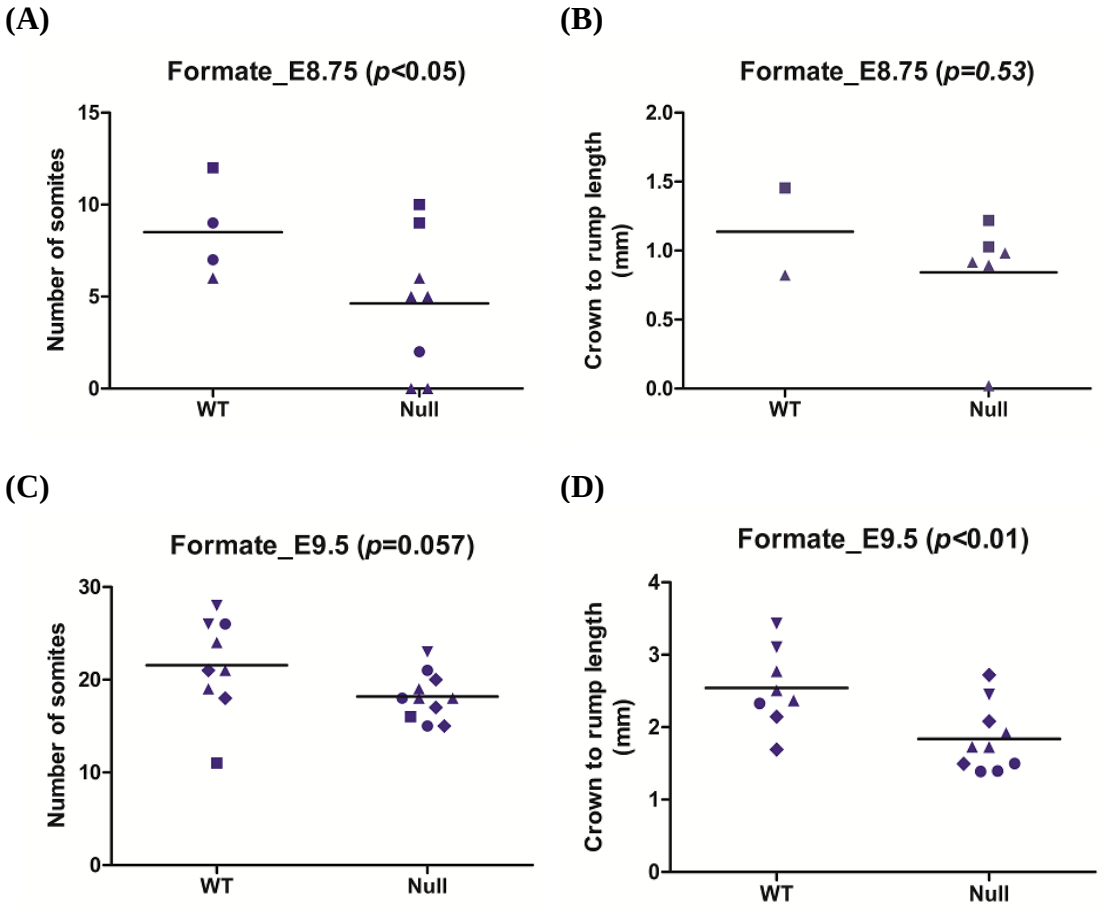

Figure 3.16 Maternal formate supplementation improves delayed embryonic growth in *Mthfd1l* nullizygous embryos. Number of somites (A, C, and E) and crown to rump length (B, D, and F) were similar in the both genotypes. Each type of symbol represents littermates. P value was calculated by Student's t-test.

The preceeding experiments reveal that loss of *Mthfd1l* causes a decrease in proliferation of neuroepithelial cells at 18-24 somite stages and a decrease in head mesenchyme density at 7-13 somite stages. In order to examine if maternal formate supplementation corrects these dysregulated cellular processes in the mutant embryos, cell proliferation at E9.5 and head mesenchyme density at E8.75 were analyzed in the formate-supplemented embryos. As shown in Figure 3.17, formate-supplemented wild type and nullizygous embryos showed the same mitotic index ($p=0.58$), confirming that formate supplementation rescued the proliferation defect. Also, formate-supplemented nulls showed improved development of head mesenchyme in center and later areas as well as in total sections (Figure 3.18).

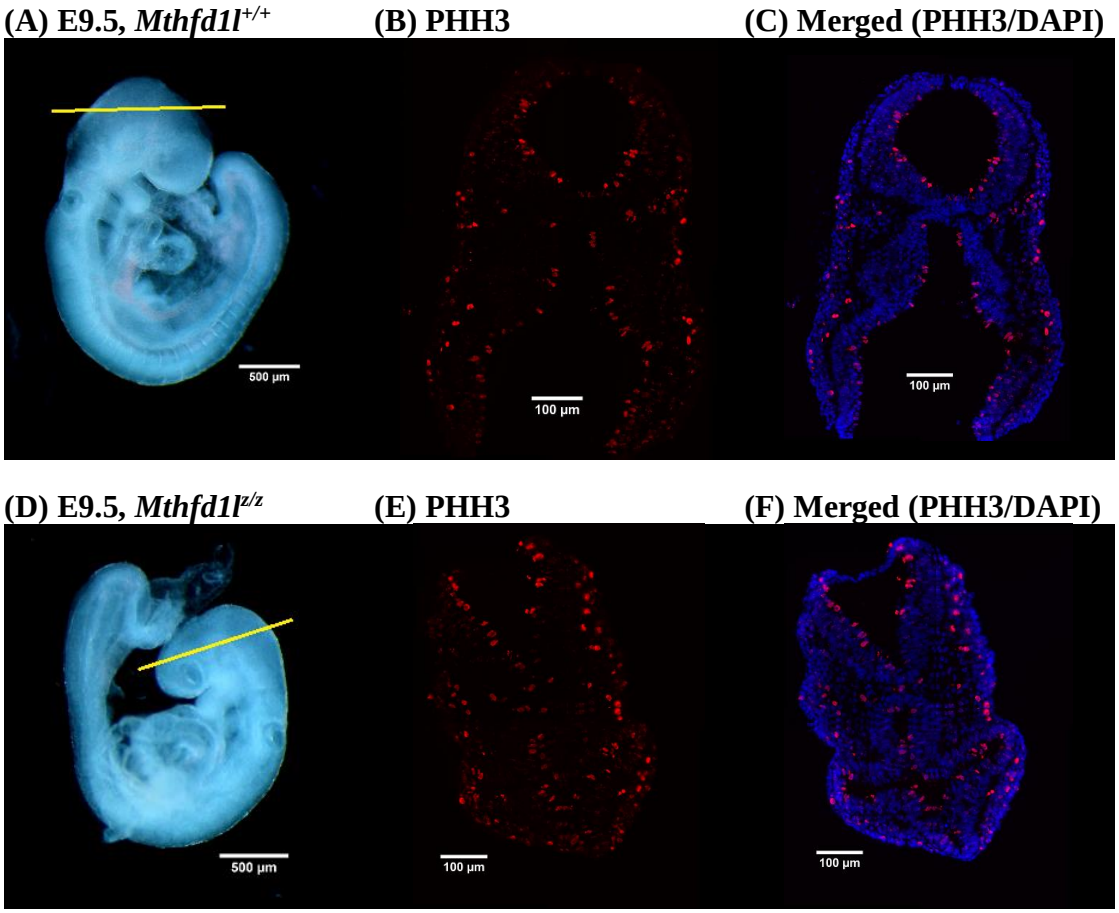

Figure 3.17 Maternal formate supplementation improves reduced proliferation of *Mthfd1l* mutant embryos at 18-24 somite stages (E9.5). The mitotic index (% phosphohistone H3-positive cells per total cells; G) was determined in the neuroepithelium at the developing hindbrain. Dashed line in the embryos (A and D) indicates the level of sections. Phosphohistone H3 (PHH3) staining is red and DAPI-stained nuclei are blue, shown in C and F. Mitotic index is not significantly different in the *Mthfd1l*$^{z/z}$ embryos compared with *Mthfd1l*$^{+/+}$ embryos. n = three embryos for both genotypes with two to four sections analyzed per embryo. P value was calculated by Student's t-test.

(A) E8.75, *Mthfd1l*$^{z/z}$

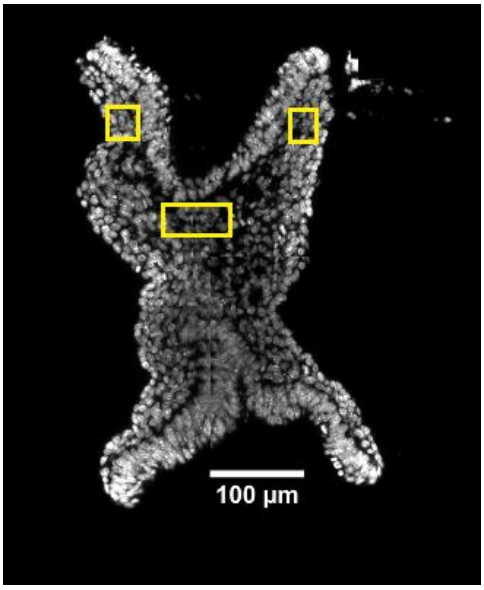

(C) Center

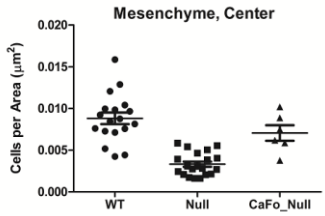

(D) Lateral

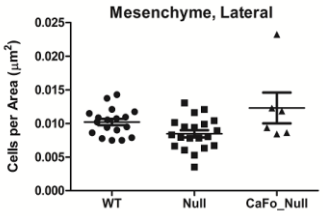

(E) Total

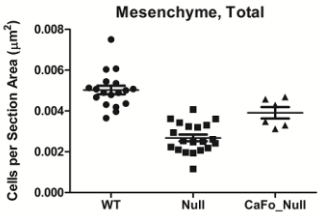

Figure 3.18 Maternal formate supplementation improves reduced head mesenchyme density in *Mthfd1l* mutant embryos at 7-13 somite stages. Representative transverse section of nullizygous embryos at E8.75 (A) show normal mesenchyme in the cranial region, especially underneath the neural plate. Head mesenchyme density is not significantly different in the center area, later area (boxed region), as well as the total mesenchyme. n = two embryos in formate-supplemented nullizygotes with three sections analyzed per embryo. P value was calculated by Student's t-test.

3.4. DISCUSSION

In this study, I have shown that the *Mthfd1l* gene is expressed ubiquitously throughout embryogenesis during neural tube closure, and significantly detected at the basal surface of the dorsal neuroepithelium. Loss of *Mthfd1l* causes retardation in growth and developmental progression. *Mthfd1l*$^{z/z}$ embryos show defects in proliferation during late neural tube closure and head mesenchyme development during early neural tube closure. However, proliferation during early neural tube closure, apoptosis, and neural crest cell migration were not affected by the loss of *Mthfd1l*. Finally, I show that maternal formate supplementation significantly improves the dysregulated cellular processes in *Mthfd1l*$^{z/z}$ embryos.

3.4.1. Proliferation

The fundamental question of how folate can prevent neural tube defects has been asked for the past 45 years, but an answer is still not clear. The most probable explanation about the role of folate may be promoting cell proliferation. Cell multiplication has an important role in neural tube closure (Copp et al., 2013), and folate is central to numerous cellular reactions including production of purines and thymidylate, encouraging the hypothesis on a key effect of folate for enhanced cell proliferation. Based on this hypothesis, my study reveals a lower rate of cellular proliferation in the cranial neural folds of *Mthfdl* mutant embryos at E9.5 (18-24 somites). This result is consistent with several publications showing reduced cellular proliferation by mutating genes or inhibiting enzyme activities in 1C metabolism at the time of E9.0 to E11.5 after neural tube closure (Dong et al., 2014; Pai et al., 2015; Tang, Santillano, Wlodarczyk, Miranda, & Finnell, 2005; Wang et al., 2014).

However, to the best of my knowledge, there are no reports on cell proliferation before/during neural tube closure with regard to 1C metabolism. I show here that cellular proliferation was not different between the two genotypes at E8.75 (7-13 somites) before neural tube closure. Tuckett and Morriss-Kay reported that differential proliferation does not play a role in the mechanisms for cranial neural tube closure at early embryonic stages in the rat (4-16 somites) (Tuckett & Morriss-Kay, 1985). A constant cell number and cell cycle time were found in the midbrain/hindbrain neural epithelium during the stages. Therefore, the lack of difference in cell proliferation at the early stage could be associated with the pre-differentiation and pre-specialization state of the neural plate during the cranial neurulation.

The reduced cellular proliferation after neural tube closure in *Mthfd1l* mutant embryos may be explained as 1) a primary effect causing failure of cranial neural folds which is incompatible with closure in the hindbrain, although permissive for closure in the forebrain and midbrain; or 2) a secondary effect caused by other dysregulated cellular processes. EdU incorporation in MEFs showed no difference between the two genotypes, suggesting a possible secondary effect. However, since the MEFs are mostly derived from mesodermal tissues, it is uncertain that the MEFs exhibit identical phenotype to the embryos *in vivo* (Yusuf et al., 2013). Also, *Mthfd1l*$^{-/-}$ nullizygotes showed no difference in proliferation compared to the wild-types in head mesenchyme, further supporting the MEFs might not be a good representative of whole embryos. Therefore, still it is unclear whether the reduced proliferation is cell autonomous or a secondary effect resulted from other processes, in the mutant mouse models of 1C metabolism.

3.4.2. Apoptosis

Apoptosis has long been observed in the non-neural surface ectoderm and the neuroepithelium during the neural tube closure (Fuchs & Steller, 2011; Lawson, Schoenwolf, England, Addai, & Ahima, 1999). From a study in chick embryos, it was suggested that apoptosis may have a functional role in neural tube closure (Weil, Jacobson, & Raff, 1997). Also, mice lacking intrinsic apoptotic pathway genes (*apaf-1, caspase-9,* and *caspase-3*) exhibit cranial neural tube defects (Honarpour et al., 2000; Kuida et al., 1998; Massa et al., 2009). By contrast, chemically inhibiting apoptosis does not affect prevent initiation or progression of neural tube closure, suggesting that apoptosis is not required for mammalian neural tube closure (Massa et al., 2009).

Association of apoptosis with 1C metabolism was reported in several studies, while the role of folate on apoptosis is still unclear. Tang et al., 2005 showed significantly increased numbers of apoptotic cells in embryos with the Folbp1 mutation (Tang et al., 2005). (Dong et al., 2014; Guan et al., 2015; Xu et al., 2016) showed that treatment with 1C metabolism inhibitors (raltitrexed, hydroxyurea, and methotrexate) increased apoptosis and decreased proliferation. These studies argue that apoptosis-mediated cell death may result in the reduction in the proliferative capacity of mitotic neural tube precursors. On the other hand, maternal folate deficiency or supplementation does not affect apoptosis in some mouse models (Barbera et al., 2002; D. Li & Rozen, 2006). My studies with the *Mthfd1l* mutant mouse model also showed that apoptosis is not affected by *Mthfd1l* mutation during the process of neural tube closure. It is not yet clear how folate and 1C metabolism mediate apoptosis, but it seems that folate may compensate for the negative effect on neural tube closure caused by other processes rather than inhibiting cell death directly.

3.4.3. Head Mesenchyme

The cranial neural plate is surrounded mainly by the head mesenchyme, which is a type of tissue composed of loosely associated cells that lack polarity and are surrounded by a large extracellular matrix. During elevation of the cranial neural folds in mammalian embryos, the head mesenchyme undergoes expansion with cell proliferation and a marked increase in the extracellular space (Copp et al., 2003). Proper head mesenchymal cell behavior has been suggested as an important factor to regulate cranial NTC. Mutant embryos lacking genes expressed in the head mesenchyme, such as *Twist* (twist homolog 1), *Cart1* (cartilage homeo ptotein 1), *Alx3* (aristaless-like homeobox 3), and *Hectd1* (HECT domain containing 1) have exencephaly, showing abnormal head mesenchyme density around the neural folds (Chen & Behringer, 1995; Lakhwani, García-Sanz, & Vallejo, 2010; Zhao, Behringer, & de Crombrugghe, 1996; Zohn et al., 2007). These mutant embryos also display a defect in dorsolateral hinge point formation in the cranial neural tube, but not in a medial hinge point formation. Importantly, while the caudal neural fold elevation does not accompany expansion of the mesenchyme, cranial neurulation seems to be highly dependent on proliferation and expansion of the cranial mesenchyme (Copp et al., 2003).

In the present study, loss of *Mthfd1l* in mouse embryos was associated with decrease in head mesenchyme density (Figure 3.13). However, proliferation in the mesenchyme was not affected by the mutation. Until now, association of head mesenchyme with folate metabolism is unknown except for a report from Dunlevy et al. (Dunlevy, Burren, Mills, et al., 2006). In their study, inhibition of methylation cycle by inhibitors of methionine adenosyl transferase reduced density of cranial mesenchyme in the inhibitor-treated embryos developing exencephaly. However, my work is the first reporting cranial mesenchyme abnormalities in mutant embryos lacking genes in folate-mediated 1C

metabolism. Surprisingly, among four mouse models having defects in the head mesenchyme (*Twist, Cart1, Alx3*, and *Hectd1*), NTDs by *Cart1* mutation are prevented by folate supplementation (Zhao et al., 1996). In addition, embryos from dams fed a folic acid-deficient diet had significantly reduced levels of Alx3 mRNA, resulting in failure of cranial neural tube closure (Lakhwani et al., 2010). Effects of supplementation on *Twist* and *Hectd1* mutant mouse models are unknown yet. These results strongly support that folate metabolism (as well as one-carbon metabolism) may have a crucial role in head mesenchyme development.

3.4.4. Neural Crest Cells and Paraxial Mesoderm

The head mesenchyme primarily originates from a mixture of cranial neural crest cells and head mesoderm (paraxial mesoderm) cells. In the head region, neural crest cells form elements of the peripheral nervous system, connective tissues and the cartilage, while the paraxial mesoderm forms the craniofacial muscles, some skeletal elements and vascular tissues (Trainor & Tam, 1995). Neural crest cells start detaching from the apices of the neural folds and migrate during neural tube closure. The neural crest cells are considered to have an important role in regulating mammalian cranial neurulation (Copp, 2005), although it is still controversial whether neural crest formation is necessary for the completion of neural tube closure or cranial neural tube closure is not required for normal migration of the neural crest. Paraxial mesoderm originates from the primitive streak and migrates to the anterior region of the embryo underlying the presumptive neural plate (Zohn & Sarkar, 2012). Paraxial mesoderm also has a key role in neural fold elevation by expansion of extracellular matrix surrounding the paraxial mesoderm cells.

My results show that loss of *Mthfd1l* results in defective head mesenchyme density, but does not affect neural crest cell migration. In the head mesenchyme, the density of cells in the center area underlying the neural plate seemed to be severely affected by the *Mthfd1l* mutation, whereas the density in the lateral area close to the tip of the neural folds only slightly decreased in the mutant embryos. High expression of MTHFD1L in the first branchial arch and limb buds also supports a possible association of MTHFD1L in anterior paraxial mesoderm compared with neural crest cells. Thus, from numerous lines of evidence, I conclude that head mesenchyme, specifically paraxial mesoderm, is a primary site of *Mthfd1l* gene action. To verify the defects on development of paraxial mesoderm and possibly on extracellular matrix formation, further experiments such as *Mesp1* labelling or alcian blue staining will be required.

3.4.5. Formate Supplementation

MTHFD1L catalyzes mitochondrial formate production in one-carbon metabolism. Mitochondrial formate provides 1C units in the cytoplasm for purine and thymidylate biosynthesis as well as the universal methylation cycle. Since *Mthfd1l* mutation affects mitochondrial formate production, it is expected that maternal formate supplementation may replace the formate in the cytoplasm. As expected, maternal formate supplementation ameliorated growth defects, neural tube defects, proliferation defects, and mesenchyme defects derived by lack of MTHFD1L. Most importantly, loss of *Mthfd1l* causes a defect in head mesenchyme formation due to cellular formate deficiency and formate supplementation corrects the abnormality of mesenchyme development.

Based on the current study, I propose a model that summarizes the possible relationship between MTHFD1L expression and neural tube closure in hindbrain

development (Figure 3.19). I propose that MTHFD1L, responsible for mitochondrial formate production, is highly expressed in neuroepithelium and underlying paraxial mesoderm. High density of mesenchymal cells support elevation of neural plates and formation of dorsolateral hinge points. However, inactivation of the *Mthfd1l* gene results in reduced mesenchymal density, leading to inadequate physical forces acting on the neural plates to elevate, ultimately resulting in failure of neural tube closure. Interestingly, expansion of the mesenchyme (specifically paraxial mesoderm) does not accompany neural fold elevation in the spinal region (Ybot-Gonzalez et al., 2002), and experimental removal of the paraxial mesoderm fails to block the spinal neural tube closure (Van Straaten et al., 1993). This model of possible involvement of MTHFD1L in head mesenchyme development is consistent with our observation that MTHFD1L mutation causes exencephaly but not spina bifida.

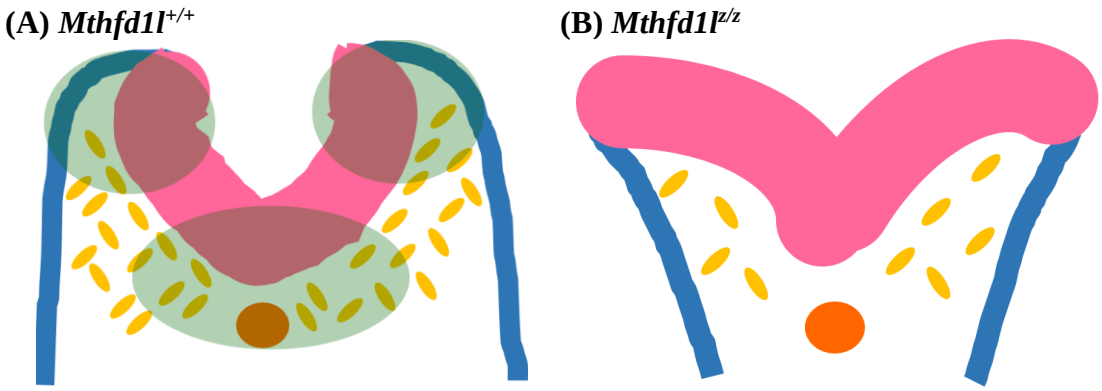

Figure 3.19 Schematic illustration of the cranial mesenchyme during neural fold elevation. Normal elevation of neural plates and formation of dorsolateral hinge point are supported by head mesenchymal cells in wild type embryos (A). Apposition and fusion of neural plates are failed in *Mthfd1l* nullizygotes (B). Neuroepithelium, surface ectoderm, mesenchyme and notochord are shown in pink, blue, yellow and orange, respectively. Green shading in panels indicates MTHFD1L expression.

How does mitochondrially-derived formate (thus, folate-mediated one-carbon metabolism) affect head mesenchyme development? One possibility is its association with the methylation cycle. Dunlevy et al reported that disruption in the methylation cycle by inhibitors (ethionine and cycloleucine) or excessive methionine cause reduction in head mesenchyme density (Dunlevy, Burren, Mills, et al., 2006; Dunlevy, Burren, Chitty, Copp, & Greene, 2006). Since more than 75 % of one-carbon units that enter the cytoplasmic methyl cycle are from mitochondrially-derived formate (Pike et al., 2010), the loss of *Mthfd1l* may cause aberrant methylation. Numerous genes encoding cytoskeletal proteins are methylated in the stage of neurulation, it is therefore possible that altered regulation of cytoskeletal proteins through the disruption of methylation could influence the neural tube closure. Further analysis on methylation cycle and cytoskeletal proteins on the *Mthfd1l* mutant embryos will be required in order to verify the association.

Another possibility of the effect of mitochondrial formate on the head mesenchyme development is its association with the extracellular matrix surrounding the mesenchyme. Extracellular matrix composes of collagen and glycosaminoglycans including hyaluronic acid. Collagen, the most abundant animal protein, is a major structural protein in the extracellular matrix, playing a critical role in neural tube closure (Sertié et al., 2000). Its polypeptide contains glycine as an every third amino acid (~ 33 % of the residues). Altered one-carbon metabolism affects serine and glycine metabolism, and it is expected that *Mthfd1l* mutation may change cellular glycine level. Further experimental studies including collagen staining and alcian blue staining for glycosaminoglycans are required to verify the role of extracellular matrix during neural tube closure.

Chapter 4. Summary AND Conclusions

4.1. SUMMARY

MTHFD2 and MTHFD2L are homologous enzymes, catalyzing the reaction of mitochondrial 5,10-methylene-THF oxidation to 10-formyl-THF. The experiments described in this dissertation demonstrate that the mammalian MTHFD2L isozyme, like MTHFD1 and MTHFD2, possesses both CH_2-THF dehydrogenase and CH^+-THF cyclohydrolase activities. The dehydrogenase activity of both MTHFD2 and MTHFD2L isozymes exhibit a higher preference for NAD^+ with monoglutamylated THF substrate than $NADP^+$. However, in the physiological CH_2-THF range, these enzyme were more active with $NADP^+$ than with NAD^+, suggesting dual cofactor specificity *in vivo*. This dual cofactor specificity was further verified by higher NADP+-preference with polyglutamylated THF substrate. Phylogenetic analysis implicates that MTHFD2L may be evolved from invertebrate MTHFD2, originally from a primitive fungal MTHFD1.

MTHFD1L, mitochondrial 10-formyl-THF synthetase, is a mono-functional enzyme catalyzing the final step in the mammalian mitochondrial pathway to formate. The *Mthfd1l* gene is expressed ubiquitously throughout embryogenesis during neural tube closure, and significantly detected at the basal surface of the dorsal neuroepithelium. Loss of *Mthfd1l* causes retardation in growth and developmental progression. Nullizygous embryos of *Mthfd1l* KO mice show defects in proliferation during late neural tube closure and head mesenchyme development during early neural tube closure, while proliferation during early neural tube closure, apoptosis, and neural crest cell migration were not affected by loss of the gene. Maternal formate supplementation significantly improves the dysregulated cellular processes in *Mthfd1l*$^{-/-}$ embryos.

4.2. CONCLUSIONS AND FUTURE DIRECTIONS

This dissertation demonstrates that mammalian mitochondrial MTHFD2 and MTHFD2L possess quite similar enzymatic characteristics including bifunctional dehydrogenase/cyclohydrolase activities, redox cofactor specificity, and unique requirement of specific ions (Mg^{2+} and P_i), except with the higher dehydrogenase activity of MTHFD2. Considering different expression profile of the two genes, *Mthfd2* (expressed only during embryogenesis) and *Mthfd2l* (expressed during late stages of embryogenesis and in adult tissues), this current study suggests that mammals have evolved sophisticated system of the two isozymes to tightly regulate flux through the mitochondrial pathway in response to changing metabolic conditions and needs. Characterization of MTHFD2 and MTHFD2L from this dissertation provides complete understanding of mammalian one-carbon metabolism in embryos as well as in adults, filling a gap in the mitochondrial pathway. This work also will be important for developing therapeutics against redox cofactor-associated birth defects as well as diseases in adults. To verify the redox cofactor specificity of the enzymes *in vivo*, further experiments such as overexpression/knockout of the genes in mammalian system will be required to compare mitochondrial redox cofactors production by MTHFD2 and MTFHD2L.

MTHFD1L is a critical enzyme in mitochondrial 1C metabolism, catalyzing the reaction of formate production. This current study first reports that proliferation during the early stages of neural tube closure is not affected by the mutation in the 1C metabolism, while head mesenchyme development is reduced by the loss of MTHFD1L. Formate supplementation rescues the abnormal head mesenchyme development. Identification of cellular processes associated with MTHFD1L from this dissertation provides the role of the mitochondrial 1C metabolism in the cranial mesenchyme development. Considering association of folate supplementation with various mesenchyme-related birth defects

including orofacial defects, congenital heart defects, and limb malformation, this work will be helpful for understanding mechanisms and developing therapeutics of the defects. To verify the origin of defects on mesenchyme (paraxial mesoderm and possibly extracellular matrix formation), further experiments such as *Mesp1* labelling or alcian blue staining will be required.

Appendix A: A Protocol of Rat MTHFD2L Purification

* Strain: *S. cerevisiae* MWY4.4

* Growth: Yeast minimal media at 30˚C, final OD 3~4

→ Centrifuge at 8000 x g, 5 min, 4˚C

→ Store at -80˚C

1) Cell lysis (2 ml/g wet cell weight)

- Buffer composition: 25 mM Tris-Cl (pH 7.5), 1% sodium carbonate (app. 100 mM), 10 mM BME, 1 mM PMSF (pH 10~11), protease inhibitor cocktail (1 tablet/10 ml)
- Cell disruption by glass beads
- Incubate for 30 min at 4˚C
- Centrifuge at 30,000 x g for 30 min at 4˚C

2) Dialysis

- Buffer composition: 25 mM Tris-Cl, 10 mM BME, 1 mM PMSF, 20% glycerol, 500 mM KCl (final pH 8.5, 4˚C)
- Use 100 ml of dialysis buffer per 1 ml of cell lysate
- Overnight

3) Column preparation

- Resin: 8~9 ml per 15 ml of the dialysate (usually from 4 L culture)
- Strip buffer (0.5 M NaCl, 100 mM EDTA, 20 mM Tris-HCl, pH 7.9)
  : 2 volume of column volume (CV)
- Water: 5 volume of CV

- 50 mM $NiSO_4$: 10 volume of CV

- Binding buffer: 5 volume of CV

4) Binding

- Buffer composition: 25 mM Tris-Cl, 20 mM imidazole, 10 mM BME, 1 mM PMSF, 20% glycerol, 500 mM KCl (final pH 8.5, 4˚C)

- Batch mode (incubation for 3 hours at 4˚C)

- Mix resin + dialysate + same volume of binding buffer (containing 40 mM imidazole)

5) Washing

- Buffer composition: 25 mM Tris-Cl, 60 mM imidazole, 10 mM BME, 1 mM PMSF, 10% isopropanol, 500 mM KCl (final pH 8.5, RT)

- 40 volume of CV

6) Elution

- Buffer composition: 25 mM Tris-Cl, 250 mM imidazole, 10 mM BME, 1 mM PMSF, 20% glycerol, 500 mM KCl (final pH 8.5, 4˚C)

- 4~5 volume of CV

Appendix B: A Protocol of Immunohistochemistry

1) Paraformaldehyde fixation

- Place dissected embryos in labeled glass vials.
- Fill vials with freshly prepared 4 % PFA fixative, 4 °C.
- Allow fixation to proceed at 4'C for 20 min (for E7.5 and E8.5), 1.5 hr (for E9.5 and E10.5), or 3 hr (for E12.5).

2) Sucrose infusion and freezing

- Wash samples twice in PBS.
- Infuse samples in 30% sucrose in PBS until tissue sinks (overnight).
- Incubate the embryos on a rocking platform in a 1:1 mixture of OCT and 30% sucrose/PBS for 30 minutes.
- Prepare dry ice/100% ethanol mixture.
- Transfer the embryos to an embedding mold containing OCT. Orient the embryos as desired.
- Freeze the cryomold in the ethanol slurry (Float the mold boat).
- Wrap samples in labeled foil and store at -80 °C
- Put samples at -20 °C for 30 min before cryosectioning.

3) Cryosectioning

- Describe orientation of the sample in a mold.
- Thickness: 7 um
- Air dry at least 30 min

4) Setting up slides

- Layer wet paper towels in a moist chamber.
- Remove slides with sections from freezer and place in moist chamber so that the slides do not touch one another.
- Once slides are at room temperature, rinse sections with PBST (0.5 % Triton x-100 in PBS) for 2 x 2 min. Do not flood the slides.
- Draw a circle on the slide around the tissue with a hydrophobic barrier pen or use rubber cement.

5) Blocking

- Block any non-specific binding by incubating the tissue sections with 5% serum in PBS-T for 30 minutes at room temperature.

6) Incubation with primary antibody

- Add primary antibody diluted in 1% serum PBS-T and incubate overnight at 4 °C (desired dilution for specific antibody, 75ul/slide, 1 drop/section).
- Wash sections twice with 1% serum PBS-T for 10 minutes each.

7) Incubation with secondary antibody (Alexa-488/555)

- Dilute secondary antibody in 1% serum PBS-T and incubate with sections at room temperature for 1 hour in dark (1:200, 75 ul/slide, 1drop/section).
- Wash sections twice with 1% serum PBS-T for 10 minutes each.
- Tap off excess wash and apply one drop of anti-fade mounting medium (vectashield+DAPI) to the slide.

Appendix C: A Protocol of Whole Mount TUNEL Assay

1) Paraformaldehyde fixation

- Place dissected embryos in labeled glass vials.
- Fill vials with freshly prepared 4 % PFA fixative, 4 °C.
- Allow fixation to proceed at 4 °C for 20 min (for E7.5 and E8.5), 1.5 hr (for E9.5 and E10.5), or 3 hr (for E12.5).
- Wash samples twice in PBS at room temp.
- Dehydrate samples in (25 % methanol/PBS > 50 % methanol/PBS > 80 % methanol/PBS > 100 % methanol) for 15 min each at room temp.
- Samples can be stored at -20 °C for 6 months

2) Rehydration

- Rehydrate samples in (80 % methanol/PBS > 50 % methanol/PBS > 25 % methanol/PBS > PBS) for 15 min each at room temp (1 ml each).
- Post-fix in pre-cooled ethanol:acetic acid (2:1) for 20 min at -20 °C (1 ml).
- Wash in PBS twice for 5 min each (1 ml each).
- Quench in 3 % hydrogen peroxide in PBS for 20 min at room temp (1 ml).
- Wash in PBS twice for 5 min each (1 ml each).

3) Equlibration and TdT incubation

- Gently tap off excess liquid.
- Immediately apply equilibration buffer (50 ul).
- Incubate for at least 1 min at room temp.
- Gently tap off excess liquid.

- Immediately add TdT enzyme (50 ul, diluted, reaction buffer:TdT enzyme, 7:3 (35 ul + 15 ul), stored on ice used in 6 hours)
- Incubate at 37 °C overnight.
- Gently tap off excess liquid.
- Immediately add stop/wash buffer (350 ul/embryo, diluted, stop buffer:dH_2O, 1:34, stored at 4 °C).
- Incubate for 1 hr at room temp.

4) Antibody incubation
- Wash in PBS three times for 1 min each (1 ml each).
- Gently tap off excess liquid.
- Immediately add anti-digoxigenin-peroxidase conjugate (50 ul).
- Incubate at 4 °C overnight.

5) Development
- Wash in PBS four times for 2 min each.
- Immediately add peroxidase substrate (250 ul 1% DAB + 250 ul 0.3% H_2O_2 in 5 ml PBS, pH 7.2)
- Stain until color developed at room temp (50 seconds).
- Wash in dH_2O three times for 1 min each.
- Incubate in dH_2O for 5 min at room temp.
- Further section the embryo and counterstain in methyl green.

References

Albe, K. R., Butler, M. H., & Wright, B. E. (1990). Cellular concentrations of enzymes and their substrates. *Journal of Theoretical Biology*, *143*(2), 163–195.

Angelakopoulou, A., Shah, T., Sofat, R., Shah, S., Berry, D. J., Cooper, J., … Hingorani, A. D. (2012). Comparative analysis of genome-wide association studies signals for lipids, diabetes, and coronary heart disease: Cardiovascular Biomarker Genetics Collaboration. *European Heart Journal*, *33*(3), 393–407.

Appling, D. R., & West, M. G. (1997). Monofunctional NAD-dependent 5,10-methylenetetrahydrofolate dehydrogenase from Saccharomyces cerevisiae. *Methods in Enzymology*, *281*, 178–188.

Atta, C. A. M., Fiest, K. M., Frolkis, A. D., Jette, N., Pringsheim, T., St Germaine-Smith, C., … Metcalfe, A. (2016). Global Birth Prevalence of Spina Bifida by Folic Acid Fortification Status: A Systematic Review and Meta-Analysis. *American Journal of Public Health*, *106*(1), e24-34. https://doi.org/10.2105/AJPH.2015.302902

Barbera, J. P. M., Rodriguez, T. A., Greene, N. D. E., Weninger, W. J., Simeone, A., Copp, A. J., … Dunwoodie, S. (2002). Folic acid prevents exencephaly in Cited2 deficient mice. *Human Molecular Genetics*, *11*(3), 283–293.

Barlowe, C. K., & Appling, D. R. (1990). Isolation and characterization of a novel eukaryotic monofunctional NAD(+)-dependent 5,10-methylenetetrahydrofolate dehydrogenase. *Biochemistry*, *29*(30), 7089–7094.

Beaudin, A. E., Abarinov, E. V., Malysheva, O., Perry, C. A., Caudill, M., & Stover, P. J. (2012). Dietary folate, but not choline, modifies neural tube defect risk in Shmt1 knockout mice. *The American Journal of Clinical Nutrition*, *95*(1), 109–114.

Beaudin, A. E., Abarinov, E. V., Noden, D. M., Perry, C. A., Chu, S., Stabler, S. P., … Stover, P. J. (2011). Shmt1 and de novo thymidylate biosynthesis underlie folate-responsive neural tube defects in mice. *The American Journal of Clinical Nutrition*, *93*(4), 789–798.

Bettembourg, C., Diot, C., & Dameron, O. (2015). Optimal Threshold Determination for Interpreting Semantic Similarity and Particularity: Application to the Comparison of Gene Sets and Metabolic Pathways Using GO and ChEBI. *PLOS ONE*, *10*(7), e0133579.

Blakley, R. L. (1957). The interconversion of serine and glycine; preparation and properties of catalytic derivatives of pteroylglutamic acid. *The Biochemical Journal*, *65*(2), 331–342.

Bolusani, S., Young, B. A., Cole, N. A., Tibbetts, A. S., Momb, J., Bryant, J. D., … Appling, D. R. (2011). Mammalian MTHFD2L Encodes a Mitochondrial Methylenetetrahydrofolate Dehydrogenase Isozyme Expressed in Adult Tissues. *Journal of Biological Chemistry*, *286*(7), 5166–5174.

Chen, Z. F., & Behringer, R. R. (1995). twist is required in head mesenchyme for cranial neural tube morphogenesis. *Genes & Development*, *9*(6), 686–699.

Cheung, M., & Briscoe, J. (2003). Neural crest development is regulated by the transcription factor Sox9. *Development*, *130*(23), 5681–5693.

Christensen, K. E., Deng, L., Leung, K. Y., Arning, E., Bottiglieri, T., Malysheva, O. V., … Rozen, R. (2013). A novel mouse model for genetic variation in 10-formyltetrahydrofolate synthetase exhibits disturbed purine synthesis with impacts on pregnancy and embryonic development. *Human Molecular Genetics*, *22*(18), 3705–3719.

Christensen, K. E., Mirza, I. A., Berghuis, A. M., & MacKenzie, R. E. (2005). Magnesium and Phosphate Ions Enable NAD Binding to Methylenetetrahydrofolate Dehydrogenase-Methenyltetrahydrofolate Cyclohydrolase. *Journal of Biological Chemistry*, *280*(40), 34316–34323.

Christensen, K. E., Patel, H., Kuzmanov, U., Mejia, N. R., & MacKenzie, R. E. (2005). Disruption of the mthfd1 gene reveals a monofunctional 10-formyltetrahydrofolate synthetase in mammalian mitochondria. *The Journal of Biological Chemistry*, *280*(9), 7597–7602.

Claros, M. G., & Vincens, P. (1996). Computational method to predict mitochondrially imported proteins and their targeting sequences. *European Journal of Biochemistry*, *241*(3), 779–786.

Copp, A. J. (2005). Neurulation in the cranial region--normal and abnormal. *Journal of Anatomy*, *207*(5), 623–635.

Copp, A. J., Greene, N. D. E., & Murdoch, J. N. (2003). The genetic basis of mammalian neurulation. *Nature Reviews Genetics*, *4*(10), 784–793.

Copp, A. J., Stanier, P., & Greene, N. D. E. (2013). Neural tube defects: recent advances, unsolved questions, and controversies. *The Lancet. Neurology*, *12*(8), 799–810.

Coppedè, F. (2009). The complex relationship between folate/homocysteine metabolism and risk of Down syndrome. *Mutation Research*, *682*(1), 54–70.

Corkey, B. E., Duszynski, J., Rich, T. L., Matschinsky, B., & Williamson, J. R. (1986). Regulation of free and bound magnesium in rat hepatocytes and isolated mitochondria. *The Journal of Biological Chemistry*, *261*(6), 2567–2574.

Curthoys, N. P., & Rabinowitz, J. C. (1971). Formyltetrahydrofolate synthetase. Binding of adenosine triphosphate and related ligands determined by partition equilibrium. *The Journal of Biological Chemistry*, *246*(22), 6942–6952.

Dereeper, A., Guignon, V., Blanc, G., Audic, S., Buffet, S., Chevenet, F., … Gascuel, O. (2008). Phylogeny.fr: robust phylogenetic analysis for the non-specialist. *Nucleic Acids Research*, *36*(Web Server issue), W465-469.

De-Regil, L. M., Peña-Rosas, J. P., Fernández-Gaxiola, A. C., & Rayco-Solon, P. (2015). Effects and safety of periconceptional oral folate supplementation for preventing birth defects. *The Cochrane Database of Systematic Reviews*, (12), CD007950.

Di Pietro, E., Sirois, J., Tremblay, M. L., & MacKenzie, R. E. (2002). Mitochondrial NAD-dependent methylenetetrahydrofolate dehydrogenase-methenyltetrahydrofolate cyclohydrolase is essential for embryonic development. *Molecular and Cellular Biology*, *22*(12), 4158–4166.

Di Pietro, E., Wang, X.-L., & MacKenzie, R. E. (2004). The expression of mitochondrial methylenetetrahydrofolate dehydrogenase-cyclohydrolase supports a role in rapid cell growth. *Biochimica Et Biophysica Acta*, *1674*(1), 78–84.

Dihazi, H., Kessler, R., & Eschrich, K. (2001). One-step purification of recombinant yeast 6-phosphofructo-2-kinase after the identification of contaminants by MALDI-TOF MS. *Protein Expression and Purification*, *21*(1), 201–209.

Dong, Y., Wang, X., Zhang, J., Guan, Z., Xu, L., Wang, J., … Niu, B. (2014). Raltitrexed's effect on the development of neural tube defects in mice is associated with DNA damage, apoptosis, and proliferation. *Molecular and Cellular Biochemistry*, 1–9.

Ducker, G. S., & Rabinowitz, J. D. (2016). One-Carbon Metabolism in Health and Disease. *Cell Metabolism*.

Dunlevy, L. P. E., Burren, K. A., Chitty, L. S., Copp, A. J., & Greene, N. D. E. (2006). Excess methionine suppresses the methylation cycle and inhibits neural tube closure in mouse embryos. *FEBS Letters*, *580*(11), 2803–2807.

Dunlevy, L. P. E., Burren, K. A., Mills, K., Chitty, L. S., Copp, A. J., & Greene, N. D. E. (2006). Integrity of the methylation cycle is essential for mammalian neural tube closure. *Birth Defects Research Part A: Clinical and Molecular Teratology*, *76*(7), 544–552.

Eichholzer, M., Tönz, O., & Zimmermann, R. (2006). Folic acid: a public-health challenge. *Lancet (London, England)*, *367*(9519), 1352–1361.

Eskes, T. K. a. B. (2006). Abnormal folate metabolism in mothers with Down syndrome offspring: review of the literature. *European Journal of Obstetrics, Gynecology, and Reproductive Biology*, *124*(2), 130–133.

Eto, I., & Krumdieck, C. L. (1982). Determination of three different pools of reduced one-carbon-substituted folates. III. Reversed-phase high-performance liquid chromatography of the azo dye derivatives of p-aminobenzoylpoly-gamma-glutamates and its application to the study of unlabeled endogenous pteroylpolyglutamates of rat liver. *Analytical Biochemistry*, *120*(2), 323–329.

Fan, J., Ye, J., Kamphorst, J. J., Shlomi, T., Thompson, C. B., & Rabinowitz, J. D. (2014). Quantitative flux analysis reveals folate-dependent NADPH production. *Nature*, *510*(7504), 298–302.

Fox, J. T., & Stover, P. J. (2008). Folate-mediated one-carbon metabolism. *Vitamins and Hormones*, *79*, 1–44.

Franceschini, N., Carty, C., Bůzková, P., Reiner, A. P., Garrett, T., Lin, Y., … Heiss, G. (2011). Association of genetic variants and incident coronary heart disease in multiethnic cohorts: the PAGE study. *Circulation. Cardiovascular Genetics*, *4*(6), 661–672.

Fuchs, Y., & Steller, H. (2011). Programmed cell death in animal development and disease. *Cell*, *147*(4), 742–758.

Geelen, J. A., & Langman, J. (1977). Closure of the neural tube in the cephalic region of the mouse embryo. *The Anatomical Record*, *189*(4), 625–640.

Gietz, R. D., & Woods, R. A. (2002). Transformation of yeast by lithium acetate/single-stranded carrier DNA/polyethylene glycol method. *Methods in Enzymology*, *350*, 87–96.

Goh, Y. I., Bollano, E., Einarson, T. R., & Koren, G. (2006). Prenatal multivitamin supplementation and rates of congenital anomalies: a meta-analysis. *Journal of Obstetrics and Gynaecology Canada: JOGC = Journal D'obstétrique et Gynécologie Du Canada: JOGC*, *28*(8), 680–689.

Golden, J. A., & Chernoff, G. F. (1993). Intermittent pattern of neural tube closure in two strains of mice. *Teratology*, *47*(1), 73–80.

Guan, Z., Wang, X., Dong, Y., Xu, L., Zhu, Z., Wang, J., … Niu, B. (2015). dNTP deficiency induced by HU via inhibiting ribonucleotide reductase affects neural tube development. *Toxicology*, *328*, 142–151.

Harris, M. J. (2009). Insights into prevention of human neural tube defects by folic acid arising from consideration of mouse mutants. *Birth Defects Research. Part A, Clinical and Molecular Teratology*, *85*(4), 331–339.

Harris, M. J., & Juriloff, D. M. (2010). An update to the list of mouse mutants with neural tube closure defects and advances toward a complete genetic perspective of neural tube closure. *Birth Defects Research Part A: Clinical and Molecular Teratology*, *88*(8), 653–669.

Hasegawa, T., Mikoda, N., Kitazawa, M., & LaFerla, F. M. (2010). Treatment of Alzheimer's disease with anti-homocysteic acid antibody in 3xTg-AD male mice. *PloS One*, *5*(1), e8593.

Hibbard, E., & Smithells, R. W. (1965). FOLIC ACID METABOLISM AND HUMAN EMBRYOPATHY. *The Lancet*, *285*(7398), 1254.

Honarpour, N., Du, C., Richardson, J. A., Hammer, R. E., Wang, X., & Herz, J. (2000). Adult Apaf-1-deficient mice exhibit male infertility. *Developmental Biology*, *218*(2), 248–258.

Horne, D. W., Patterson, D., & Cook, R. J. (1989). Effect of nitrous oxide inactivation of vitamin B12-dependent methionine synthetase on the subcellular distribution of folate coenzymes in rat liver. *Archives of Biochemistry and Biophysics*, *270*(2), 729–733.

Hubacek, J. A., Staněk, V., Gebauerová, M., Poledne, R., Aschermann, M., Skalická, H., … Pitˇha, J. (2015). Rs6922269 marker at the MTHFD1L gene predict cardiovascular mortality in males after acute coronary syndrome. *Molecular Biology Reports*, *42*(8), 1289–1293.

Jain, M., Nilsson, R., Sharma, S., Madhusudhan, N., Kitami, T., Souza, A. L., … Mootha, V. K. (2012). Metabolite Profiling Identifies a Key Role for Glycine in Rapid Cancer Cell Proliferation. *Science*, *336*(6084), 1040–1044.

Jaquier, M., Klein, A., & Boltshauser, E. (2006). Spontaneous pregnancy outcome after prenatal diagnosis of anencephaly. *BJOG: An International Journal of Obstetrics & Gynaecology*, *113*(8), 951–953.

Kallen, R. G., & Jencks, W. P. (1966). The mechanism of the condensation of formaldehyde with tetrahydrofolic acid. *The Journal of Biological Chemistry*, *241*(24), 5851–5863.

Kennedy, R. B., Ovsyannikova, I. G., Pankratz, V. S., Haralambieva, I. H., Vierkant, R. A., & Poland, G. A. (2012). Genome-wide analysis of polymorphisms associated

with cytokine responses in smallpox vaccine recipients. *Human Genetics*, *131*(9), 1403–1421.

Kos, R., Reedy, M. V., Johnson, R. L., & Erickson, C. A. (2001). The winged-helix transcription factor FoxD3 is important for establishing the neural crest lineage and repressing melanogenesis in avian embryos. *Development*, *128*(8), 1467–1479.

Koufaris, C., Gallage, S., Yang, T., Lau, C.-H., Valbuena, G. N., & Keun, H. C. (2016). Suppression of MTHFD2 in MCF-7 Breast Cancer Cells Increases Glycolysis, Dependency on Exogenous Glycine, and Sensitivity to Folate Depletion. *Journal of Proteome Research*, *15*(8), 2618–2625.

Kuida, K., Haydar, T. F., Kuan, C. Y., Gu, Y., Taya, C., Karasuyama, H., … Flavell, R. A. (1998). Reduced apoptosis and cytochrome c-mediated caspase activation in mice lacking caspase 9. *Cell*, *94*(3), 325–337.

Kumar, S., Stecher, G., & Tamura, K. (2016). MEGA7: Molecular Evolutionary Genetics Analysis Version 7.0 for Bigger Datasets. *Molecular Biology and Evolution*, *33*(7), 1870–1874.

Lakhwani, S., García-Sanz, P., & Vallejo, M. (2010). Alx3-deficient mice exhibit folic acid-resistant craniofacial midline and neural tube closure defects. *Developmental Biology*, *344*(2), 869–880.

Lawson, A., Schoenwolf, G. C., England, M. A., Addai, F. K., & Ahima, R. S. (1999). Programmed cell death and the morphogenesis of the hindbrain roof plate in the chick embryo. *Anatomy and Embryology*, *200*(5), 509–519.

Lehtinen, L., Ketola, K., Mäkelä, R., Mpindi, J.-P., Viitala, M., Kallioniemi, O., & Iljin, K. (2013). High-throughput RNAi screening for novel modulators of vimentin expression identifies MTHFD2 as a regulator of breast cancer cell migration and invasion. *Oncotarget*, *4*(1), 48–63.

Li, D., & Rozen, R. (2006). Maternal Folate Deficiency Affects Proliferation, but Not Apoptosis, in Embryonic Mouse Heart. *The Journal of Nutrition*, *136*(7), 1774–1778.

Li, M. Z., & Elledge, S. J. (2007). Harnessing homologous recombination in vitro to generate recombinant DNA via SLIC. *Nature Methods*, *4*(3), 251–256.

Liu, F., Liu, Y., He, C., Tao, L., He, X., Song, H., & Zhang, G. (2014). Increased MTHFD2 expression is associated with poor prognosis in breast cancer. *Tumour Biology: The Journal of the International Society for Oncodevelopmental Biology and Medicine*, *35*(9), 8685–8690.

Liu, X., Huang, Y., Jiang, C., Ou, H., Guo, B., Liao, H., … Yang, D. (2016). Methylenetetrahydrofolate dehydrogenase 2 overexpression is associated with tumor aggressiveness and poor prognosis in hepatocellular carcinoma. *Digestive and Liver Disease: Official Journal of the Italian Society of Gastroenterology and the Italian Association for the Study of the Liver*, *48*(8), 953–960.

Ma, X.-Y., Yu, J.-T., Wu, Z.-C., Zhang, Q., Liu, Q.-Y., Wang, H.-F., Tan, L. (2012). Replication of the MTHFD1L gene association with late-onset Alzheimer's disease in a Northern Han Chinese population. *Journal of Alzheimer's Disease: JAD*, *29*(3), 521–525.

Martin, B., Brenneman, R., Becker, K. G., Gucek, M., Cole, R. N., & Maudsley, S. (2008). iTRAQ analysis of complex proteome alterations in 3xTgAD Alzheimer's mice: understanding the interface between physiology and disease. *PloS One*, *3*(7), e2750.

Marttinen, P., Pirinen, M., Sarin, A.-P., Gillberg, J., Kettunen, J., Surakka, I., … Kaski, S. (2014). Assessing multivariate gene-metabolome associations with rare variants using Bayesian reduced rank regression. *Bioinformatics (Oxford, England)*, *30*(14), 2026–2034.

Massa, V., Savery, D., Ybot-Gonzalez, P., Ferraro, E., Rongvaux, A., Cecconi, F., … Copp, A. J. (2009). Apoptosis is not required for mammalian neural tube closure. *Proceedings of the National Academy of Sciences of the United States of America*, *106*(20), 8233–8238.

Mejia, N. R., & MacKenzie, R. E. (1985). NAD-dependent methylenetetrahydrofolate dehydrogenase is expressed by immortal cells. *The Journal of Biological Chemistry*, *260*(27), 14616–14620.

Mejia, N. R., Rios-Orlandi, E. M., & MacKenzie, R. E. (1986). NAD-dependent methylenetetrahydrofolate dehydrogenase-methenyltetrahydrofolate cyclohydrolase from ascites tumor cells. Purification and properties. *The Journal of Biological Chemistry*, *261*(20), 9509–9513.

Mitchell, H. K., Snell, E. E., & Williams, R. J. (1941). THE CONCENTRATION OF "FOLIC ACID." *Journal of the American Chemical Society*, *63*(8), 2284–2284.

Momb, J., & Appling, D. R. (2014). Mitochondrial one-carbon metabolism and neural tube defects. *Birth Defects Research Part A: Clinical and Molecular Teratology*, *100*(8), 576–583.

Momb, J., Lewandowski, J. P., Bryant, J. D., Fitch, R., Surman, D. R., Vokes, S. A., & Appling, D. R. (2013). Deletion of Mthfd1l causes embryonic lethality and neural tube and craniofacial defects in mice. *Proceedings of the National Academy of Sciences*, *110*(2), 549–554.

Moran, D. M., Trusk, P. B., Pry, K., Paz, K., Sidransky, D., & Bacus, S. S. (2014). KRAS mutation status is associated with enhanced dependency on folate metabolism pathways in non-small cell lung cancer cells. *Molecular Cancer Therapeutics*, *13*(6), 1611–1624.

Morgan, T. M., House, J. A., Cresci, S., Jones, P., Allayee, H., Hazen, S. L., … Spertus, J. A. (2011). Investigation of 95 variants identified in a genome-wide study for association with mortality after acute coronary syndrome. *BMC Medical Genetics*, *12*, 127.

MRC Vitamin Study Research Group. (1991). Prevention of neural tube defects: results of the Medical Research Council Vitamin Study. *Lancet (London, England)*, *338*(8760), 131–137.

Naj, A. C., Beecham, G. W., Martin, E. R., Gallins, P. J., Powell, E. H., Konidari, I., … Pericak-Vance, M. A. (2010). Dementia revealed: novel chromosome 6 locus for late-onset Alzheimer disease provides genetic evidence for folate-pathway abnormalities. *PLoS Genetics*, *6*(9), e1001130.

Narisawa, A., Komatsuzaki, S., Kikuchi, A., Niihori, T., Aoki, Y., Fujiwara, K., … Kure, S. (2012). Mutations in genes encoding the glycine cleavage system predispose to neural tube defects in mice and humans. *Human Molecular Genetics*, *21*(7), 1496–1503.

NCBI Resource Coordinators. (2015). Database resources of the National Center for Biotechnology Information. *Nucleic Acids Research*, *43*(Database issue), D6-17.

Nijhout, H. F., Reed, M. C., Lam, S.-L., Shane, B., Gregory, J. F., & Ulrich, C. M. (2006). In silico experimentation with a model of hepatic mitochondrial folate metabolism. *Theoretical Biology & Medical Modelling*, *3*, 40.

Nilsson, R., Jain, M., Madhusudhan, N., Sheppard, N. G., Strittmatter, L., Kampf, C., … Mootha, V. K. (2014). Metabolic enzyme expression highlights a key role for MTHFD2 and the mitochondrial folate pathway in cancer. *Nature Communications*, *5*, 3128.

Pai, Y. J., Leung, K.-Y., Savery, D., Hutchin, T., Prunty, H., Heales, S., … Greene, N. D. E. (2015). Glycine decarboxylase deficiency causes neural tube defects and features of non-ketotic hyperglycinemia in mice. *Nature Communications*, *6*, 6388.

Palmer, B. R., Slow, S., Ellis, K. L., Pilbrow, A. P., Skelton, L., Frampton, C. M., … Cameron, V. A. (2014). Genetic polymorphism rs6922269 in the MTHFD1L gene is associated with survival and baseline active vitamin B12 levels in post-acute coronary syndromes patients. *PloS One*, *9*(3), e89029.

Palmer, K. F., & Williams, D. (1974). Optical properties of water in the near infrared*. *JOSA*, *64*(8), 1107–1110.

Parle-McDermott, A., Pangilinan, F., O'Brien, K. K., Mills, J. L., Magee, A. M., Troendle, J., … Brody, L. C. (2009). A common variant in MTHFD1L is associated with neural tube defects and mRNA splicing efficiency. *Human Mutation*, *30*(12), 1650–1656.

Pawelek, P. D., & MacKenzie, R. E. (1998). Methenyltetrahydrofolate Cyclohydrolase Is Rate Limiting for the Enzymatic Conversion of 10-Formyltetrahydrofolate to 5,10-Methylenetetrahydrofolate in Bifunctional Dehydrogenase-Cyclohydrolase Enzymes. *Biochemistry*, *37*(4), 1109–1115.

Pelletier, J. N., & MacKenzie, R. E. (1995). Binding and interconversion of tetrahydrofolates at a single site in the bifunctional methylenetetrahydrofolate dehydrogenase/cyclohydrolase. *Biochemistry*, *34*(39), 12673–12680.

Piedrahita, J. A., Oetama, B., Bennett, G. D., van Waes, J., Kamen, B. A., Richardson, J., … Finnell, R. H. (1999). Mice lacking the folic acid-binding protein Folbp1 are defective in early embryonic development. *Nature Genetics*, *23*(2), 228–232.

Pike, S. T., Rajendra, R., Artzt, K., & Appling, D. R. (2010). Mitochondrial C1-Tetrahydrofolate Synthase (MTHFD1L) Supports the Flow of Mitochondrial One-carbon Units into the Methyl Cycle in Embryos. *Journal of Biological Chemistry*, *285*(7), 4612–4620.

Pikman, Y., Puissant, A., Alexe, G., Furman, A., Chen, L. M., Frumm, S. M., … Stegmaier, K. (2016). Targeting MTHFD2 in acute myeloid leukemia. *The Journal of Experimental Medicine*, *213*(7), 1285–1306.

Pincus, T., Yazici, Y., Sokka, T., Aletaha, D., & Smolen, J. S. (2003). Methotrexate as the "anchor drug" for the treatment of early rheumatoid arthritis. *Clinical and Experimental Rheumatology*, *21*(5 Suppl 31), S179-185.

Prasannan, P., Pike, S., Peng, K., Shane, B., & Appling, D. R. (2003). Human mitochondrial C1-tetrahydrofolate synthase: gene structure, tissue distribution of the mRNA, and immunolocalization in Chinese hamster ovary calls. *The Journal of Biological Chemistry*, *278*(44), 43178–43187.

Ren, R.-J., Wang, L.-L., Fang, R., Liu, L.-H., Wang, Y., Tang, H.-D., … Chen, S.-D. (2011). The MTHFD1L gene rs11754661 marker is associated with susceptibility to Alzheimer's disease in the Chinese Han population. *Journal of the Neurological Sciences*, *308*(1–2), 32–34.

Ron-Harel, N., Santos, D., Ghergurovich, J. M., Sage, P. T., Reddy, A., Lovitch, S. B., … Haigis, M. C. (2016). Mitochondrial Biogenesis and Proteome Remodeling Promote One-Carbon Metabolism for T Cell Activation. *Cell Metabolism*, *24*(1), 104–117.

Ross, J., Green, J., Baugh, C. M., MacKenzie, R. E., & Matthews, R. G. (1984). Studies on the polyglutamate specificity of methylenetetrahydrofolate dehydrogenase from pig liver. *Biochemistry*, *23*(8), 1796–1801.

Rydström, J. (2006). Mitochondrial NADPH, transhydrogenase and disease. *Biochimica Et Biophysica Acta*, *1757*(5–6), 721–726.

Saade, S., Cazier, J.-B., Ghassibe-Sabbagh, M., Youhanna, S., Badro, D. A., Kamatani, Y., … FGENTCARD consortium. (2011). Large scale association analysis identifies three susceptibility loci for coronary artery disease. *PloS One*, *6*(12), e29427.

Saleet Jafri, M., & Kotulska, M. (2006). Modeling the mechanism of metabolic oscillations in ischemic cardiac myocytes. *Journal of Theoretical Biology*, *242*(4), 801–817.

Schirch, V., & Strong, W. B. (1989). Interaction of folylpolyglutamates with enzymes in one-carbon metabolism. *Archives of Biochemistry and Biophysics*, *269*(2), 371–380.

Scrimgeour, K. G., & Huennekens, F. M. (1960). Occurrence of a DPN-linked, N5,N10-methylene tetrahydrofolic dehydrogenase in Ehrlich ascites tumor cells. *Biochemical and Biophysical Research Communications*, *2*(3), 230–233.

Seither, R. L., Trent, D. F., Mikulecky, D. C., Rape, T. J., & Goldman, I. D. (1989). Folate-pool interconversions and inhibition of biosynthetic processes after exposure of L1210 leukemia cells to antifolates. Experimental and network thermodynamic analyses of the role of dihydrofolate polyglutamylates in antifolate action in cells. *The Journal of Biological Chemistry*, *264*(29), 17016–17023.

Selhub, J. (2002). Folate, vitamin B12 and vitamin B6 and one carbon metabolism. *The Journal of Nutrition, Health & Aging*, *6*(1), 39–42.

Sertié, A. L., Sossi, V., Camargo, A. A., Zatz, M., Brahe, C., & Passos-Bueno, M. R. (2000). Collagen XVIII, containing an endogenous inhibitor of angiogenesis and tumor growth, plays a critical role in the maintenance of retinal structure and in neural tube closure (Knobloch syndrome). *Human Molecular Genetics*, *9*(13), 2051–2058.

Shin, M., Bryant, J. D., Momb, J., & Appling, D. R. (2014). Mitochondrial MTHFD2L is a Dual Redox Cofactor Specific Methylenetetrahydrofolate Dehydrogenase/Methenyltetrahydrofolate Cyclohydrolase Expressed in Both Adult and Embryonic Tissues. *Journal of Biological Chemistry*, jbc.M114.555573.

Sievers, F., Wilm, A., Dineen, D., Gibson, T. J., Karplus, K., Li, W., … Higgins, D. G. (2011). Fast, scalable generation of high‐quality protein multiple sequence alignments using Clustal Omega. *Molecular Systems Biology*, *7*(1), 539.

Soo, K., O'Rourke, M. P., Khoo, P.-L., Steiner, K. A., Wong, N., Behringer, R. R., & Tam, P. P. L. (2002). Twist Function Is Required for the Morphogenesis of the Cephalic Neural Tube and the Differentiation of the Cranial Neural Crest Cells in the Mouse Embryo. *Developmental Biology*, *247*(2), 251–270.

Strickland, K. C., Krupenko, N. I., & Krupenko, S. A. (2013). Molecular mechanisms underlying the potentially adverse effects of folate. *Clinical Chemistry and Laboratory Medicine*, *51*(3), 607–616. https://doi.org/10.1515/cclm-2012-0561

Strong, W., Joshi, G., Lura, R., Muthukumaraswamy, N., & Schirch, V. (1987). 10-Formyltetrahydrofolate synthetase. Evidence for a conformational change in the enzyme upon binding of tetrahydropteroylpolyglutamates. *The Journal of Biological Chemistry*, *262*(26), 12519–12525.

Sudiwala, S., De Castro, S. C. P., Leung, K.-Y., Brosnan, J. T., Brosnan, M. E., Mills, K., … Greene, N. D. E. (2016). Formate supplementation enhances folate-dependent nucleotide biosynthesis and prevents spina bifida in a mouse model of folic acid-resistant neural tube defects. *Biochimie*, *126*, 63–70.

Suliman, H. S., Sawyer, G. M., Appling, D. R., & Robertus, J. D. (2005). Purification and properties of cobalamin-independent methionine synthase from Candida albicans and Saccharomyces cerevisiae. *Archives of Biochemistry and Biophysics*, *441*(1), 56–63.

Tang, L. S., Santillano, D. R., Wlodarczyk, B. J., Miranda, R. C., & Finnell, R. H. (2005). Role of Folbp1 in the regional regulation of apoptosis and cell proliferation in the developing neural tube and craniofacies. *American Journal of Medical Genetics Part C: Seminars in Medical Genetics*, *135C*(1), 48–58.

Tibbetts, A. S., & Appling, D. R. (2010). Compartmentalization of Mammalian Folate-Mediated One-Carbon Metabolism. *Annual Review of Nutrition*, *30*(1), 57–81.

Trainor, P. A., & Tam, P. P. (1995). Cranial paraxial mesoderm and neural crest cells of the mouse embryo: co-distribution in the craniofacial mesenchyme but distinct segregation in branchial arches. *Development (Cambridge, England)*, *121*(8), 2569–2582.

Tremblay, G. B., Sohi, S. S., Retnakaran, A., & MacKenzie, R. E. (1995). NAD-dependent methylenetetrahydrofolate dehydrogenase-methenyltetrahydrofolate cyclohydrolase is targeted to the cytoplasm in insect cell lines. *FEBS Letters*, *368*(1), 177–182.

Tuckett, F., & Morriss-Kay, G. M. (1985). The kinetic behaviour of the cranial neural epithelium during neurulation in the rat. *Journal of Embryology and Experimental Morphology*, *85*, 111–119.

Wagner, W., Breksa, A. P., Monzingo, A. F., Appling, D. R., & Robertus, J. D. (2005). Kinetic and structural analysis of active site mutants of monofunctional NAD-dependent 5,10-methylenetetrahydrofolate dehydrogenase from Saccharomyces cerevisiae. *Biochemistry*, *44*(39), 13163–13171.

Walkup, A. S., & Appling, D. R. (2005). Enzymatic characterization of human mitochondrial C1-tetrahydrofolate synthase. *Archives of Biochemistry and Biophysics*, *442*(2), 196–205.

Wallingford, J. B., Niswander, L. A., Shaw, G. M., & Finnell, R. H. (2013). The continuing challenge of understanding and preventing neural tube defects. *Science (New York, N.Y.)*, *339*(6123), 1222002.

Wang, X., Wang, J., Guan, T., Xiang, Q., Wang, M., Guan, Z., … Niu, B. (2014). Role of methotrexate exposure in apoptosis and proliferation during early neurulation. *Journal of Applied Toxicology*, *34*(8), 862–869.

Ward, M. (2001). Homocysteine, folate, and cardiovascular disease. *International Journal for Vitamin and Nutrition Research. Internationale Zeitschrift Für*

Vitamin- Und Ernährungsforschung. Journal International De Vitaminologie Et De Nutrition, *71*(3), 173–178.

Weil, M., Jacobson, M. D., & Raff, M. C. (1997). Is programmed cell death required for neural tube closure? *Current Biology: CB*, *7*(4), 281–284.

West, M. G., Barlowe, C. K., & Appling, D. R. (1993). Cloning and characterization of the Saccharomyces cerevisiae gene encoding NAD-dependent 5,10-methylenetetrahydrofolate dehydrogenase. *The Journal of Biological Chemistry*, *268*(1), 153–160.

Wright, E., Hargrave, M. R., Christiansen, J., Cooper, L., Kun, J., Evans, T., … Koopman, P. (1995). The Sry-related gene Sox9 is expressed during chondrogenesis in mouse embryos. *Nature Genetics*, *9*(1), 15–20.

Xu, L., Wang, L., Wang, J., Zhu, Z., Chang, G., Guo, Y., … Niu, B. (2016). The effect of inhibiting glycinamide ribonucleotide formyl transferase on the development of neural tube in mice. *Nutrition & Metabolism*, *13*(1), 56.

Yamaguchi, Y., & Miura, M. (2013). How to form and close the brain: insight into the mechanism of cranial neural tube closure in mammals. *Cellular and Molecular Life Sciences: CMLS*, *70*(17), 3171–3186.

Yang, H., Yang, T., Baur, J. A., Perez, E., Matsui, T., Carmona, J. J., … Sinclair, D. A. (2007). Nutrient-sensitive mitochondrial NAD+ levels dictate cell survival. *Cell*, *130*(6), 1095–1107.

Yang, X. M., & MacKenzie, R. E. (1993). NAD-dependent methylenetetrahydrofolate dehydrogenase-methenyltetrahydrofolate cyclohydrolase is the mammalian

homolog of the mitochondrial enzyme encoded by the yeast MIS1 gene. *Biochemistry*, *32*(41), 11118–11123.

Yi, Y., Lindemann, M., Colligs, A., & Snowball, C. (2011). Economic burden of neural tube defects and impact of prevention with folic acid: a literature review. *European Journal of Pediatrics*, *170*(11), 1391–1400.

Yu, J., Valerius, M. T., Duah, M., Staser, K., Hansard, J. K., Guo, J., … McMahon, A. P. (2012). Identification of molecular compartments and genetic circuitry in the developing mammalian kidney. *Development*, *139*(10), 1863–1873.

Yusuf, B., Gopurappilly, R., Dadheech, N., Gupta, S., Bhonde, R., & Pal, R. (2013). Embryonic fibroblasts represent a connecting link between mesenchymal and embryonic stem cells. *Development, Growth & Differentiation*, *55*(3), 330–340.

Zaganjor, I., Sekkarie, A., Tsang, B. L., Williams, J., Razzaghi, H., Mulinare, J., … Rosenthal, J. (2016). Describing the Prevalence of Neural Tube Defects Worldwide: A Systematic Literature Review. *PloS One*, *11*(4), e0151586.

Zhang, L., Joshi, A. K., & Smith, S. (2003). Cloning, expression, characterization, and interaction of two components of a human mitochondrial fatty acid synthase. Malonyltransferase and acyl carrier protein. *The Journal of Biological Chemistry*, *278*(41), 40067–40074.

Zhang, Z., Hailat, Z., Falk, M. J., & Chen, X. (2014). Integrative analysis of independent transcriptome data for rare diseases. *Methods (San Diego, Calif.)*, *69*(3), 315–325.

Zhao, Q., Behringer, R. R., & de Crombrugghe, B. (1996). Prenatal folic acid treatment suppresses acrania and meroanencephaly in mice mutant for the Cart1 homeobox gene. *Nature Genetics*, *13*(3), 275–283.

Zohn, I. E., Anderson, K. V., & Niswander, L. (2007). The Hectd1 ubiquitin ligase is required for development of the head mesenchyme and neural tube closure. *Developmental Biology*, *306*(1), 208–221.

Zohn, I. E., & Sarkar, A. A. (2012). Does the cranial mesenchyme contribute to neural fold elevation during neurulation? *Birth Defects Research Part A: Clinical and Molecular Teratology*, *94*(10), 841–848.